ผลของหมู่แทนที่ของอนุพันธ์เฮกซะฟีนิลเบนซีนต่อการเปล่งแสงที่ถูกเหนี่ยวนำโดยการรวมกลุ่มและการประยุกต์เพื่อเป็นตัวรับรู้ทางเคมี

นายวีระวัฒน์ ศรีเพชร

วิทยานิพนธ์นี้เป็นส่วนหนึ่งของการศึกษาตามหลักสูตรปริญญาวิทยาศาสตรมหาบัณฑิต
สาขาวิชาเคมี ภาควิชาเคมี
คณะวิทยาศาสตร์ จุฬาลงกรณ์มหาวิทยาลัย
ปีการศึกษา 2557

SUBSTITUENT EFFECTS OF HEXAPHENYLBENZENE DERIVATIVES ON AGGREGATION-INDUCED EMISSION AND THEIR APPLICATIONS AS CHEMOSENSORS

Mr. Weerawat Sripet

A Thesis Submitted in Partial Fulfillment of the Requirements
for the Degree of Master of Science Program in Chemistry
Department of Chemistry
Faculty of Science
Chulalongkorn University
Academic Year 2014

Thesis Title	SUBSTITUENT EFFECTS OF HEXAPHENYLBENZENE DERIVATIVES ON AGGREGATION-INDUCED EMISSION AND THEIR APPLICATIONS AS CHEMOSENSORS
By	Mr. Weerawat Sripet
Field of Study	Chemistry
Thesis Advisor	Assistant Professor Sumrit Wacharasindhu, Ph.D.
Thesis Co-Advisor	Associate Professor Mongkol Sukwattanasinitt, Ph.D.

Accepted by the Faculty of Science, Chulalongkorn University in Partial Fulfillment of the Requirements for the Master's Degree

.....Dean of the Faculty of Science
(Professor Supot Hannongbua, Dr.rer.nat.)

THESIS COMMITTEE

.....Chairman
(Associate Professor Vudhichai Parasuk, Ph.D.)

.....Thesis Advisor
(Assistant Professor Sumrit Wacharasindhu, Ph.D.)

.....Thesis Co-Advisor
(Associate Professor Mongkol Sukwattanasinitt, Ph.D.)

.....Examiner
(Thanit Praneenararat, Ph.D.)

.....External Examiner
(Assistant Professor Rakchart Traiphol, Ph.D.)

วีระวัฒน์ ศรีเพชร : ผลของหมู่แทนที่ของอนุพันธ์เฮกซะฟีนิลเบนซีนต่อการเปล่งแสงที่ถูกเหนี่ยวนำโดยการรวมกลุ่มและการประยุกต์เพื่อเป็นตัวรับรู้ทางเคมี (SUBSTITUENT EFFECTS OF HEXAPHENYLBENZENE DERIVATIVES ON AGGREGATION-INDUCED EMISSION AND THEIR APPLICATIONS AS CHEMOSENSORS) อ.ที่ปรึกษาวิทยานิพนธ์หลัก: ผศ. ดร.สัมฤทธิ์ วัชรสินธุ์, อ.ที่ปรึกษาวิทยานิพนธ์ร่วม: รศ. ดร.มงคล สุขวัฒนาสินิทธิ์, 115 หน้า.

โดยทั่วไปการเปล่งแสงฟลูออเรสเซ็นส์ของสารเรืองแสงจะถูกยับยั้งภายใต้สภาวะรวมตัวกัน (aggregation-caused quenching, ACQ) เมื่อไม่นานมานี้ได้มีการค้นพบปรากฏการณ์รวมตัวกันเหนี่ยวนำให้เกิดการเปล่งแสง (aggregation-induced emission, AIE) จากปรากฏการณ์ดังกล่าวนำมาสู่การออกแบบและพัฒนาตัวรับรู้ทางเคมีให้มีประสิทธิภาพมากขึ้น ในงานวิจัยชิ้นนี้จึงศึกษาผลของหมู่แทนที่ของอนุพันธ์เฮกซะฟีนิลเบนซีน (HPB) ต่อการเปล่งแสงที่ถูกเหนี่ยวนำโดยการรวมกลุ่มและการประยุกต์เพื่อเป็นตัวรับรู้ทางเคมี โดยส่วนแรกศึกษาเปรียบเทียบสมบัติเชิงแสงระหว่างในสภาวะการรวมตัวกันและในสภาวะสารละลายของอนุพันธ์ HPB ที่มีหมู่แทนที่ต่างกัน HPB-2Me, HPB-2OMe, HPB-2Cl และ HPB-2NAP จากการศึกษาพบว่าในอัตราส่วนของน้ำที่สูง HPB-2Me, HPB-2OMe และ HPB-2NAP แสดงปรากฏการณ์ AIE ขณะที่ HPB-2Cl มีการเปลี่ยนแปลงสัญญาณของฟลูออเรสเซ็นส์ที่ไม่ชัดเจน ส่วนที่สองเราทำการสังเคราะห์สารประกอบกลุ่มอนุพันธ์ของไพรีน (FL1 และ FL2) จากการศึกษาการเปรียบเทียบสมบัติเชิงแสงในสภาวะรวมตัวกันพบว่าที่ 60 เปอร์เซ็นต์ของน้ำในตัวทำละลายอินทรีย์ (THF) ของ FL1 มีการเปล่งแสงของฟลูออเรสเซนส์เพิ่มขึ้นในขณะที่ FL2 มีการเปลี่ยนแปลงสัญญาณของฟลูออเรสเซ็นส์ที่ไม่ชัดเจน อีกทั้งยังพบว่าในสภาวะที่รวมตัวกันของ FL1 สามารถใช้เป็นตัวรู้ทางเคมีที่มีจำเพาะกับ picric acid ในระดับความเข้มข้นต่ำสุด 0.880 μM ส่วนที่สามเราได้สังเคราะห์สารประกอบอนุพันธุ์ HPB [SW(2-6)] ที่ประกอบด้วยส่วนของอิมมีนสำหรับเป็นตัวตรวจวัดกับโลหะ พบว่าสัญญาณฟลูออเรสเซนส์ของ SW2 เพิ่มขึ้นเมื่อจับกับโลหะอะลูมิเนียมในขณะที่สัญญาณฟลูออเรสเซนส์ของ SW(4-6) มีจำเพาะกับโลหะสังกะสีในลักษณะเพิ่มสัญญาณ SW4 และ SW5 สามารถตรวจวัดโลหะสังกะสีที่มีความเข้มข้นที่ต่ำสุดเท่ากับ 0.160 μM และ 0.035 μM ตามลำดับซึ่งน้อยกว่าองค์การอนามัยโลกกำหนดไว้ในน้ำดื่ม และน่าสนใจอย่างมากสำหรับ SW5 ที่แสดงความสามารถต่อการตรวจวัดโลหะสังกะสีในเซลล์สิ่งมีชีวิต อีกทั้งสารประกอบเชิงซ้อน SW5-Zn^{2+} สามารถนำมาเป็นตัวรับรู้ทางเคมีสำหรับตรวจวัดสารประกอบกลุ่ม organophosphate pesticides ชนิด Diazinon ในระดับส่วนในล้านส่วน

ภาควิชา เคมี	ลายมือชื่อนิสิต .....
สาขาวิชา เคมี	ลายมือชื่อ อ.ที่ปรึกษาหลัก .....
ปีการศึกษา 2557	ลายมือชื่อ อ.ที่ปรึกษาร่วม .....

5572117523 : MAJOR CHEMISTRY
KEYWORDS:

WEERAWAT SRIPET: SUBSTITUENT EFFECTS OF HEXAPHENYLBENZENE DERIVATIVES ON AGGREGATION-INDUCED EMISSION AND THEIR APPLICATIONS AS CHEMOSENSORS. ADVISOR: ASST. PROF. SUMRIT WACHARASINDHU, Ph.D., CO-ADVISOR: ASSOC. PROF. MONGKOL SUKWATTANASINITT, Ph.D., 115 pp.

Typical flurophore molecules usually display aggregation caused quenching emission (ACQ) but a recent discovery on the aggregation-induced emission (AIE) leads to new designs of fluorescent sensor. In this work, we would like to report the systematic study of the substituent effects toward emission in the aggregation state of hexaphenylbenzene (HPB) derivatives and their application as chemosensor. Firstly, we compared photophysical properties between the aggregation state and the solution state of five different HPB derivatives HPB-2Me, HPB-2OMe, HPB-2Cl and HPB-2NAP. In high content of water, HPB-2Me, HPB-2OMe and HPB-2NAP showed AIE effect while HPB-2Cl gave no change in fluorescence intensity. Secondly, we synthesized two novel oligophenylene-based pyrene derivatives (FL1 and FL2) in good yields (86-96%). Comparison study of photophysical properties of both compound toward aggregate effect suggested that FL1 showed maximum fluorescence intensity in 60% water in THF (aggregate state) while FL2 displayed no significant change in fluorescence signal. The aggregate state FL1 exhibited specific response towards the picric acid over other nitroaromatic compounds. The detection limit was determined to be 0.880 μM. Finally, we prepared new hexaphenylbenzenes (HPBs) containing imine moiety [SW (4-6)] for metal ions detection. The addition of Al^{3+} to SW2 resulted in the strong enhancement as orange emission while the SW (4-6) showed selective turn-on fluorescence toward Zn^{2+} ion in different degrees. Moreover, the detection limits of SW4 and SW5 toward Zn^{2+} ion were calculated to be 0.160 μM and 0.035 μM, respectively which are lower than drinking water permission concentration by world health organization (WHO). The complex between SW5 and Zn^{2+} was investigated by NMR titration, Job's plot, SEM and DLS technique suggesting the formation of nano aggregates in 2:1 complex ratio. We were able to detect Zn^{2+} in living cell using SW5 and also the emissive SW5-Zn^{2+} complex can selectively detect organophosphate pesticides, Diazinon in ppm level.

Department:	Chemistry	Student's Signature	.....
Field of Study:	Chemistry	Advisor's Signature	.....
Academic Year:	2014	Co-Advisor's Signature	.....

ACKNOWLEDGEMENTS

The accomplishment of this thesis can be attributed to the assistance and support from Assistant Professor Dr. Sumrit Wacharasindhu as my thesis advisor and Associate Professor Dr. Mongkol Sukwattanasinitt as my co-adviser, invaluable guidance and encouragement throughout the course of this research.

I would like to gratefully acknowledge the committee, Associate Professor Dr. Vudhichai Parasuk, Dr. Thanit Praneenararat, and Assistant Professor Dr. Rakchart Traiphol for their comments, guidance and extending cooperation over my presentation. I would like to thank Assistant Professor Dr. Anawat Ajavakom, Associate Professor Dr. Paitoon Rashatasakhon and Dr. Sakulsuk Unarunotai for their attention and suggestions during our research group meeting. I also would like to thank Associate Professor Dr. Suchada Chantrapromma for her helpful suggestion during my studying. Furthermore, I would like to thank my appreciation is also given to many people in our research group; Ms. Nopparat Thavornsin, Ms. Kanoktorn Boonkitpatarakul, Mr. Waroton Paisuwan, Ms. Kunnigar Vongnam and Ms. Pornpat Sam-ang for their helpful suggestion and everyone in MAPS group for spirit, smile, good wish and their helps in everything.

This study is financially supported by the Thailand Research Fund (RSA5780055) and nanotechnology Center (NANOTEC), NSTDA, Ministry of Science and Technology, Thailand, through its program of Center of Excellence Network. This work is part of the Project for Establishment of Comprehensive Center for Innovative Food, Health Products and Agriculture supported by the Thai Government Stimulus Package 2 (TKK2555, SP2), the Higher Education Research Promotion and National Research University Project of Thailand, Office of the Higher Education Commission (AM1006A-56) and the Ratchadaphiseksomphot Endowment Fund of Chulalongkorn University (RES560530126-AM).

Finally, I would like to express my thankfulness to my beloved parents and friends for their encouragement and understanding throughout. I would not be able to reach this success without them.

CONTENTS

Page

Page

Page

Page

Page

LIST OF FIGURES

Figure **Page**

LIST OF SCHEMES

LIST OF ABBREVIATIONS

A	acceptor
Ar	aromatic
Calcd	calculated
^{13}C NMR	carbon-13 nuclear magnetic resonance
$CDCl_3$	deuterated chloroform
D	donor
d	doublet (NMR)
dd	doublet of doublet (NMR)
ESIMS	electrospray ionization mass spectrometry
Equiv	Equivalent (s)
g	gram (s)
^{1}H NMR	proton nuclear magnetic resonance
Hz	Hertz
HRMS	high resolution mass spectrum
hrs	hour (s)
ICT	internal charge transfer
J	coupling constant
mg	milligram (s)
mL	milliliter (s)
mmol	mill mole (s)
m/z	mass per charge
m	multiplet (NMR)
M.W.	Molecular weight
M	molar
MHz	megahertz
rt	room temperature

s	singlet (NMR)
TEA	triethylamine
THF	tetrahydrofuran
UV	ultraviolet
δ	Chemical shift
^{o}C	degree Celsius
µL	microliter (s)
µM	micro molar (s)
Φ	Quantum yield

CHAPTER I
INTRODUCTION

1.1 Overviews

1.1.1 Nitroaromatic compounds

Nitroaromatic compounds are well-known primary constituents of many unexploded land mines worldwide [1] and are also considered to be environmental contaminants because the soil and groundwater of war zone and military facilities can contain toxic level of these compounds. Examples of nitroaromatic compounds are shown in **Figure 1.1.** Trinitrotoluene (TNT) is one of the most used chemicals for construction of explosive material while picric acid (PA) is a common reagent used in the leather, pharmaceutical, dye industries and manufacturing of explosives[2]. The widespread use of both compounds has made them a significant environmental pollutant. Those are strong irritant and very harmful to human in respirator, gastrointestinal and central nervous system [3]. The traditional techniques for the detection of nitroaromatic compounds are gas chromatography coupled with mass spectrometry, energy dispersive X-ray diffraction and cyclic voltammetry [4, 5] which are expensive and time-consuming in practice. Recently, fluorescence spectroscopy has gained attention for the detection of toxic chemicals due to convenient method, high sensitivity and ability to perform on-site analysis.

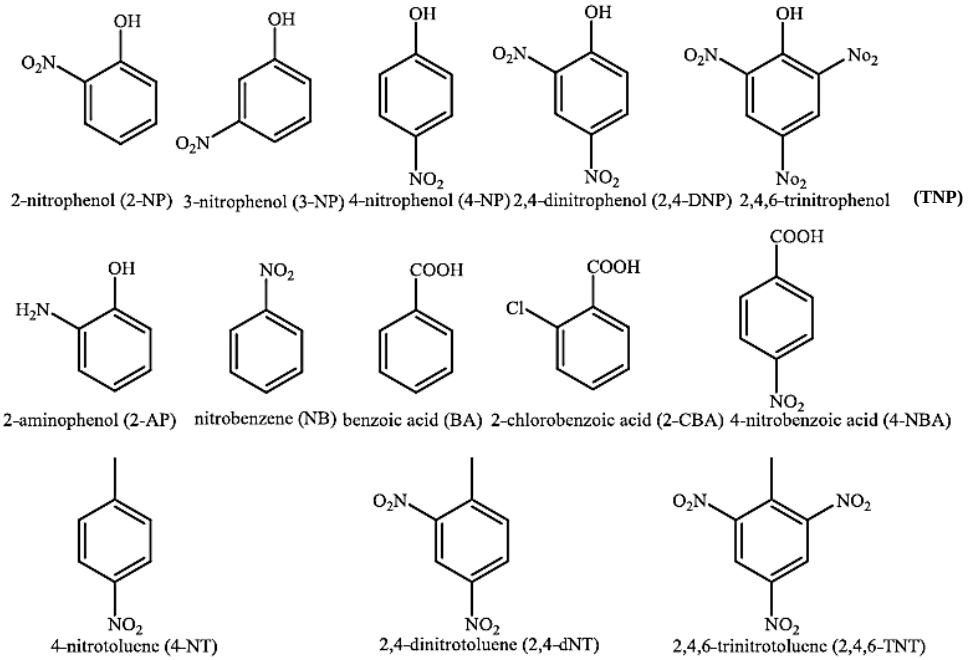

Figure 1.1 Structures of all nitroaromatic compounds

1.1.2. Zinc (Zn^{2+}) and aluminum (Al^{3+}) ions

The development of detection methods for metal ions has received considerable attention [6] due to their importance in biological and environmental roles. Among various metal ions, zinc ion (Zn^{2+}) has attracted a great deal of attention ascribing to its biological significance. Zinc ion plays significant role in various fundamental biological processes, such as gene transcription and DNA binding or recognition. Also, excessive amount of zinc in human cause many severe diseases such as Alzheimer's disease, Friedreich's ataxia and Parkinson's disease [7]. On the other hand, aluminum is widely used in many applications such as textile industry, medicines, paper industry and food additive. An excess amount of aluminum in human body not only damages the central nervous system but also causes various diseases such as Alzheimer's, Parkinson's and breast cancer[8]. Therefore, detection of Zn^{2+} and Al^{3+} are necessary. Traditional analytical methods, such as atomic

absorption spectroscopy, inductively coupled plasma mass spectroscopy and electrochemical analysis, have been used for the trace-quantity determination of metal ions. Nevertheless, most of those methods are expensive and time-consuming in practice. Therefore development for the detecting Al^{3+} and Zn^{2+} traces is required.

1.2 Principle of fluorescence

Fluorescence activity can be schematically illustrated with the classical Jablonski diagram as seen in **Figure 1.2** when a molecular system absorbs, then emits light. Initially, molecule absorbs high energy light (short wavelength) and promotes electron within the molecule from the ground state to the excited state (purple arrow). In the excited state the electrons rapidly, in a few pico-seconds, relax to the lowest available energy state (red arrow). Once in this state, and after a lag period of several nano-seconds (the fluorescence lifetime), the electrons will relax back to ground state (green arrow), releasing their stored energy in an emitted photon. Due to the higher energy relaxation mechanism, this emitted light is of a lower energy (longer wavelength) than the absorbed light[9]. The difference between the excitation and the emission energy (wavelength) is termed the Stokes shift.

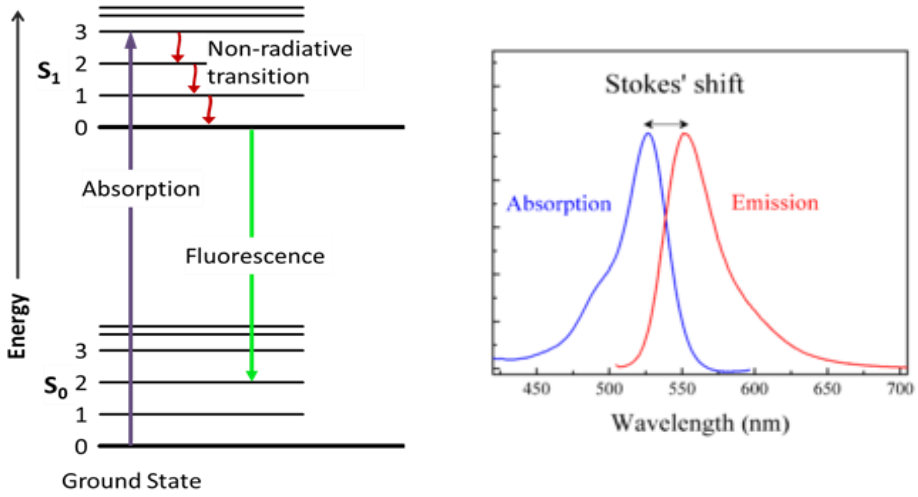

Figure 1.2 Jablonski diagram[9] (Left) and the difference wavelength between the absorption and the emission [10] (Right).

1.3. Mechanism of changing fluorescent signals

A decrease in fluorescence intensity is referred to as quenching. This is caused by several mechanisms such as Photo-induced Electron Transfer (PET), Forster Resonance Energy Transfer (FRET), Internal Charge Transfer (ICT), Aggregation Effect, Excited-State Proton Transfer (ESPT), and C=N isomerization. In this work, we focused on the Aggregation Effect, ESIPT, ICT, C=N isomerization process.

1.3.1. Internal Charge Transfer (ICT) effect

In gernal, molecules will emit fluorescent signal when they return from locally exicited stae (LE) to ground state. On the other hand, if molecule compose both of strong electron-donor and electron acceptor substituents, an electron can delocalize via the pi-conjugated system. The LE excited state will convert to the ICT state which is the more stable state following the Frank-Condon principle [11] (**Figure 1.3**). Then, the fluorescence intensity will be lower and the molecules show a large Stoke shift emission wavelength so called “red shift”.

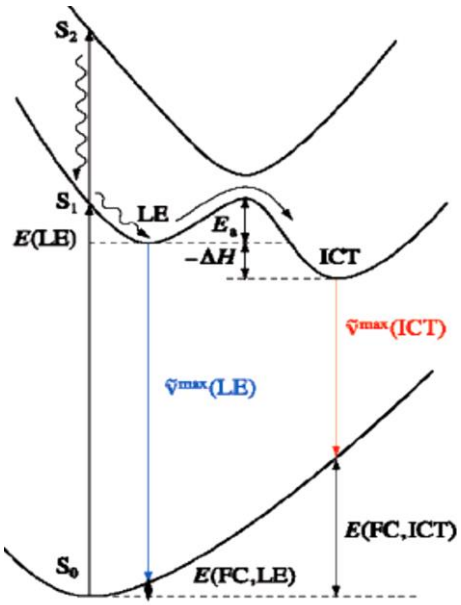

Figure 1.3 Potential energy surfaces of the ground state (S_0) is excited to and S_1 or S_2 and then relaxed to LE, and ICT (FC = Franck-Condon)

1.3.2 Photoinduced electron transfer (PET) effect

PET effect is one of the well-known processes of the fluorescence signal quenching [9].Ordinarily, when a flurophore is excited by light energy, an electron of the molecules moves from the highest occupied molecular orbital (HOMO) to the lowest unoccupied molecular orbital (LUMO). If the HOMO of the receptor unit in system is located in between HOMO and LUMO of flurophore, the electron move from HOMO receptor unit to HOMO of flurophore and from LUMO of flurophore to HOMO receptor unit, resulting in quenching of fluorescence signal as seen in **Figure 1.4**

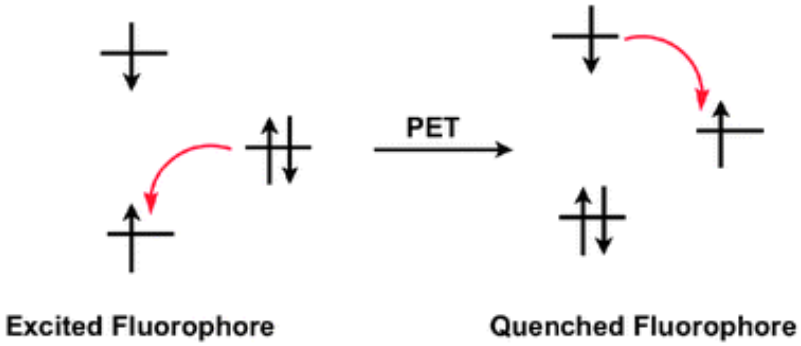

Figure 1.4 Photoinduced electron transfer (PET), modified from reference[12]

1.3.3 Excited-state proton transfer (ESPT) process

The intramolecular proton transfer in excited states (ESIPT) is based on acidity and basicity relations in an intramolecular hydrogen bond. The excited-enol (E*) can be significantly altered to an excited-keto (K*) via phototautomerization process of as illustrated in **Figure 1.5**. For example, in keto-enol tautomerization, the proton donor consists of a hydroxyl group and the acceptor is a nitrogen atom or a carbonyl group. Eventually, the excited keto (K*) structure decays to the ground state K(S_0) either by radiative (fluorescence) or non-radiative (internal conversion) processes (red arrow). Then it undergoes reverse proton transfer returning to the original ground state, enol structure. This pathway suppresses the enol emission (blue arrow).

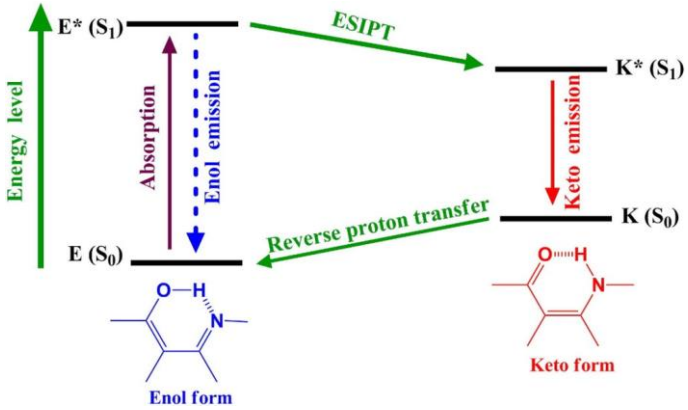

Figure 1.5 Illustration of a typical ESIPT photocycle , modified from reference [13]

1.3.4 Double bond isomerization process

Double bond isomerization is known as a fluorescence quenching mechanism that occurs though the rotation of double bond. The geometry structure in the ground state of flurophore was excited by light energy to higher energy level [14, 15]. It is the predominant decay process of excited states in compounds with an unabridged double bond structure so those compounds are often non-fluorescent. On the other hand, the fluorescence of their analogs containing a covalently bridged double bond structure increases dramatically due to the suppression of double bond isomerization in the excited states as seen in **Figure 1.6**.

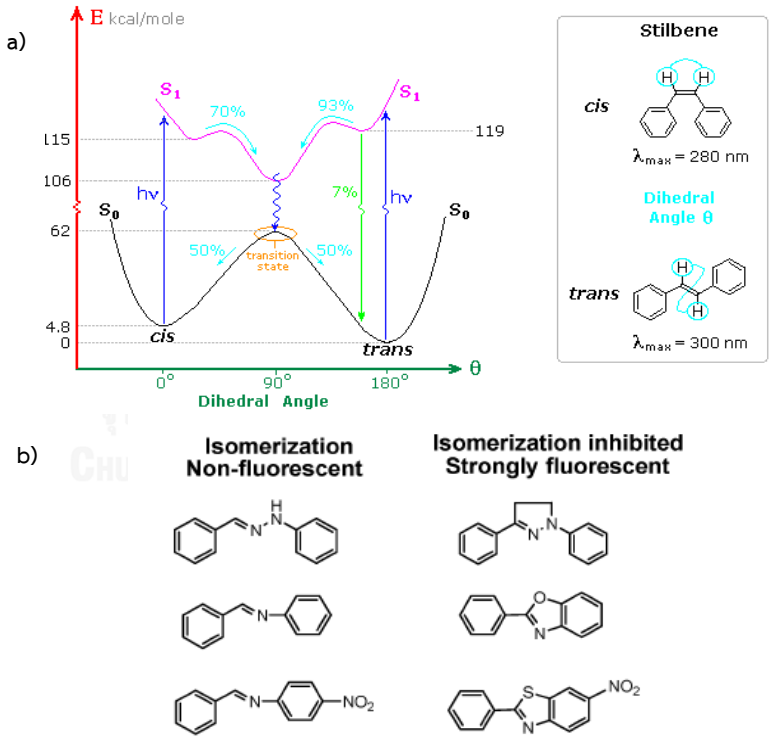

Figure 1.6 a) Potential energy surfaces of the ground state (S_0) is excited to S_1 b) Molecular structures of unabridged and bridged C=N compounds, modified from reference [16]

1.3.5 Aggregation effect

The common fluorphores are highly emissive in dilute, but they become weakened with an increasing concentration or in solids state. This low emission caused by the formation of sandwich-shaped excimer and exciplex aided (**ΠΠ**-**ΠΠ** stacking interactions) between the planar molecule in excited and ground state [17] which supported by the formation of aggregates with ordered or random structures. In this case the aggregates in excited states often decay via non-radiative pathways, which is known as aggregation-caused quecning (ACQ) [18] of ligth emission as seen in **Figure 1.7a**. This cause several advantages. For example, emissions from dilute solutions are often weak, leading to poor sensitivity in fluorescence sensor system[19]. However, some organic molecules that are the most non-fluorescent in dilute solution are able to exhibit strong emission in high concentration and in aggrgate state which is called “aggregation-induced emission” (AIE) which was first discovered in 2001 by Tang *et al*[20]. This phenomenon usually occurs with the propeller-like structure which induces a free intramolecular rotation resulting to non-luminescence in solution state. Upon aggregation in a suitable system, intramolecular rotation was restricted and the formation of eximers was prohibited leading to fluorescence enhancement (**Figure 1.7b**).

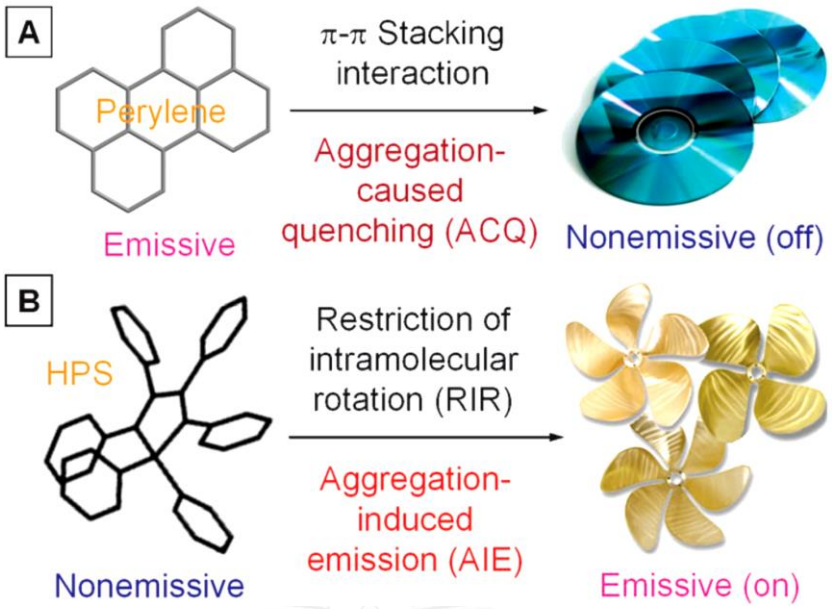

Figure 1.7 a) Planar fluorphore such as perylene tend to aggregate as discs pile up, due to the strong **π–π** stacking interactions between the aromatic rings, which commonly turns ‘‘off’’ light emission b) Propeller-like molecules such as hexaphenylsilole (HPS) behave oppositely, with their light emissions turned ‘‘on’’ by aggregate formation, due to the restriction of the intramolecular rotation (RIR) of the multiple phenyl rotors against the silole stator in the aggregate state, modified from reference [21].

Not only hexaphenylsilole (HPS), there are reports on other AIE-active flurophore molecules such as tetraphenylethylene (TPE) [22] and hexaphenylbenzene (HPB) [23-25] showing aggregation induced emission effect as seen in **Figure 1.8.** These allow such flurophores to perform the detection of metal ions in solid state or aqueous solution. However, there was no report on the effect of substituent groups on HPB derivatives toward their photopysical properties. Therefore, in this work, we are interested in the photophysical poroperties of hexaphenylbenzene derivatives on aggregation state and their application as chemosensors.

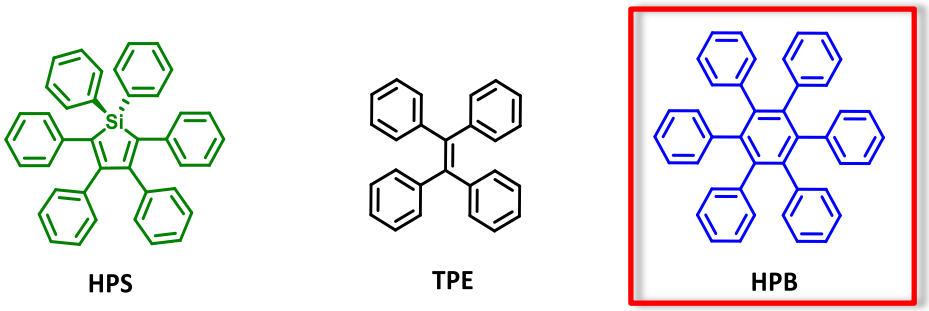

Figure 1.8 Structures of AIE-active flurophore molecules

1.4 Fluorescence sensor

In general, the chemosensor is composed of two units; receptor unit for binding with analytes and for giving readout as seen **Figure 1.9**. The chemosensor can be categorized into two modes based on the changes in fluorescent signal. The "turn-off" mode is those which exhibit of quenching fluorescence signal under the presence of analyte (**Figure 1.9a**). The opposite changes fluorescence signal would call "turn-on" mode (**Figure 1.9b**).

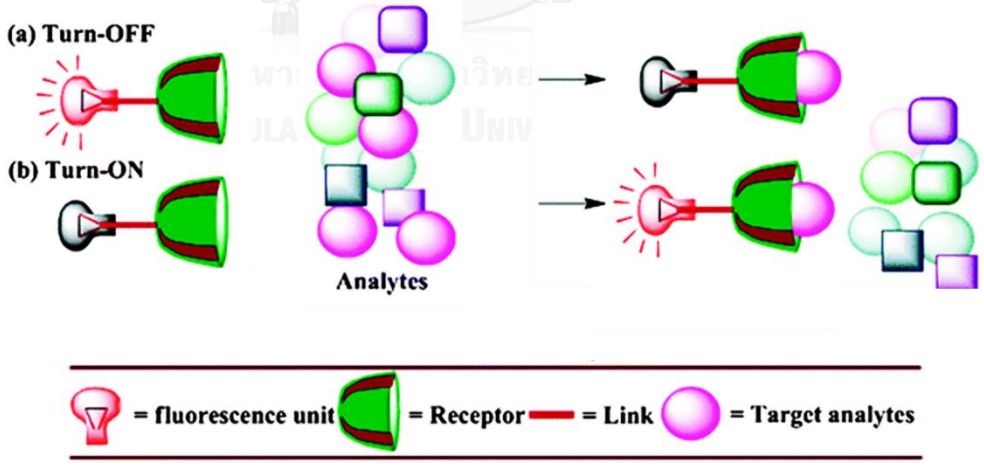

Figure 1.9 Schematic illustration of two modes fluorescent chemosensor [26]

1.5 Literature review on Hexaphenylbenzene (HPB) based fluorescence chemosensor

Recently, there has been an increase in the number of studies about hexaphenylbenzene (HPB) as fluorescence chemosensor. In general, it is an aromatic molecule self-possessed of a benzene ring substituted with six phenyl rings (**Figure 1.10**). It was obtained from Diels-Alder reaction. Due to their advantages such as convenient synthesis, high photo stability, insensitive to pH and most importantly AIEE-active molecule, HPB was reported as fluorescence sensor domain which we will be discussed in this section.

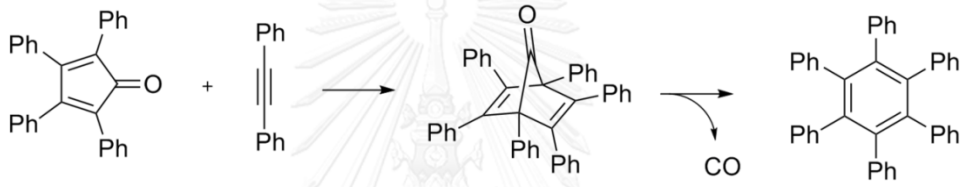

Figure 1.10 The synthetic scheme of HPB and structure

In 2006, Robert G. and co-worker [27] reported the method for the synthesis of heterosubstituted HPB (**Figure 1.11**) starting from asymmetric carbonylative couplings of benzyl halides to produce ketones, followed by Knoevenagel condensations to generate cyclopentadienenone. Then the cycloaddition reaction between cyclopentadienenone and diaryethyne give the product in excellent yield.

Figure 1.11 Hexaarylbenzenes with specific, unique groups at the 1, 4 positions

In 2012, Vandana Bhalla and co-worker [28] reported a novel “turn-on” fluorescent chemosensor of hexaphenylbenzene derivative containing quinolone moiety. The sensing mechanism is based on the Photoinduced electron transfer (PET) from imine nitrogen to a photoexcited hexaphenylbenzene moiety. The chemosensor has shown Zn^{2+} selectivity over other metal ions as seen in **Figure 1.12**.

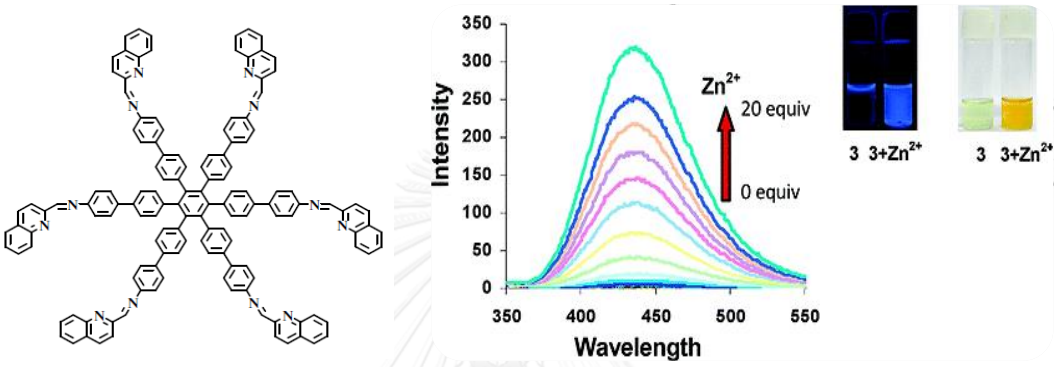

Figure 1.12 HPB derivative compound 3 and change in fluorescence on the presence of Zn^{2+} ions (Inset) Change in (left) fluorescence and (right) color on addition of 20 equiv. of Zn^{2+} ions in 5 μM solution in ethanol/ THF (3:1, v/v)

Also, this report showed the applications of the sensor in visualizing prostate cancer cells. Their Blue fluorescence images of cells were recorded at 37 ^{0}C in 20 min (**Figure 1.13**).

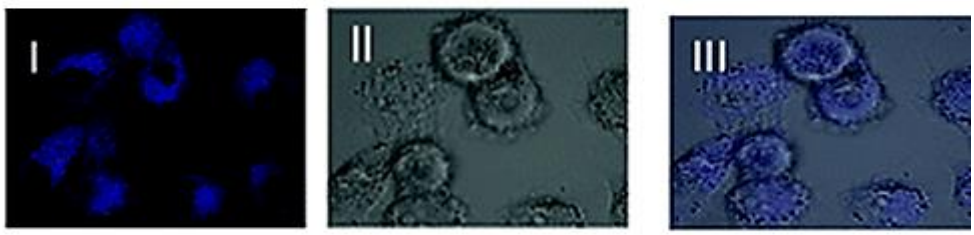

Figure 1.13 Blue fluorescence images of cells treated with HPB derivative compound 3 (1.0 M) only for 20 min at 37 ^{0}C. (**II**) Brightfield image of (**I**). (**III**) Overlay of (**I**) and (**II**)

In 2012, Manoj Kumar and co-worker [23] developed a new chemosensor, heterooligophenylene-based carbazole derivatives **3** and **4** exhibiting weak emission at weak emission (Φ_F = 0.0018) at 363 nm when excited at 290 nm. Upon addition of an 80% volume fraction of water the emission band at 363 nm showed a maximum enhancement (Φ_{AIEE} = 0.59) in emission intensity due to AIEE effect which resulted in restriction of the intramolecular rotation. The AIEE-active derivatives **3** and **4** showed selective fluorescent sensors for the nanomolar detection of TNT in solution, solid, and vapor. The detection limit of **3** as fluorescent sensors for TNT was found to be 30 × 10^{-9} mol.L^{-1}. The Stern–Volmer plots of aggregates compound was linear and gave quenching constants (K_{SV}) of 13.3 × 10^5 and M^{-1} (**Figure 1.14**)

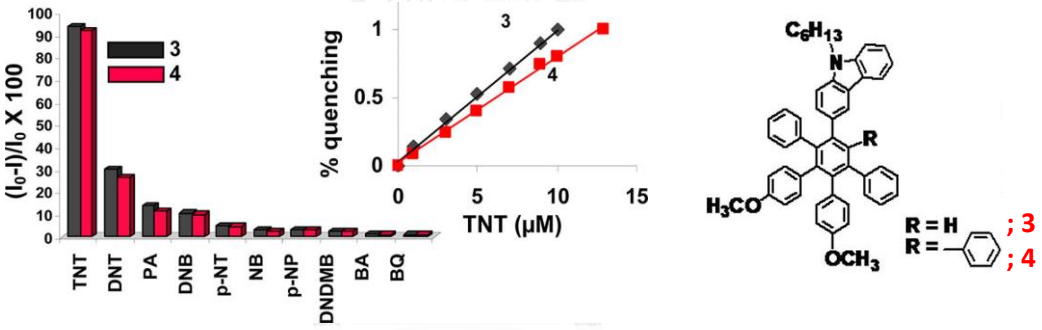

Figure 1.14 Selectivity graphs of **3** and **4** toward TNT for 10 and 13 μM analyte, respectively. The inset shows the Stern–Volmer plot of % quenching vs TNT concentration

In 2013, Vandana Bhalla and co-workers [29] designed and synthesized hexaphenylbenzene-based derivative **5**. This compound exhibited aggregation-induced emission (AIEE) in a mixed aqueous medium because of the presence of free rotors. In addition, these aggregates of derivative **5** have a strong affinity for Hg^{2+} ions and undergo metal-induced modulation in the presence of Hg^{2+} ions to form nanorods. Compound **5**-Hg^{2+} ensemble exhibited remarkable selectivity toward PA among other nitro derivatives with a detection limit of 6.87 ppb and K_{SV}=1.92 × 10^5 M^{-1} (**Figure 1.15**).

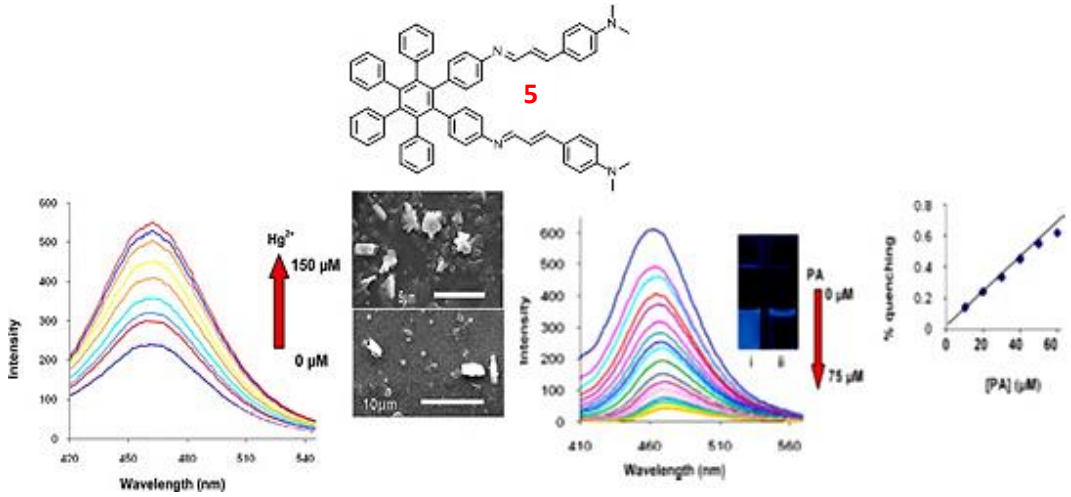

Figure 1.15 (upper) HPB derivative compound **5** (left) change in fluorescence on the presence of Hg^{2+} ions Inset and SEM images (right) Change in the fluorescence of **5**-Hg^{2+} (5 μM) upon the addition of PA (75 μM) Inset difference in the fluorescence of **5** (i) before and (ii) after the addition of PA to the **5**-Hg^{2+} ensemble; Stern–Volmer plot in H_2O/THF, (4:6 v/v)

In 2013, Vandana Bhalla and co-worker[24] designed and synthesized AIEE-active HPB based receptor **6**. The increase in fluorescence intensity of **6** in the presence of an increasing percentage of the water fraction suggests that AIE effect existed. The aggregates of this derivative underwent modulation in the presence of CN^- ions and it showed rod like self-assemblies. Interestingly, self-assemblies of this ensemble work as an efficient fluorogenic sensor for the detection of trinitrotoluene (TNT) with a detection limit of 10.21 ppq (parts per quadrillion) as shown in **Figure 1.16**.

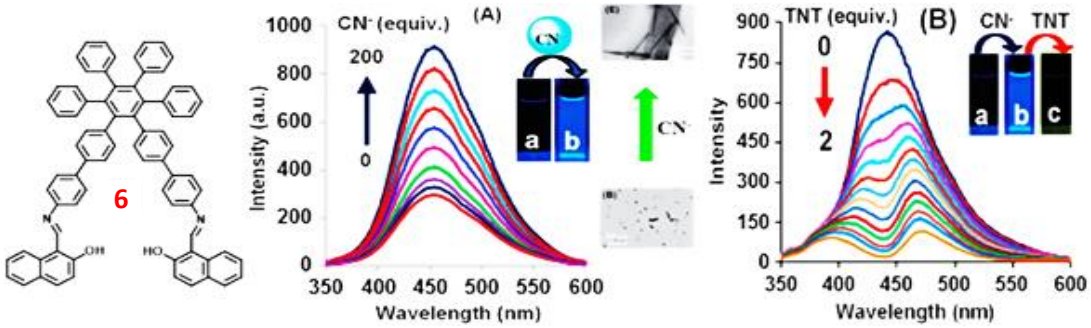

Figure 1.16 HPB derivative compound **6** a) change in fluorescence on the presence of CN^- b) Change in fluorescence on addition of 2 equiv. of TNT ions in 5 μM solution in H_2O/EtOH (6 : 4, v/v) buffered with HEPES, pH = 7.0

In 2013, Subhamay Pramanikand and co-workers [25]successfully designed and synthesized a new AIEE-active HPB compound **7**. This aggregates of compound **7** showed network of fluorescent nanofibres in presence of mercury ions. Interestingly, the **7**-Hg^{2+}supramolecular ensemble exhibited sensitive and pronounced response towards the picric acid. This supramolecular ensemble can detect picric acid in the range of 50 × 10^{-12} M with Stern–Volmer constant of 1.71 × 10^5 M^{-1} (**Figure 1.17**).

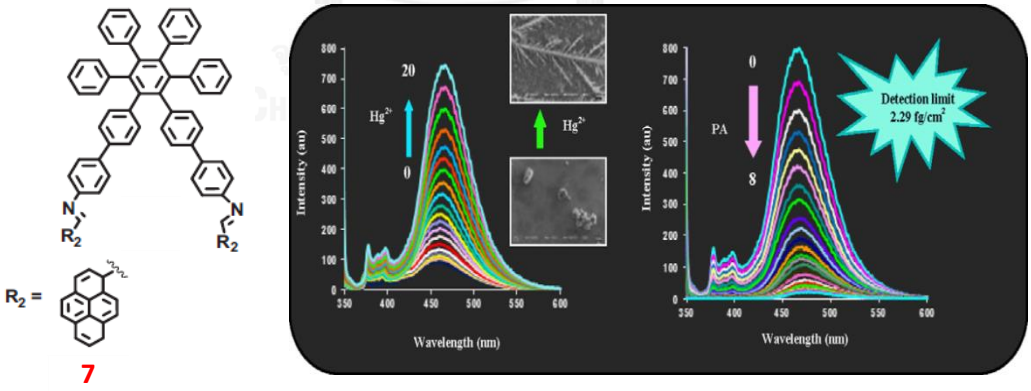

Figure 1.17 Chemical structure of HPB compound **7**, its selectivity toward Hg^{2+} ion and Change in fluorescence on addition of 8 equiv. of PA in H_2O/EtOH (5:5, v/v) buffered with HEPES, pH = 7.05

1.6 Literature review on imine based fluorescence chemosensor for the detection of metal ions

A general equation for the formation of an imine from a primary amine and an aldehyde or ketone is shown in **Figure 1.18.** Imine formation is an acid catalyzed reaction, and the product can form as a mixture of (E) and (Z) isomers. Recently, chemosensor for the detection of environmentally important metal has been actively investigated and imine moiety is used as receptor unit for the detection of metal ions in many reports.

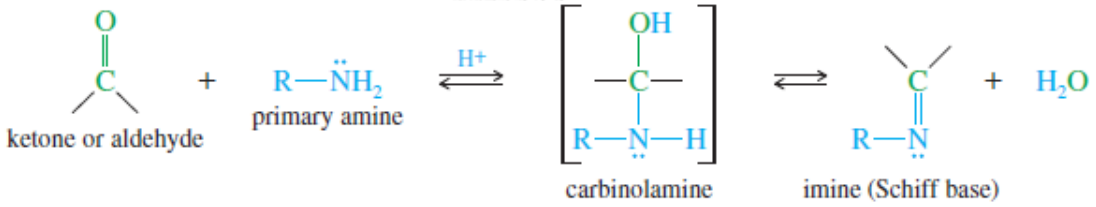

Figure 1.18 Equation reaction of imine formation[30]

In 2007, Jia-Sheng Wuand co-worker [31] successfully synthesized coumarin derivatives as new fluorescence sensors. The free rotation of imine bridged C=N is suppressed in the excited states because of the binding between Zn^{2+} and ligand. In addition, the solution of ligand showed about 200-fold increase of fluorescence quantum yield (about 30%) upon addition of Zn^{2+} (**Figure 1.19**).

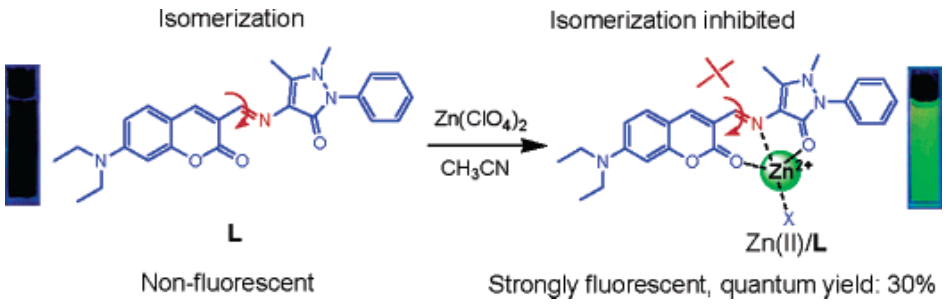

Figure 1.19 Schematic illustration of increase in fluorescence achieved by inhibiting C=N isomerization

In 2012, Hsiang-Yi Lin and co-workers [32] synthesized Schiff base-type fluorescent receptor **1** which was prepared from 2-hydroxynaphthalene-1-carboxaldehyde with 2-aminoethanol. It showed a selective turn-on response to Zn^{2+} in the blue emission (**Figure 1.20**). In addition, the detection limit of this sensor was found to be 3.04 $\times 10^{-6}$ M. The association constant for **1**–Zn^{2+} in methanol was determined as 2.2×10^{5} M^{-1} by a Hill plot and a Job plot indicated a 2:1 complexation. The complex **1**–Zn^{2+} uses the phenolic proton for complex formation to prevent ESIPT processing and C=N isomerization.

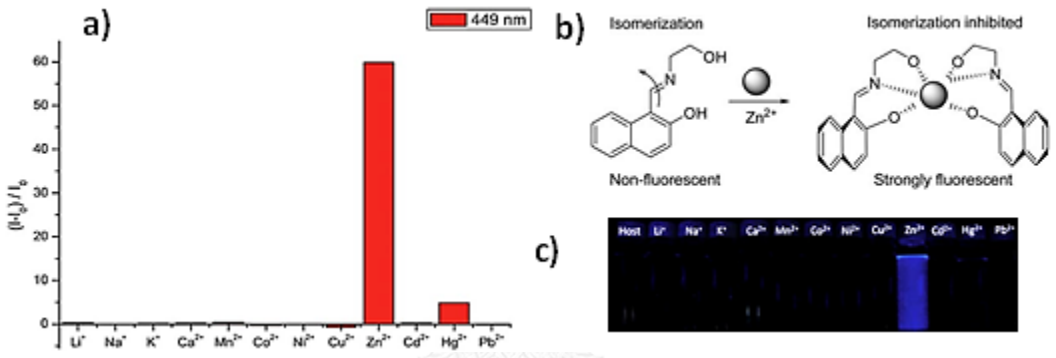

Figure 1.20 a) Selectivity graphs of receptor **1** toward various cations in methanol b) Proposed binding mechanism c) Fluorescence changes excited by UV lamp upon addition of 10 equiv.

In 2013, Ji Young Choi and co-workers [33] synthesized new chemosensor based on imine moiety **2** in a single step via imine formation between hydroxypyrene-2-carboaldehyde and 2-aminoaniline. It gave low fluorescence at 588 nm in CH_3CN-HEPES buffer (0.01 M, pH 7.4) (2:1, v/v). In addition, upon addition of Zn^{2+}, it induced a highly selective "turn-on" fluorescence enhancement. This inhibited the internal charge transfer (ICT) mechanism and also caused fluorescence enhancement which observed by naked-eyes under black light (**Figure 1.21**).

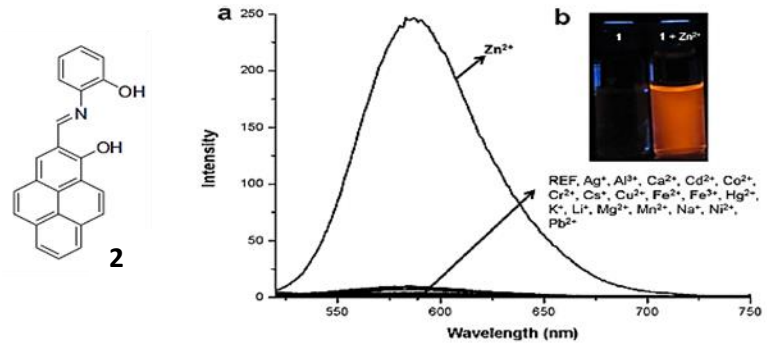

Figure 1.21 Chemosensor **2** and a) fluorescence spectra respond upon various metal ions (10 equiv.) b) Fluorescence picture of 1 (10 mM), before and after addition of 10 equiv. of Zn^{2+}

In 2014, Mengyu Zhan and co-worker [34] designed a naphthol derivative **3** containing an imine moiety that gives weak emission at 451 nm in methanol caused by the photoinduced electron transfer (PET) and C=N isomerization mechanisms. Interestingly, the chemosensor shows highly selective to Zn^{2+} ion in enhanced fluorescence responses. The detection limit of this sensor was found to be 2.50×10^{-6} M. In addition, **3**-Zn^{2+}complex exhibited remarkable selectivity toward $H_2PO_4^-$ by fluorescence turn-off signaling (**Figure1.22**).

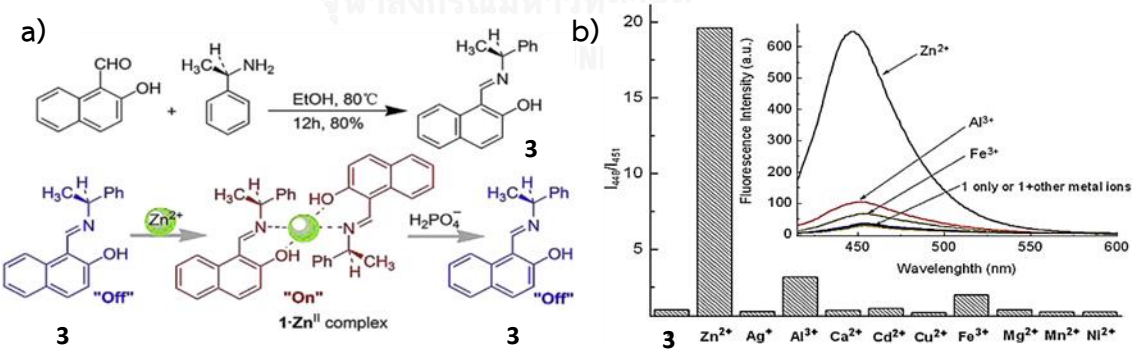

Figure 1.22 a) the synthetic procedure for receptor **3** and schematic representative of fluorescent sensing toward Zn^{2+} and $H_2PO_4^-$. b) fluorescence responses upon addition various metal ions in methanol

In 2012, Hongde Xiao and co-workers [35] demonstrated that coumarin derivative containing imine probe (**CN**) can selectively detect Al^{3+} in aqueous systems. In addition, Al^{3+} induced a highly selective "turn-on" fluorescence enhancement. This enhancement can be ascribed to the cation-induced inhibition of the ESIPT process **(Figure 1.23)**. The binding ratio of **CN**–Al^{3+} complexes was determined from the Job plot to be 1:1. The binding constant was calculated to be 9.55×10^{4} M^{-1} from a Benesi–Hildebrand plots and the detection limit was evaluated to be as low as 0.10 μM (**Figure1.23**).

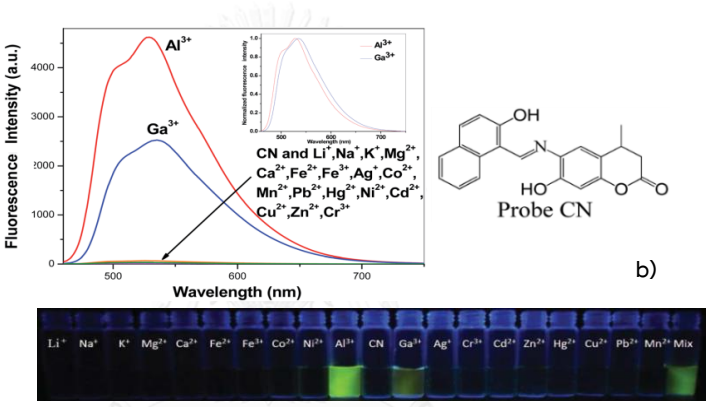

Figure 1.23 a) Fluorescence responses of to various metal ions in ethanol–Tris–HCl buffer (v/v, 1/9, pH= 7.3) and strcture **CN** probe b) Fluorescence changes excited by UV lamp upon addition of 10 equiv.

1.7 Objective of this research

From the above literature reveiws, there is no report on the effect of substituent groups on HPB toward AIEE. Also, in the chemosensor application, most sensors were reported as turn-off mode based on the initial strong emissive HPB in aggregates state. Therefore, in this work ours objectives are devided into three parts.

1. We will synthesize hexaphenylbenzene derivatives containing various substituent groups including electron donating and withdrawing groups (**Figure 1.24**). These

prepared HPB should have AIEE effect but their fluorescence enhancement ratio should depend on substituent groups on HPB.

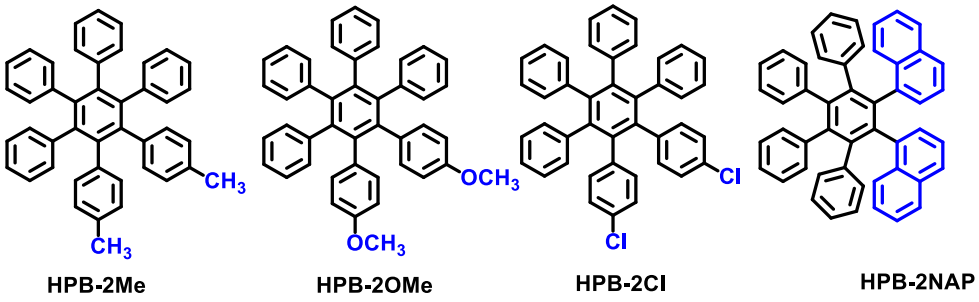

Figure 1.24 Structure of substituented hexaphenylbenzene derivative

2. Oligophenylene based pyrene derivatives (**FL1** and **FL2**) as seen in **Figure 1.25.** will be synthesized and investigated for their exhibition of aggregaton induced emission (AIE) effect. Their appliaction as sensing ability toward a variety of nitroaromatic compounds in aqueous media will also be investigated.

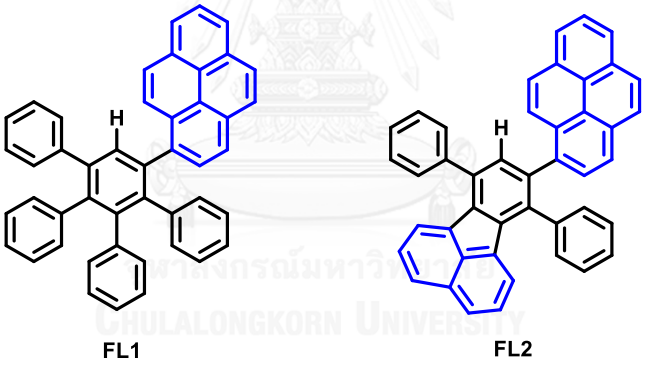

Figure 1.25 Structure of oligophenylene based pyrene derivatives (**FL1** and **FL2**)

3. We will synthesize new hexaphenylbenzenes (HPBs) containing imine moiety **SW (2-6)** as shown in **Figure 1.26**). These new compounds should display relatively low emission efficiency due to the intramolecular rotation, C=N isomerization and ESIPT process even in high concent of water. The presence of metal ions should inhibit queching processes resulting in fluorescence enhancement.

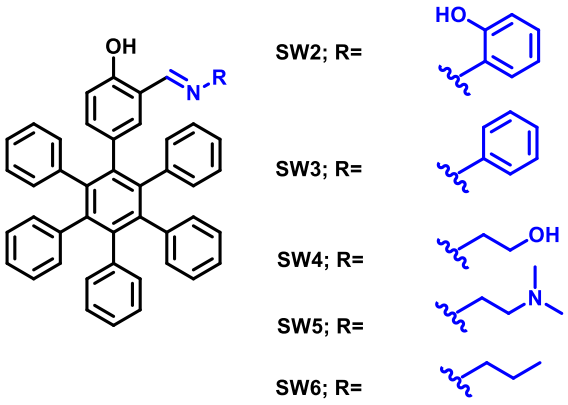

Figure 1.26 Structures of hexaphenylbenzene (HPB) containing with imine moiety derivatives **SW (2-6)**

CHAPTER II

Experiment

2.1 Analytical instruments

All ^{1}H- and ^{13}C-NMR spectra were recorded on a Varian Mercury NMR spectrometer, which operated at 400 MHz for ^{1}H and 100 MHz for ^{13}C (Varian Company, CA, USA) using $CDCl_3$, d_6-DMSO or d_8-THF as the solvents. Mass spectra were recorded on a Micro flex MALDI-TOF mass spectrometer (Bruker Daltonics) using doubly recrystallized 2-cyano-4-hydroxy cinnamic acid (CCA) or dithranol as a matrix. Melting points were uncorrected and determined by a melting point apparatus (Electrothermal 9100, Fisher Scientific, USA). Absorption spectra were measured by a UV-2550 UV-Vis spectrophotometer (SHIMADZU. Japan). Fluorescence spectra were obtained from a Carry Eclipse Fluorescence Spectrophotometer (Agilent Technologies) using a mixture of water and THF as solvents. Particle size of all flurophores was measured by Zetatract Dynamic Light Scattering (DLS) particle size analyzer with zeta potential capability.

2.2 Materials and chemicals

All reagent grade chemicals were obtained from Merck® (Germany), Sigma-Aldrich (USA), or Fluka®, (Switzerland). For general reactions, solvents such as methylene chloride (CH_2Cl_2 and ethanol (CH_3CH_2OH) were reagent grade and stored over molecular sieves for at least 24 h prior uses. In anhydrous reactions, solvents such as tetrahydrofuran (THF) were dried and distilled before use according to the standard procedures. All column chromatography were operated using silica gel 60 (70-230 mesh) purchased from Merck. Thin layer chromatography (TLC) was performed on silica gel plates (Merck F245). Solvents used for extraction and chromatography were commercial grade and distilled before use. Ethyl acetate

(EtOAc) and *n*-hexane (C_6H_{14}) used for extraction was reagent grade. De-ionized water was used in all fluorescence experiments unless specified otherwise. All reactions were carried out under positive pressure of N_2 filled in rubber balloons.

2.3 Synthesis

2.3.1 General procedure for Pd-catalyzed coupling reaction of calcium carbide with aryl iodides[36]

A 100 mL round bottom flask with a magnetic stir bar was charged with copper iodide (0.1 equiv.), palladium acetate (0.05 equiv.), and triphenylphosphine (0.1 equiv.) in acetonitrile. The solution was degassed with nitrogen for 20 min. Then, triethylamine (3 equiv.), aryl iodides (1 equiv.), and calcium carbide (3 equiv.) were added. The mixture was stirred at room temperature overnight under nitrogen atmosphere. The reaction mixture was then filtrated through a separation funnel and evaporated under vacuum to give the desired compound and the compound was purified by column chromatography using 10%ethyl acetate in hexane as an eluent to give compound.

Synthesis of compound 1, 2-di-p-tolylethyn

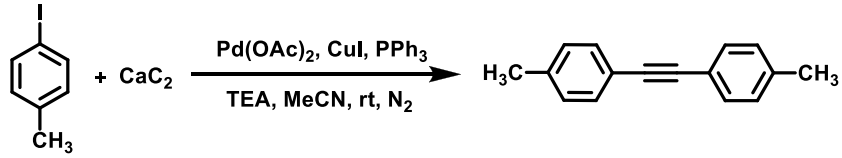

Synthesized according to general procedure from 4-iodotoluene (100 mg, 0.459 mmol), calcium carbide (88mg, 1.375 mmol), copper iodide (8.6 mg, 0.046 mmol), palladium(II)acetate (5.6 mg, 0.023 mmol), triphenylphosphine (12.0 mg, 0.046 mmol), and triethylamine (138 mg, 0.046 mmol) to afford 1,2-di-p-tolylethyn as a white solid 81 % yield: ^{1}H NMR (400 MHz, $CDCl_3$) **δ** 7.41 (d, J = 8.0 Hz, 4H), 7.14 (d, J = 7.9 Hz, 4H), 2.36 (s, 6H).

Synthesis of compound 1, 2-bis (4-methoxyphenyl) ethyne

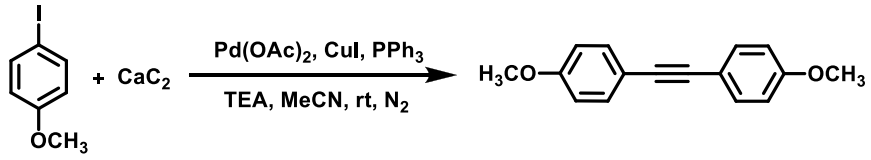

Synthesized according to general procedure from 4-iodoanisole (1000 mg, 4.27 mmol), calcium carbide (81.9 mg, 12.81 mmol), copper iodide (81.1 mg, 0.427 mmol), palladium(II)acetate (52.1mg, 21.3 mmol), triphenylphosphine (111 mg, 0.427 mmol), and triethylamine (1293 mg, 12.81 mmol) to afford 1,2-bis(4-methoxyphenyl)ethyne as a white solid 81% yield: ^{1}H NMR (400 MHz, $CDCl_3$) δ 7.45 (d, J = 8.8 Hz, 4H), 6.87 (d, J = 8.8 Hz, 4H), 3.83 (s, 6H).

Synthesis of compound 1, 2-di (naphthalen-1-yl) ethyne

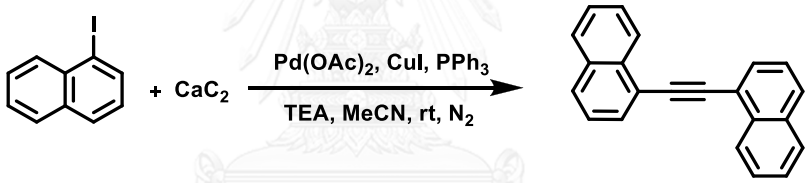

Synthesized according to general procedure from 1-iodonaphthalene (300 mg, 1.180 mmol), calcium carbide (227 mg, 3.54 mmol), copper iodide (22.4 mg, 0.118 mmol), palladium(II)acetate (14.4 mg, 0.059 mmol), triphenylphosphine (30.9 mg, 0.118 mmol), and triethylamine (357 mg, 3.54 mmol) to afford 1,2-di(naphthalen-1-yl)ethyne as a white solid 93% yield: ^{1}H NMR (400 MHz, $CDCl_3$) δ 8.57 (d, J = 8.1 Hz, 2H), 7.90 (t, J = 5.9 Hz, 6H), 7.64 (t, J = 7.0 Hz, 2H), 7.57 (t, J = 7.0 Hz, 2H), 7.54 (m, 2H).

Synthesis of compound 1, 2-bis (4-chlorophenyl) ethyne

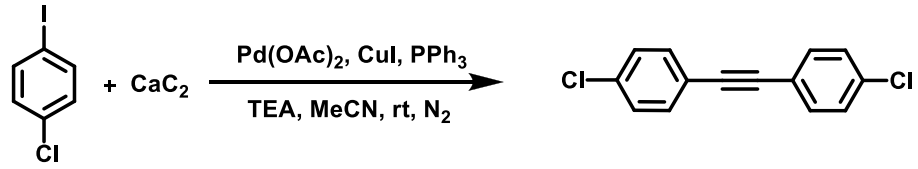

Synthesized according to general procedure from 4-iodochlorobenzene (1000.0 mg, 4.19 mmol), calcium carbide (804.4 mg, 12.57 mmol), copper iodide (79.6 mg,0.419 mmol),palladium(II)acetate (35.9 mg, 0.147 mmol) triphenylphosphine (109.8 mg, 0.419 mmol), and triethylamine (126.0 mg, 12.57 mmol) to afford 1,2-bis(4-chlorophenyl)ethyne as a white solid 25 % yield: ^{1}H NMR (400 MHz, $CDCl_3$) δ 7.45 (d, J = 7.6 Hz, 4H), 7.33 (d, J = 7.6 Hz, 4H).

2.3.2 General procedure for the synthesis of hexaphenylbenzene derivatives

A mixture of diaryethyne and tetraphenylcyclopentadienone in diphenylether under refluxed heating and stirring 24hr. After cooling, the dark-red mixture was diluted with dichloromethane (1 mL), poured in methanol (50 mL) and stirred; the off white precipitate was filtered, washed with methanol and vacuum dried. The product was recrystallized by partial evaporation (24 h) of a mixture of DCM (2.5 mL) and ethanol (5 mL).

Synthesis of compound HPB-2Me

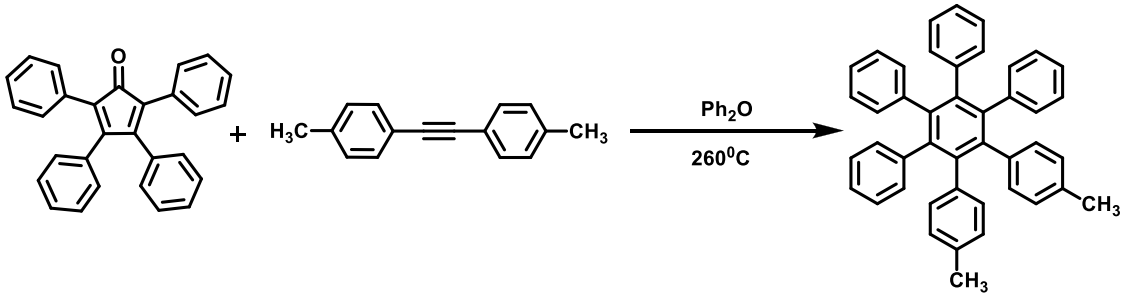

Synthesized according to general procedure from 1, 2-di-p-tolylethyn (200 mg, 0.967 mmol) and tetraphenylcyclopenta-2,4-dienone (410 mg 1.066mmol).

Afford to HPB-2Me as a white solid 40% yield: ^{1}H NMR (400 MHz, $CDCl_3$) **δ** 6.96 (m, 20H), 6.70 (d, *J* = 8.1 Hz, 4H), 6.65 (d, *J* = 8.1 Hz, 4H), 2.10 (s, 6H).^{13}C NMR (100 MHz, $CDCl_3$) **δ** 141.0, 140.9, 140.5, 140.3, 137.8, 134.5, 131.6, 131.4, 127.4, 126.6, 125.2, 125.1, 21.1.

Synthesis of compound HPB-2OMe

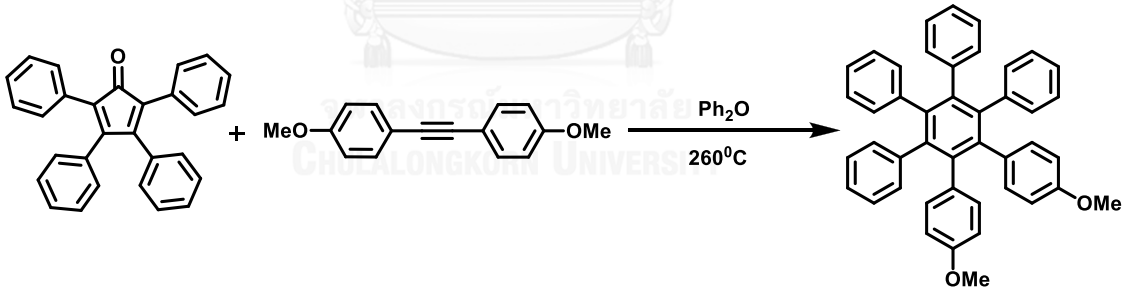

Synthesized according to general procedure from 1,2-bis(4-methoxyphenyl) ethyne (300mg, 1.25 mmol) and tetraphenylcyclopenta-2,4-dienone (480 mg 1.25 mmol). Afford to HPB-2OMe as a white solid 42% yield: ^{1}H NMR (400 MHz, $CDCl_3$) **δ** 6.91 (m, 20H), 6.75 (d, *J* = 8.7 Hz, 4H), 6.42 (d, *J* = 8.7 Hz, 4H), 3.62 (s, 6H).^{13}C NMR (100 MHz, $CDCl_3$) **δ** 156.4, 140.5, 140.4, 140.2, 139.8, 139.7, 132.7, 132.0, 131.0, 126.2, 126.1, 124.7, 124.6, 111.9, 54.4.

Synthesis of compound HPB-2Cl

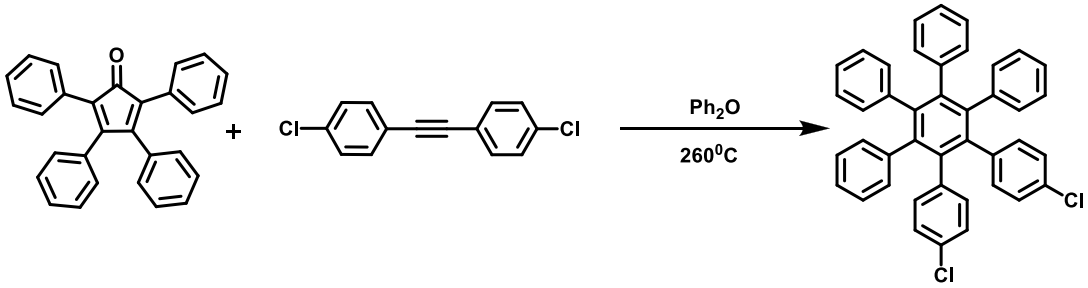

Synthesized according to general procedure from 1,2-bis(4-chlorophenyl)ethyne (100mg, 0.410 mmol) and tetraphenylcyclopenta-2,4-dienone (151 mg, 0.410 mmol). Afford to HPB-2Cl as a brown solid 39% yield: ^{1}H NMR (400 MHz, $CDCl_3$) **δ** 7.44 (d, *J* = 8.0 Hz, 1H), 7.33 (d, *J* = 8.0 Hz, 4H), 6.91 – 6.70 (m, 21H).^{13}C NMR (100 MHz, $CDCl_3$) **δ** 140.0, 139.7, 139.5, 139.3, 138.1, 133.7, 131.9, 131.8, 130.7, 130.5, 127.9, 126.3, 126.0, 125.8, 124.7, 124.54, 120.8.

Synthesis of compound HPB-2NAP

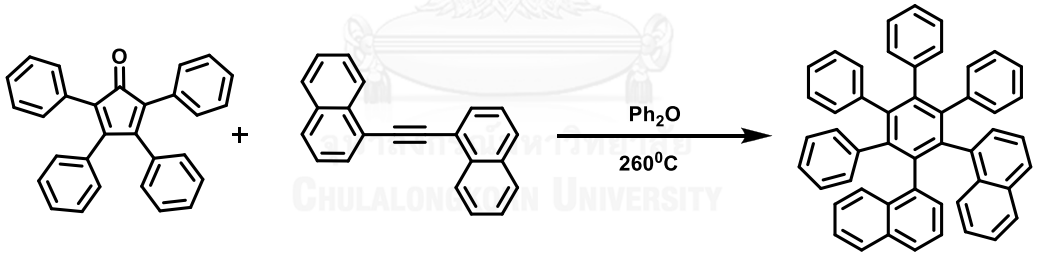

Synthesized according to general procedure from 1,2-di(naphthalen-1-yl)ethyne (300mg, 1.18 mmol) and tetraphenylcyclopenta-2,4-dienone (453 mg 1.18mmol). Afford to HPB-2NAP as a brown solid 13% yield: ^{1}H NMR (400 MHz, $CDCl_3$) **δ** 7.92, 7.90, 7.86, 7.84, 7.46, 7.44, 7.40, 7.38, 7.36, 7.31, 7.29, 7.22, 7.21, 7.19, 7.16, 7.15, 7.03, 7.01, 7.00, 6.98, 6.95, 6.94, 6.92, 6.90, 6.88, 6.86, 6.79, 6.77, 6.74, 6.72, 6.70, 6.68, 6.63, 6.61, 6.59, 6.54, 6.52, 6.50, 6.48.

2.3.3 Synthesis of oligophenylene based pyrene derivatives (FL1 and FL2)

Synthesis of compound 7, 9-diphenyl-8H-cyclopenta[l]acenaphthylen-8-one

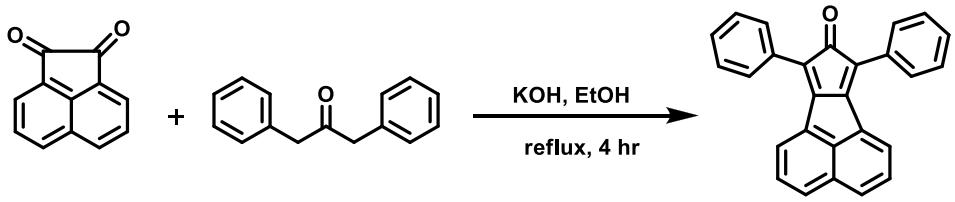

Acenaphthenedione (546.5 mg, 3 mmol) were added into the ethanol (5 mL) solution of 1,3-diphenylacetone (630.8 mg, 3 mmol) under heating and stirring. Under refluxing and stirring, the ethanol solution (2 mL) of KOH (94.1 mg) was drop wised in the above mixture. After reacting 5 min, the product was obtained after the above solution was cooled for 12 h and was filtrated. The yield: 1.038 g, 90%. Characterization of compound: ^{1}H NMR (400 MHz, $CDCl_3$) **δ** 8.07 (d, *J* = 7.0 Hz, 2H), 7.85 (dd, *J* = 16.2, 7.9 Hz, 6H), 7.59 (t, *J* = 7.4 Hz, 2H), 7.53 (t, *J* = 7.3 Hz, 4H), 7.42 (d, *J* = 6.8 Hz, 2H).

Synthesis of compound 1-pyrene-2, 3, 4, 5-tetraphenylbenzene (FL1)

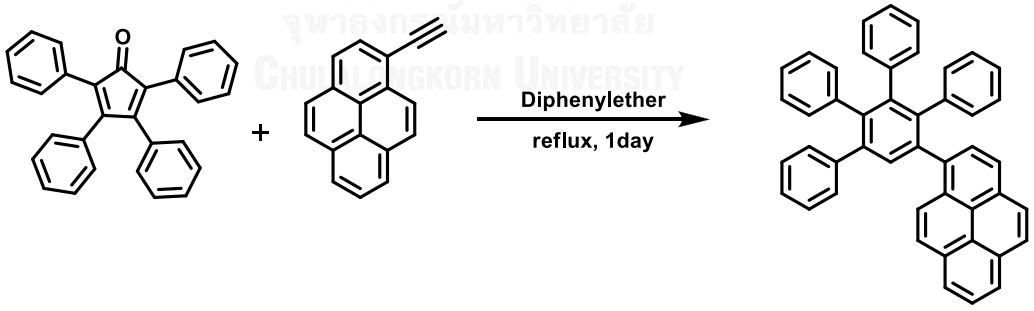

A solution of tetraphenylcyclopentadienone (611g, 1.59mmol) and 1-Ethynylpyrene (300 mg, 1.33mmol) in 2 mL of diphenylether was refluxed for overnight under a nitrogen atmosphere. The dark-red mixture was diluted with dichloromethane (1 mL), poured in methanol (50 mL) and stirred; the off white precipitate was filtered, washed with methanol and vacuum dried. The product was recrystallized by partial evaporation (24 h) of a mixture of dichloromethane (2.5 mL)

and ethanol (5 mL). The yield: 0.666 g, 86%. Characterization of compound: ^{1}H NMR (400 MHz, $CDCl_3$) **δ** 8.24 (d, *J* = 9.2 Hz, 1H), 8.18 – 8.11 (m, 2H), 8.05 – 7.93 (m, 5H), 7.74 (d, *J* = 7.9 Hz, 1H), 7.66 (s, 1H), 7.22 – 7.10 (m, 5H), 6.98 (s, 5H), 6.88 (s, 6H), 6.81 – 6.70 (m, 2H), 6.65 (t, *J* = 7.3 Hz, 1H), 6.58 – 6.48 (m, 1H). ^{13}C NMR (100 MHz, $CDCl_3$) **δ** 142.0, 141.8, 141.2, 140.5, 140.4, 140.3, 140.1, 139.8, 139.7, 137.4, 132.9, 131.8, 131.7, 131.5, 131.1, 130.2, 129.4, 128.9, 127.7, 127.6, 127.3, 127.2, 127.1, 126.8, 126.8, 126.4, 126.1, 125.9, 125.8, 125.6, 125.5, 125.1, 124.9, 124.8, 124.1. HRMS (ESI); m/z calcd for $C_{44}H_{26}$ + H^+: 583.2348 [M+H^+]: Found 583.2427.

Synthesis of compound 7, 10- diphenyl-8-pyrenefluoranthene (FL2)

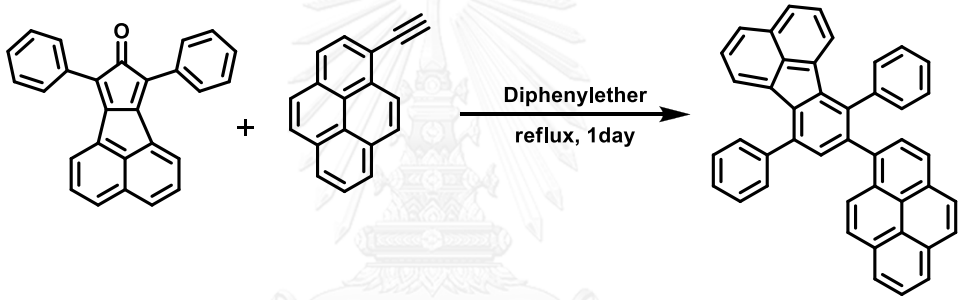

A solution of compound 3 (566 mg, 1.59 mmol) and 1-Ethynylpyrene (300 mg, 1.33 mmol) in 2 mL of diphenylether was refluxed for overnight under a nitrogen atmosphere. The dark-red mixture was diluted with dichloromethane (1 mL), poured in methanol (50 mL) and stirred; the off white precipitate was filtered and the compound was purified by column chromatography using ethyl acetate as an eluent to give compound **FL2**. The yield: 0.709 g, 96%. Characterization of compound: ^{1}H NMR (400 MHz, $CDCl_3$) **δ** 8.06 (dd, *J* = 7.9, 4.7 Hz, 3H), 7.91 (p, *J* = 8.8 Hz, 5H), 7.71 (dt, *J* = 12.6, 8.1 Hz, 5H), 7.52 – 7.38 (m, 4H), 7.38 – 7.31 (m, 3H), 7.22 (dd, *J* = 15.3, 7.3 Hz, 2H), 7.02 (dd, *J* = 16.4, 7.7 Hz, 2H), 6.87 (t, *J* = 7.3 Hz, 1H), 6.63 (d, *J* = 7.1 Hz, 1H). ^{13}C NMR (100 MHz, $CDCl_3$) **δ** 141.18, 140.21, 139.57, 138.79, 138.23, 138.04, 137.07, 136.99, 136.56, 133.65, 132.75, 131.83, 131.44, 130.64, 130.60, 130.31, 130.09, 129.70, 129.60, 129.11, 129.00, 128.82, 128.37, 128.31, 128.19, 128.09, 127.92, 127.62,

127.57, 127.53, 127.27, 127.23, 125.07, 124.29, 123.92, 123.60. . HRMS (ESI); m/z calcd for $C_{44}H_{26}$ + H^+: 555.2035 [M+H^+]: Found 555.2115.

2.3.4 Synthesis of hexaphenylbenzene derivatives containing imine moiety SW (2-6)

Synthesis of 5-iodosalicylaldehyde (1)

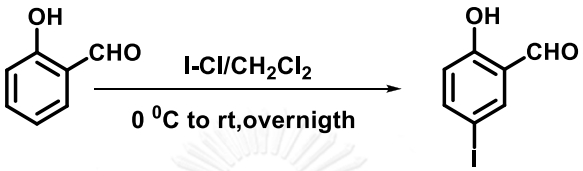

Salicylaldehyde (0.870 mL, 8.189 mmol) was dissolved in dichloromethane, and followed by addition of iodine-mono-chloride (0.692 mL, 13.228 mmol) at 0 ^{o}C to room temperature. The reaction mixture was left overnight. After the reaction was completed, the reaction mixture was extracted with CH_2Cl_2 and the organic solution was washed with $Na_2S_2O_3$, respectively. The organic layer was dried over anhydrous magnesium sulfate and solvent was removed by evaporator then recrystallized from hot hexane temperature to afford the white solid compound 1 (65%). ^{1}H NMR (400 MHz, $CDCl_3$) **δ** 10.95 (s, 1H), 9.83 (s, 1H), 7.85 (s, 1H), 7.77 (d, *J* = 8.5 Hz, 1H), 6.80 (d, *J* = 8.5 Hz, 1H). ^{13}C NMR (100MHz, $CDCl_3$) **δ** ppm 195.3, 161.3, 145.5, 142.0, 122.7, 120.1, 80.4.

Synthesis of 2-hydroxy-5-(phenylethynyl) benzaldehyde (2)

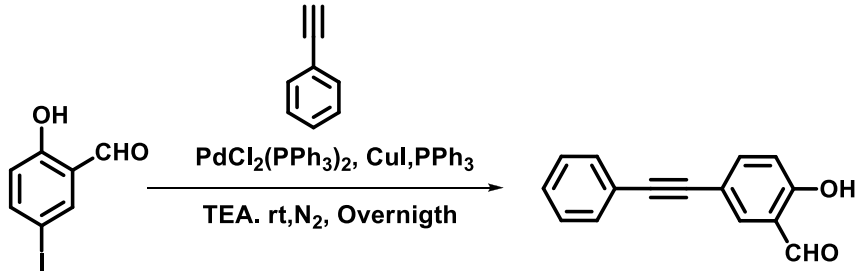

5-Iodosalicylaldehyde (1.80 g, 7.258 mmol) was mixed with $Pd(PPh_3)_2Cl_2$ (0.457g, 0.653 mmol), CuI (0.124 g, 0.653mmol) and PPh_3 (0.085 g, 0.326 mmol) in round bottom flask under N_2 atmosphere. After that, THF and TEA were added and kept stirred for 15 min. Then, phenylacetylene (2.38 mL, 21.77 mmol) was gradually added. The mixture was left overnight. The rotary evaporator was used to evaporate solvent from the mixture. The residue was purified by column chromatography on silica gel (10% EtOAc in hexane) to give compound 2 (79% yield). ^{1}H NMR (400 MHz, DMSO) δ (ppm) 11.17 (s, 1H), 10.25 (s, 1H), 7.78 (s, 1H), 7.65 (d, *J* = 8.5 Hz, 1H), 7.58 – 7.47 (m, 2H), 7.47 – 7.34 (m, 3H), 7.04 (d, *J* = 8.5 Hz, 1H).^{13}C NMR (100 MHz, $CDCl_3$) δ (ppm) 196.5, 162.8, 161.9, 140.3, 137.3, 132.0, 128.9, 123.4, 120.8, 118.3, 115.7, 89.7, 87.6.

Synthesis of compound SW1

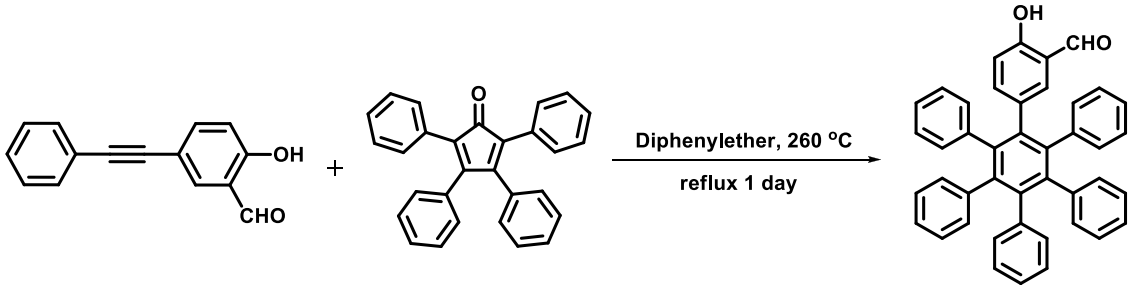

A solution of compound 2 (0.300 g, 1.34 mmol) and tetraphenylcyclopenta-2,4-dienone (0.468 g 0.218mmol) in 3 mL of diphenylether was refluxed for overnight under nitrogen atmosphere. The dark-brown mixture was diluted with dichloromethane (2 mL), poured in methanol (50 mL) and stirred; the off white precipitate was filtered and recrystallized from methanol to afford compound SW1 (51% yield). ^{1}H NMR (400 MHz, DMSO) **δ** (ppm) 10.29 (s, 1H), 9.89 (s, 1H), 7.09 (d, *J* = 1.8 Hz, 1H), 7.00 (d, *J* = 8.5 Hz, 1H), 6.95 – 6.72 (m, 25H), 6.45 (d, *J* = 8.5 Hz, 1H).^{13}C NMR (100 MHz, DMSO) **δ** (ppm) 191.13, 157.9, 140.1, 140.1, 139.9, 139.9, 138.7, 138.5, 131.6, 131.4, 130.8, 130.8, 130.7, 126.6, 126.4, 125.3, 125.2, 120.5, 115.5, 47.2.

Synthesis of compound SW2

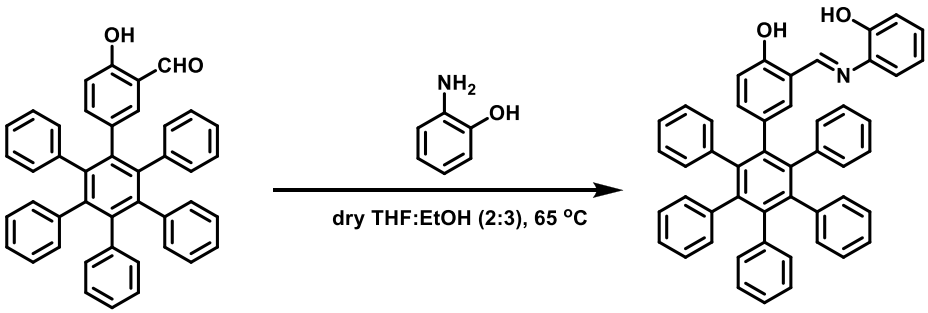

A clear solution of compound SW1 (0.100 g, 0.173 mmol) and 2-aminophenol (0.0283 g, 0.260 mmol) in dry THF: EtOH (2:3) was stirred at 65 °C. After 24 hrs, the reaction mixture turned turbid. The reaction mixture was concentrated under the reduced pressure and dry ethanol was poured into it, solid appeared. The solid was filtered and recrystallized from methanol to afford the light yellow solid compound SW2 (74% yield); ^{1}H NMR (400 MHz, DMSO) **δ** 13.36 (s, 1H), 9.67 (s, 1H), 8.53 (s, 1H), 7.18 (d, *J* = 7.7 Hz, 1H), 7.13 – 7.06 (m, 2H), 6.97 – 6.76 (m, 28H), 6.41 (d, *J* = 8.5 Hz, 1H). ^{13}C NMR (100MHz, DMSO) **δ** (ppm) 161.3, 158.1, 150.9, 140.3, 140.1, 140.0, 140.0, 139.0, 135.4, 134.8, 134.6, 130.9, 130.8, 130.7, 127.9, 126.6, 126.5, 126.4, 125.3, 125.2, 119.5, 119.4, 117.8, 116.5, 115.5, 114.9. HRMS (ESI); m/z calcd for $C_{49}H_{35}NO_2$ + H^+: 670.2668 [M+H^+]: Found 670.2740.

Synthesis of compound SW3

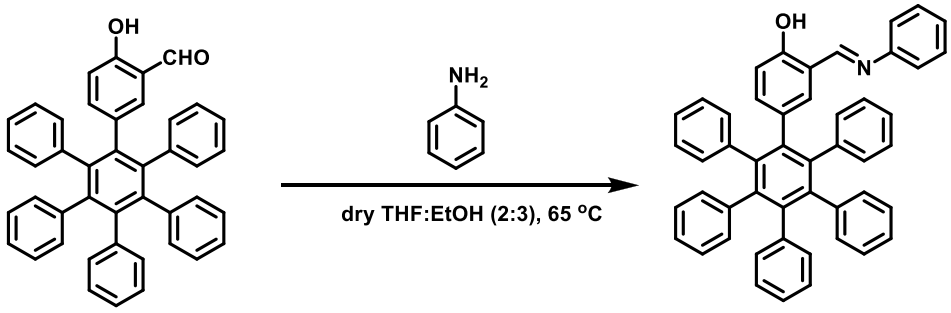

A clear solution of compound SW1 (0.100 g, 0.173 mmol) and aniline (0.0283 g, 0.260 mmol) in dry THF: EtOH (2:3) was stirred at 65 °C. After 24 hrs, the reaction mixture turned turbid. The reaction mixture was concentrated under the reduced pressure and dry ethanol was poured into it, solid appeared. The solid was filtered and recrystallized from methanol to afford the white solid compound SW3 (82% yield); ^{1}H NMR (400 MHz, DMSO) **δ** 12.71 (s, 1H), 8.51 (s, 1H), 7.41 (t, *J* = 6.9 Hz, 2H), 7.26 (d, *J* = 6.9 Hz, 2H), 7.08 (d, *J* = 11.7 Hz, 1H), 6.93 – 6.73 (m, 27H), 6.42 (d, *J* = 8.4 Hz, 1H).^{13}C NMR (101 MHz, DMSO) **δ** 163.3, 157.8, 148.1, 140.5, 140.2, 138.9, 135.9, 135.2, 131.0, 129.6, 126.8, 126.6, 125.5, 125.2, 121.3, 117.6, 114.9. HRMS (ESI); m/z calcd for $C_{49}H_{35}NO_2$ + H+: 654.2719 [$M+H^+$]: Found 654.2794.

Synthesis of compound SW4

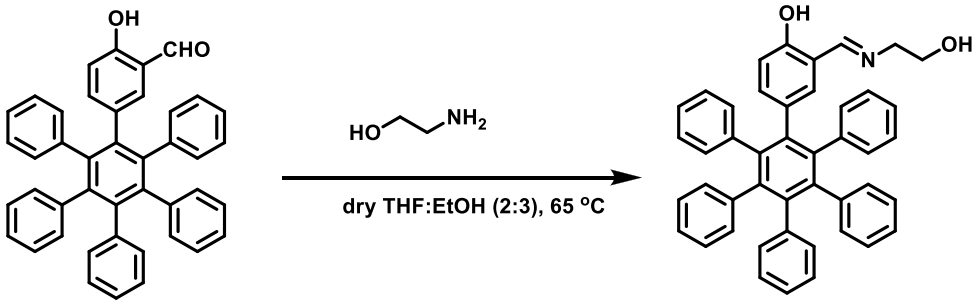

A clear solution of compound SW1 (0.100 g, 0.173 mmol) and 2-aminoethanol (0.0158 g, 0.260 mmol) in dry THF: EtOH (2:3) was stirred at 65 °C. After 24 hrs, the reaction mixture turned turbid. The reaction mixture was concentrated under the reduced pressure and dry ethanol was poured into it, solid appeared. The solid was filtered and recrystallized from methanol to afford the light yellow solid compound SW4 (89% yield); ^{1}H NMR (400 MHz, DMSO) **δ** (ppm) 13.26 (s, 1H), 8.10 (s, 1H), 6.99 – 6.73 (m, 27H), 6.31 (d, *J* = 8.6 Hz, 1H), 4.70 (d, *J* = 4.9 Hz, 1H), 3.54 (t, *J* = 4.5, 2H), 3.50 (t, *J* = 4.5 Hz, 2H). ^{13}C NMR (100 MHz, DMSO) **δ** (ppm) 165.7, 158.3, 140.3, 140.1, 140.1, 139.9, 139.9, 139.1, 134.7, 133.8, 130.8, 130.2, 126.5, 126.4, 125.3, 125.3, 116.9, 114.8, 60.8, 60.5. HRMS (ESI); m/z calcd for $C_{45}H_{35}NO_2$ + H^+: 622.2668 [M+H^+]: Found 622.2745.

Synthesis of compound SW5

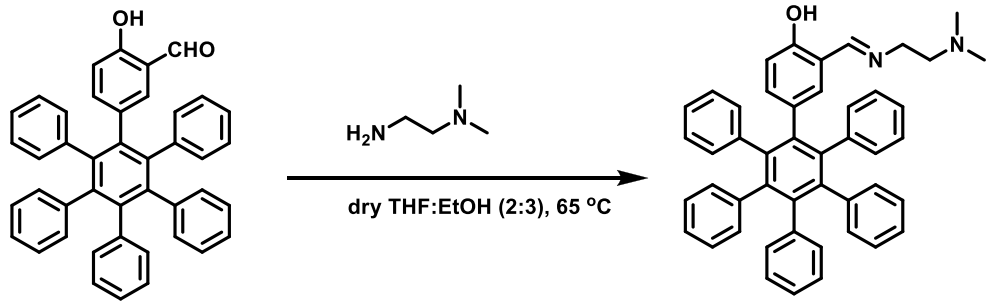

A clear solution of compound SW1 (300 mg, 0.518 mmol) and *N,N*-dimethyl-ethylene-di-amine (68.5 mg, 0.777 mmol) in dry THF: EtOH (2:3) was stirred at 65 °C. After 24 hrs, the reaction mixture turned turbid. The reaction mixture was concentrated under the reduced pressure and dry ethanol was poured into it, solid appeared. The solid was filtered and recrystallized from methanol to afford the light yellow solid compound SW5 (79% yield); ^{1}H NMR (400 MHz, $CDCl_3$) **δ** 13.14 (s, 1H), 7.91 (s, 1H), 6.94 – 6.77 (m, 25H), 6.74 (dd, *J* = 8.5, 2.1 Hz, 1H), 6.65 (d, *J* = 2.1 Hz, 1H), 6.45 (d, *J* = 8.5 Hz, 1H), 3.58 (t, *J* = 6.9 Hz, 2H), 2.56 (t, *J* = 6.9 Hz, 2H), 2.26 (s, 6H).^{13}C NMR (100 MHz, $CDCl_3$) **δ** 165.31, 158.61, 140.78, 140.61, 140.52, 139.37, 135.58, 134.33, 131.55, 131.15, 126.99, 126.88, 126.72, 125.42, 125.35, 118.05, 115.66, 59.98, 57.33, 45.94. HRMS (ESI); m/z calcd for $C_{47}H_{40}NO_2$ + H^+: 649.3141 [M+H^+]: Found 649.3218.

Synthesis of compound SW6

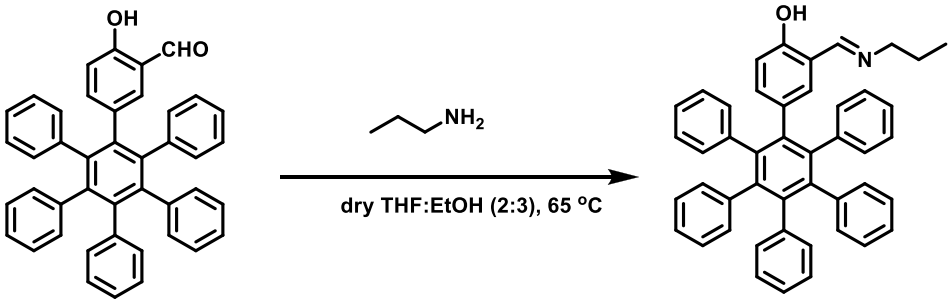

A clear solution of compound SW1 (0.150g, 0.259mmol) and propan-1-amine (0.023g, 0.388mmol) in dry THF: EtOH (2:3) was stirred at 65 °C. After 24 hrs, the reaction mixture turned turbid. The reaction mixture was concentrated under the reduced pressure and dry ethanol was poured into it, solid appeared. The solid was filtered and recrystallized from methanol to afford the light yellow solid compound SW6 (88% yield); ^{1}H NMR (400 MHz, $CDCl_3$) δ (ppm) 7.78 (s, 1H), 6.76 (s, 26H), 6.66 (d, *J* = 8.6 Hz, 1H), 6.54 (s, 1H), 6.36 (d, *J* = 8.0 Hz, 1H), 3.33 (d, *J* = 5.8 Hz, 1H), 1.13 (d, *J* = 6.2 Hz, 6H).^{13}C NMR (100MHz, $CDCl_3$) δ (ppm) 161.9, 140.6, 140.4, 140.3, 139.2, 134.1, 131.3, 126.9, 126.7, 126.6, 125.2, 125.2, 24.0. HRMS (ESI); m/z calcd for $C_{46}H_{37}NO + H^+$: 620.2875 [$M+H^+$]: Found 620.2958.

2.3 Photophysical property study

The stock solution of **SW5** that concentration is 400 μM was prepared by dissolving in THF 50 ml. The stock solutions of other flurophores are prepared by the same condition.

2.4 UV-Visible spectroscopy

The each of stock solutions is diluted to 10 μM in THF. The UV-Visible absorption spectra were recorded from 400 nm to 700 nm at room temperature.

2.5 Fluorescence spectroscopy

The emission spectra of flurophores which were diluted from THF solution were recorded from 300 nm to 700 nm at room temperature using an excitation wavelength at 280 for substituent **HPB**, 346 nm for **FL(1-2)**, 280 nm for **SW (2,3,4,6)**, 290 nm for **SW5**, respectively.

2.6 Effect of water content

The stock solutions are diluted into 20 μM by varied water content between 10% - 90% water in THF. The UV-Visible absorption spectra were recorded from 200 nm to 700 nm at room temperature and the emission spectra of flurophores were recorded from 300 nm to 700 nm at room temperature using an excitation wavelength at 280 nm for **SW (2, 3, 4** and **6)**, 290 nm for **SW5**, respectively.

2.7 Fluorescence sensor study

2.7.1 Nitroaromatic compounds sensor

Stock solution nitroaromatic compound were prepared in Milli-Q water. Concentrations of all stock nitroaromatic compound solutions were adjusted to 1000 μM and were added with desired volumes (1000 μL) to the flurophore solutions.

2.8.2 Cations sensor

The excitation wavelength was 280 nm for **SW (2, 3, 4** and **6)**, 290 nm for **SW5**, respectively and the emission was recorded from 300-700 nm. Cations solutions were prepared in Milli-Q water. Concentrations of all stock sodium Cation solutions were adjusted to 2mM and were added with desired volumes (10 μL) to the flurophore solutions.

CHAPTER III
RESULTS AND DISCUSSION

3.1 Synthesis and characterization of substituent hexaphenylbenzene derivatives

Even though hexaphenylbenzene (HPB) derivatives has been synthesized and used in many sensor applications [23-25, 29], the relationship between substituents on the benzene ring in HPB and AIE behavior has not been explored. Therefore in this part, we will prepare a variety of HPB carrying different substituents and study their AIE property.

3.1.1 Synthesis of substituent hexaphenylbenzene (HPB) derivatives

Initially, we planned to synthesize four different HPB derivatives containing chloro, methyl and methoxy and naphthalene group as seen in **scheme 3.1.** The iodobenzenes (**1a-1d**) reacted with calcium carbide in the presence of $Pd(OAc)_2$ by means of Sonogashira coupling reaction under developed method from our research group [36] to produce the corresponding diarylethynes (**2a-2d**) in 25-91% yields. Then **[4+2]** cycloaddition between diarylethynes (**2a-2d**) and 2, 3, 4, 5-tetraphenyl-2,4- cyclopentadien-1-one (**3**) gave rise to the formation target HPB include **HPB-2Me**, **HPB-2OMe**, **HPB-2Cl** and **HPB-2NAP** in good yields (13-42%) as depicted in **Scheme 3.1.**

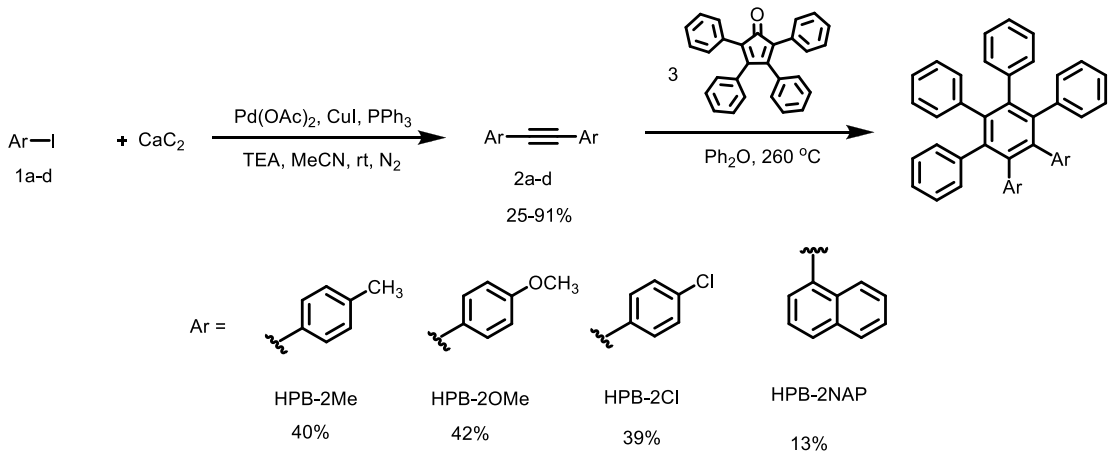

Scheme 3.1 Synthetic route to compound **HPB-2Me**, **HPB-2OMe**, **HPB-2Cl** and **HPB-2NAP**

3.1.2 NMR Characterization

All prepared HPBs were characterized by NMR spectroscopy. The ^{1}H NMR spectra of diaryethyne derivatives (**2a-2d**) are represented in **Figure 3.1.1.** All signals were assigned to all protons in each corresponding compound structure and matched with previous report [36]. Moreover, the ^{1}H NMR spectra of **HPB-2Me**, **HPB-2OMe**, **HPB-2Cl** and **HPB-2NAP** are represented in **Figure 3.1.2.** All signals were assigned to all protons in each corresponding compound structure. As evidence of **HPB** moiety, the multiplet groups of aromatic protons belonging to unsubstituted benzene moiety displayed at around 7.00-6.40 ppm for all prepared HPB. For ^{1}H NMR of **HPB-2Me and HPB-2OMe,** the proton on substituted benzenes (a) average shift up field as seen in **Figure 3.1.2a** and **b** while the proton on substituted benzenes on **HPB-2Cl** maintain the same chemical shift in comparison with their starting diarylethynes. In case of **HPB-2NAP** spectrum, it is more complicated and we observed two set of naphthalene signal (a, b, c, d, e, f and g) ring. This is caused by the restrict rotation two naphthalene ring resulting in the formation of atropisomerism [37].

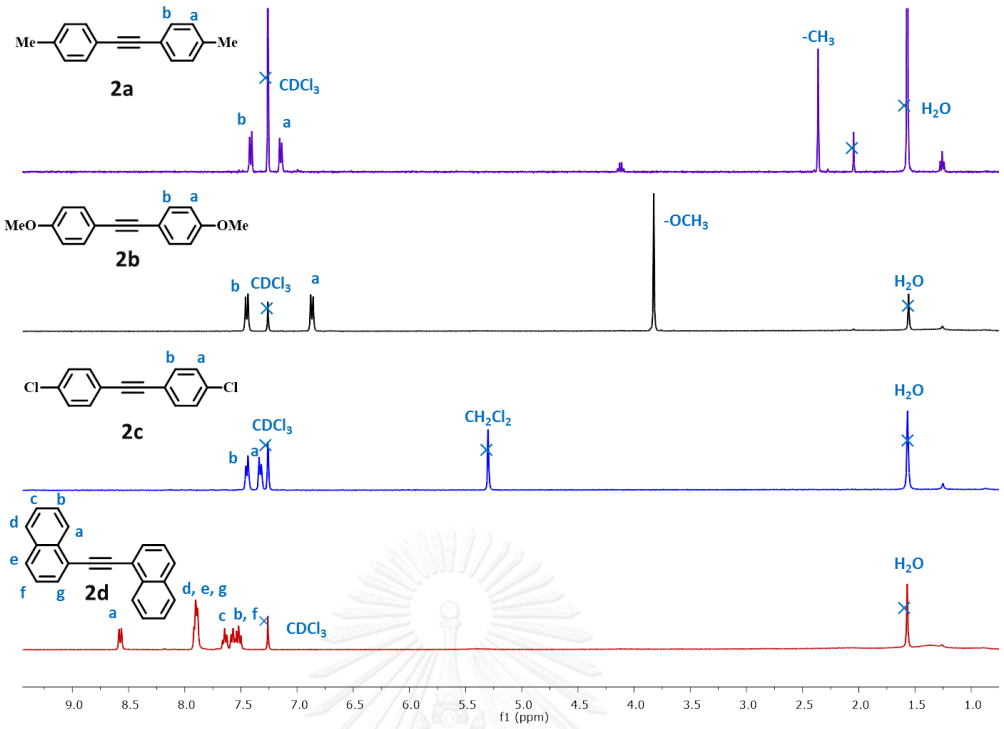

Figure 3.1.1 ^{1}H NMR (400) MHz of diarylethynes (**2a-2d**) derivatives

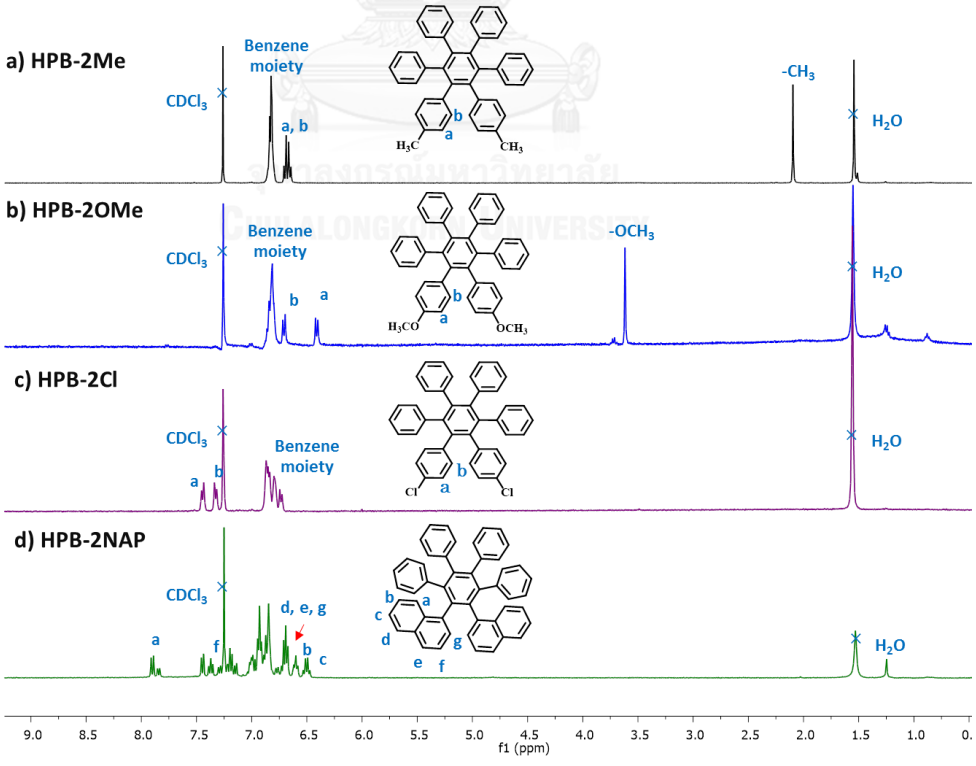

Figure 3.1.2 ^{1}H NMR (400) MHz of hexaphenylbenzene derivative compounds

3.1.3 Water fraction effect on photophysical properties

3.1.3.1 Absorption properties

The UV-vis spectra of **HPB-2Me**, **HPB-2OMe**, **HPB-2Cl** and **HPB-2NAP** in THF exhibited two-peak absorption bands at 240-250 and 280-295 nm (**Figure 3.1.3)**. Upon increase of water fraction in THF solution, the tail of UV-vis spectra of all HPB increased. This phenomenon is known as "leveling-off tail". This behavior suggests the formation of nanoparticle suspensions[38], confirming the existence of aggregates at 70%water contents.

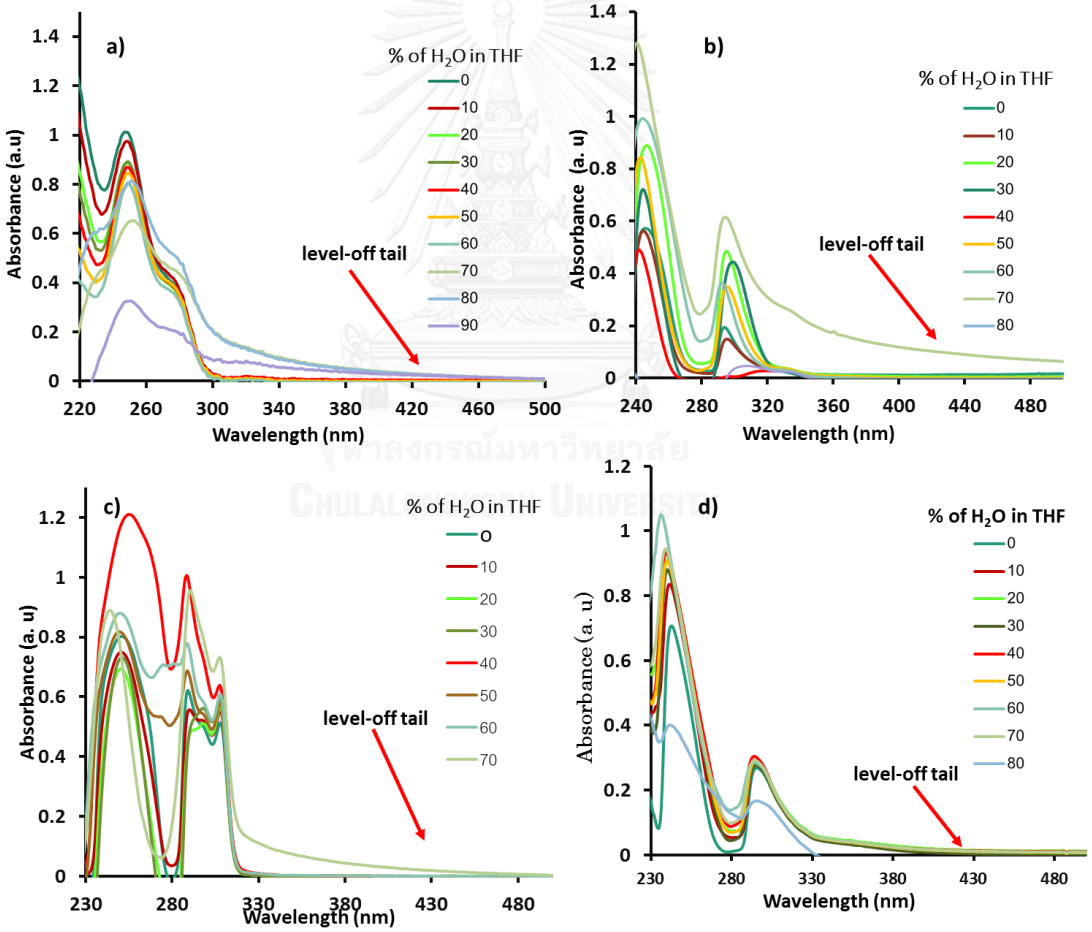

Figure 3.1.3 UV–Vis spectra of a) **HPB-2Me**, **b**) **HPB-2OMe**, c) **HPB-2Cl** and d) **HPB-2NAP** (50 μM) in H_2O/THF mixture (0–90% volume fraction of water in THF)

3.1.3.2 Fluorescence properties

Next, the fluorescence of **HPB-2Me, HPB-2OMe, HPB-2Cl** and **HPB-2NAP** in different water fraction in THF solution was further investigated **(Figure 3.1.4**.). **HPB-2Me**, **HPB-2OMe** and **HPB-2NAP** shows emission peak at 340, 368 and 373 nm respectively, in THF solution as shown in **Figure 3.1.4a**, **b** and **d** addition of water into the THF solution resulted in the fluorescence enhancement and when water content reach 70%, the fluorescence intensity decreased. This observation can be explained that in 0-70% water fraction, the HPB undergo aggregation resulting in restrict intramolecular rotation (RIR) process. Such process will suppress the non radiative decay and increase the fluorescence signal. However, when the water fraction is higher than 70%, the solubility of **HPB-2Me**, **HPB-2OMe** and **HPB-2NAP** in the solvent mixture is relatively low and the number of emissive molecules per unit volume is decreased. The fluorescence enhancement due to the restriction-in-rotation process could not contend with the decreasing trend in the intensity caused by the smaller number of emitting molecules. Hence, fluorescence intensity in this case is decreased [1]. In case of **HPB-2Cl**, changes in the fluorescence intensities versus water fraction of the mixture were plotted, as shown in **Figure 3.1.4c**. When the water fraction was increased from 0% to 90%, there was no change in fluorescence intensities along with red shift from 335 to 360 nm. In order to see the effect of water more clearly, we constructed the plot between fluorescence enhancement ratio of HPB before and after addition of water again such water fraction as presented **Figure 3.1.5.** With this plot, it allow us to compare fluorescence intensities between HPB in aggregation state (60:40 water/THF) and in solution state (100% THF) as shown in red line in **Figure 3.1.5. HPB-2Me**, **HPB-2OMe** and **HPB-2NAP** displayed fluorescence enhancement at 1.60, 3.05 and 1.53 folds respectively. On the other hand the fluorescence enhancement ratio of **HPB-2Cl**

maintained at ca. 1. We hypothesized that the low emission of **HPB-2Cl** is cause by the **ICT** from donor core benzene into chlorobenzenes acceptor. When increased of water fraction to **HPB-2Cl** solution, the greater **ICT** effect was observed. This is caused by the ability to stabilize excited state from water as polar solvent. Even though **HPB-2Me**, **HPB-2OMe** and **HPB-2NAP** served as good **AIE** molecules showing ability on induced fluorescence intensity on aggregation state, their emission intensities are relatively low and maximum emission wavelengths fall in range between 300-380 nm which is a nonvisible region. Therefore, in order to turn **HPB** molecules into naked eyes fluorescence chemosensor, we planned to increase **π**-conjugation system or incorporate hetero atoms into **HPB** system in the hope that they can emit fluorescence light in longer wavelength with higher intensity. The strategy and detail will be further discussed in the next two sections.

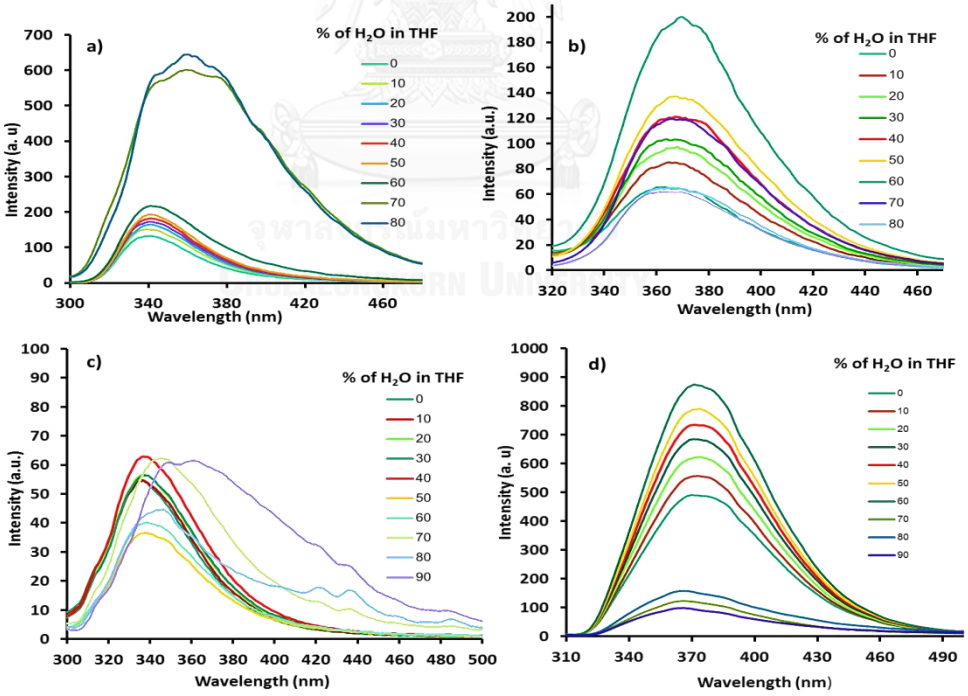

Figure 3.1.4 Fluorescence spectra of a) **HPB-2Me**, b) **HPB-2OMe**, c) **HPB-2Cl**, d) **HPB-2NAP** (50 μM) in H_2O/THF mixture (0–90% volume fraction of water in THF) when excited at 280 nm

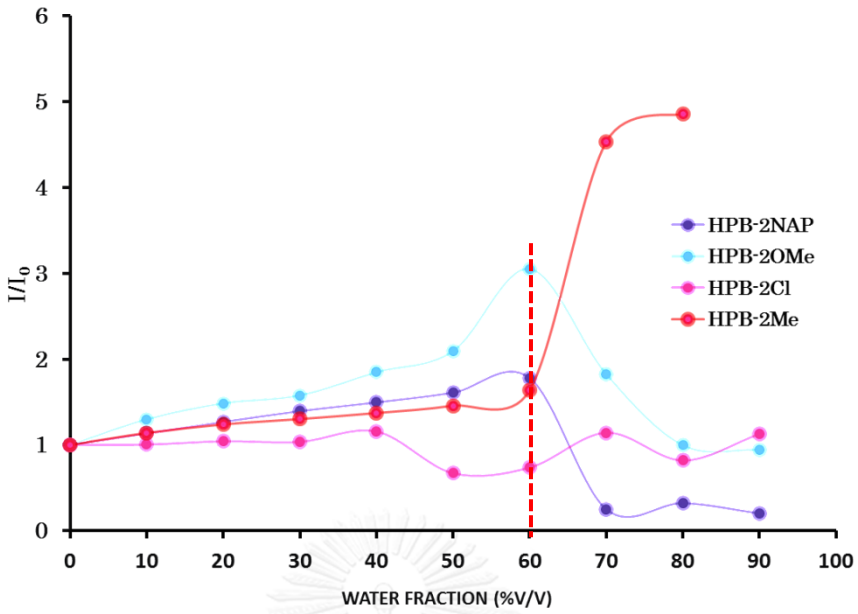

Figure 3.1.5 Plots of emission intensity VS the composition of the aqueous mixture of **HPB-2Me (λ_{em} 336 nm)**, **HPB-2OMe (λ_{em} 370 nm)**, **HPB-2Cl (λ_{em} 340 nm)** and **HPB-2NA (λ_{em} 366 nm)** (50 μM) when excited at 280 nm

3.2 Synthesis and characterization of oligophenylene-based pyrene derivatives (FL1 and FL2) and their application in metal sensing.

3.2.1 Synthesis of oligophenylene based pyrene derivatives (FL1 and FL2)

The synthesis of **FL1** and **FL2** was outlined in scheme 3.2.1. The [**4+2**] cycloaddition reaction between 1-ethynylpyrene (**5**) and tetraphenylcyclopentadienone (4) in diphenylether furnished compound **FL1** in 86% yield in **scheme 3.2.** To synthesize **FL2**, we began with the condensation reaction between dione (**1**) and ketone (**2**) generating the intermediate 7,9-diphenyl-8H-cyclopenta[l]acenaphthylen-8-one (**3**) in 96% yield. Then heating 1-ethynylpyrene (**5**) with cyclopentadienenone (**3**) gave rise to the formation of target **FL2** in excellent yield (**scheme 3.2**).

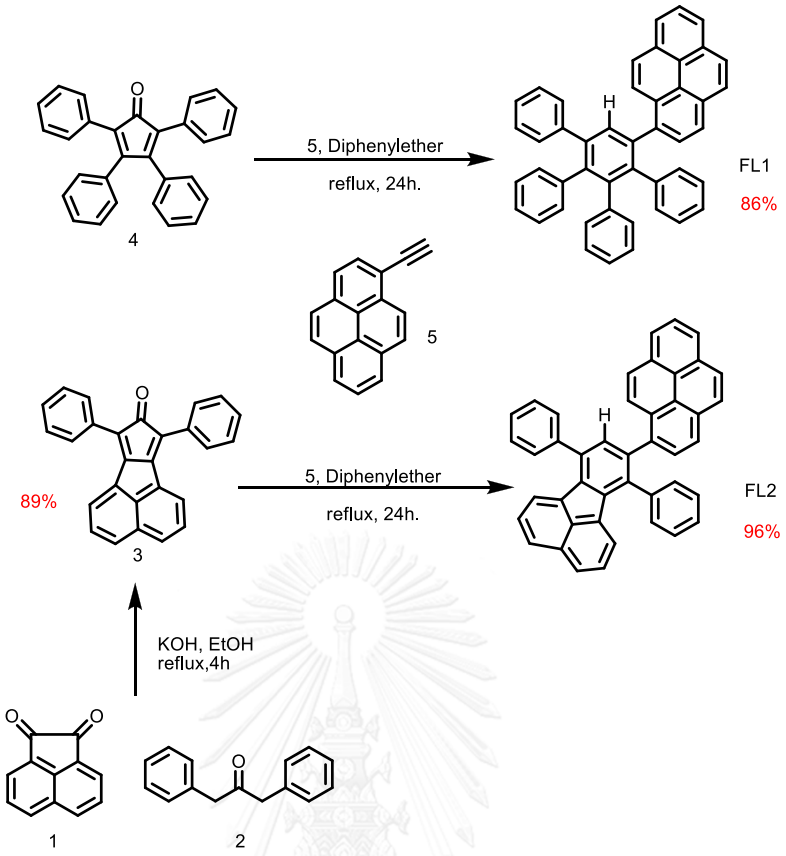

Scheme 3.2 Synthetic route to compound **FL1** and **FL2**

The structures of compounds **FL1** and **FL2** were confirmed from their NMR spectroscopy and HRMS data as shown in **Figure 3.2.1** and **Figure S.17.** The ^{1}H NMR spectra of compound **FL1** showed proton resonances in benzene substituent (k-p) in **δ** between 7.65–6.50 ppm with a singlet peak at 7.65 ppm belonging to signal of hydrogen (H_j) of core benzene. Also, pyrene moiety (a-i) corresponds to peaks in the range between **δ** 8.3-7.7 ppm. In case of compounds **FL2**, It was assigned in according to the similar compound reported by *M. L. Keshtova and co-worker* [39]. In addition, molecular weights of both compounds were matched with the HRMS data **Figure S.17.**

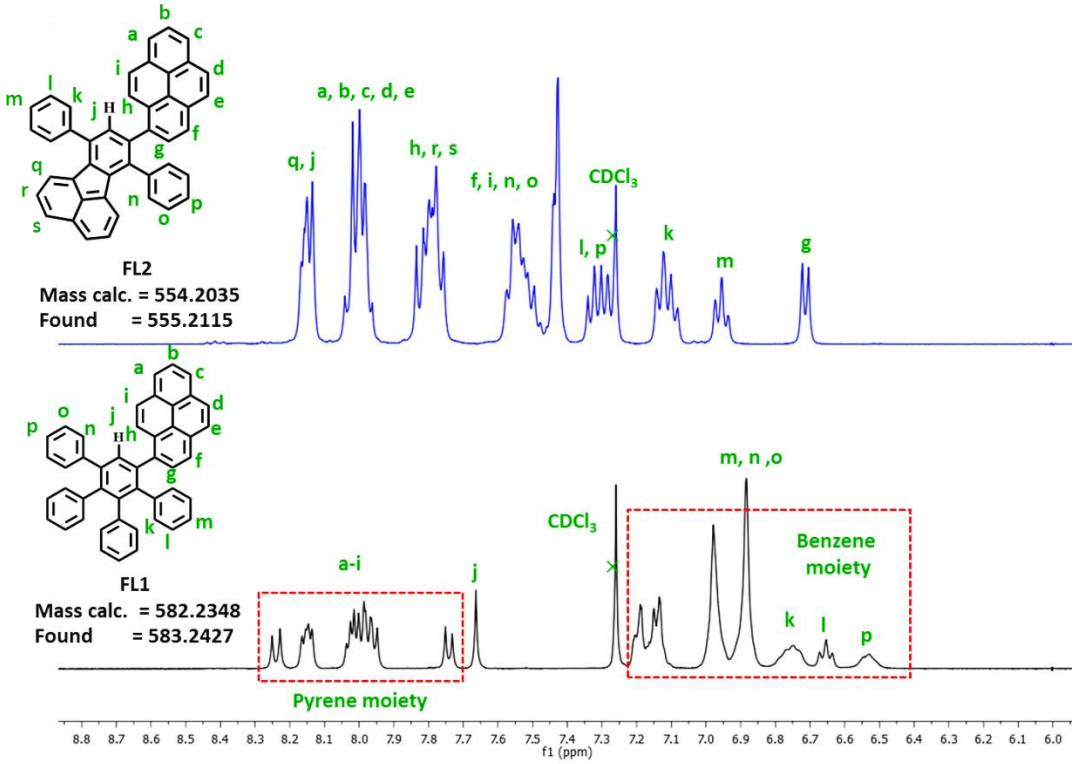

Figure 3.2.1 ^{1}H NMR (400) MHz of **FL1** and **FL2** in $CDCl_3$

3.2.2 Water fraction effect on photophysical properties

The fluorescence intensity of compounds **FL1** and **FL2** were measured in various ratios of mixed solvent of THF and water. In case of **FL1** in pure THF solution, it exhibited weak absorption bands at 249 nm, 282 nm and 346nm as seen in **figure 3.2.2a** as well as showed weak emission peaks at 382 and 402 nm when excited at 346 nm as seen in **figure 3.2.2b**. With the increase of water content up to 60% (volume fraction), the intensity of entire absorption spectra gradually increased with the appearance of a level-off long wavelength tail in the visible region 400–500 nm as shown in **Figure 3.2.2a**, which is attributed to the Mie scattering due to formation of nanoaggregates [38]. As expected, the fluorescence intensity also strongly increased upon the increase of water content up to 60% as depicted in fluorescence spectrum in **Figure 3.2.2b** and the plot of water fraction VS maximum emission in

Figure 3.2.3. We also observed the change in quantum efficiency (Φ) from 47 to 99% when water content increases from 0 to 60% showing a strong blue emissive solution under black light (**Figure 3.2.3inset**). This suggested that compound **FL1** possess aggregation induced emission (AIE) behavior and also observable by naked eyes.

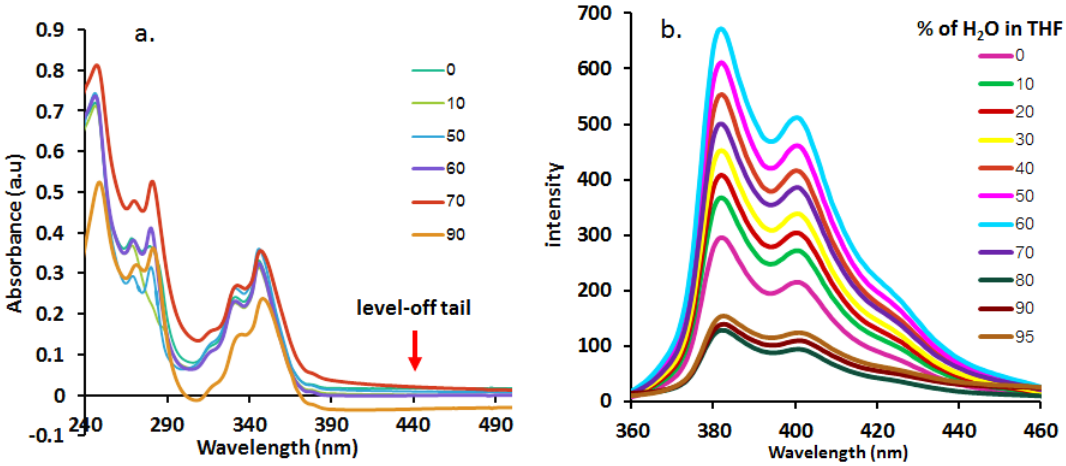

Figure 3.2.2 a) Absorption and b) fluorescence emission spectra of **FL1** (0.5 μM) when excited at 346 nm in variable H_2O/THF

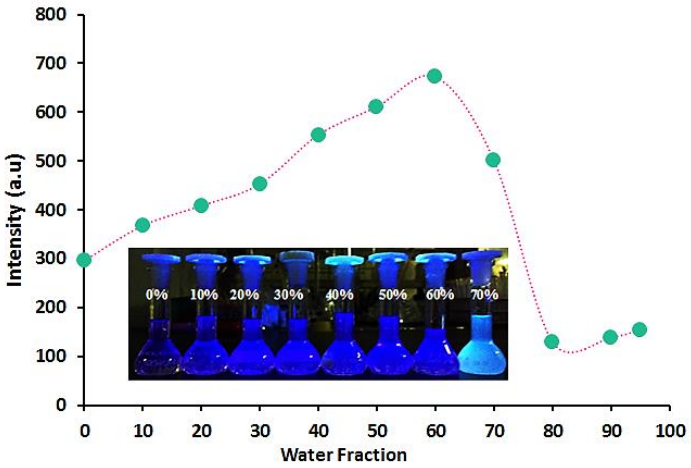

Figure 3.2.3 Fluorescence responses of **FL1** (0.5 μM) in variable H_2O/THF at 382 nm Inset: Fluorescence photographs of compound **FL1** (100 μM) in variable H_2O/THF

On the other hand, the compound **FL2** showed no significant fluorescence enhancement when the amount of H_2O of compound **FL2** was added gradually as seen in **Figure 3.2.4.** This is because its structure has more rigidity from fluoranthene moiety which resulted in restricted rotation even in nonaggregates state leading to the strong fluorescence intensity in pure THF [40].

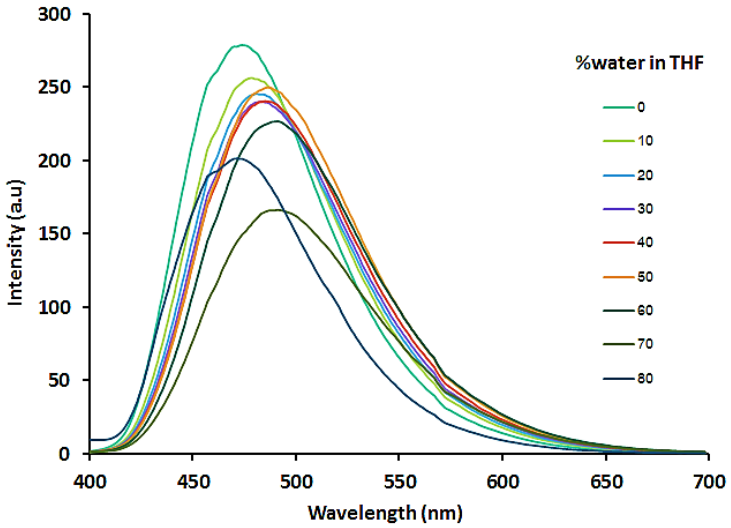

Figure 3.2.4 Fluorescence emission spectra of **FL2** (2 μM) in variable H_2O/THF when excited at 346 nm

This clearly justifies the role of two benzene moiety emergence of AIE phenomenon and we believe that intramolecular rotations of compound **FL1** in aqueous media are restricted by the formation of aggregates that block the non-radiative channels and populate the radiative excitons[1].That makes the molecule emit in the aggregate state. In an effort to further understand the mechanism operating in this AIE system, we checked the geometries and packing arrangements of **FL1** in the crystal state by recrystallization by CH_3OH and CH_2Cl_2 (1:1v/v). Based on X-ray data, the packing models of crystals of **FL1** are resembled to anchors (**Figure 3.2.5.**). The planar aromatic rings are situated between two pyrene units, which efficiently hampers their **π–π** interactions and allow excimer formation. The pyrene

units are also sandwiched between two planar units. This formation indicated rigidify in molecule which lock the molecular rotation. As a result, the excited state energy consumed by the restriction of intramolecular rotation process is greatly reduced, which enables the molecule to emit intensely in the aggregates state. Of this result, the **FL1** molecule may assume to be in non-emissive state in high water fraction (> 60%). This enhances the **π–π** stacking interactions of the planar pyrene units causing vivid precipitation and hence leads to red-shift and decrease fluorescence intensity.

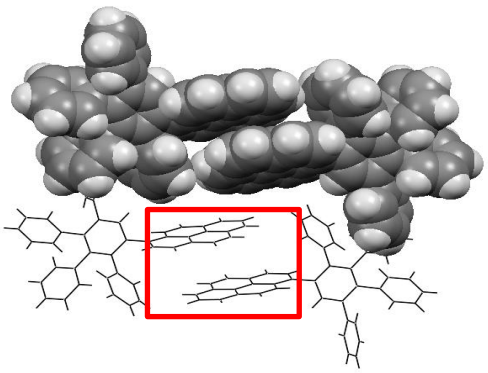

Figure 3.2.5 The packing models crystal of compound **FL1** from X-ray data

3.2.3 Nitroaromatic compounds sensing

It is well known that the poly aromatic compounds which has electron rich property can undergo the electron transfer process with electron poor species such as nitro aromatic compounds (NACs) causing fluorescence quenching property[41-43]. Therefor we selected the compound **FL1** in the aggregates state which has the strong quantum efficiency as a flurophore for NACs detection. We studied fluorescence response of compound **FL1** in H_2O/THF (60:40, v/v) which has the maximum emission intensity toward different NACs such as 2,4,6-trinitrotoluene(TNT), 2,4-dinitrotoluene (2,4 DNT), picric acid (PA), 1,4-dinitrobenzoic acid (DNBA), benzoquinone (BQ), 3-nitrophenol (3NP), 4-nitrophenol (4NP), 4-nitrotoluene (4NT),

(2CB). Upon the treatment of NACs at 100 μM concentration, there are several NACs that can quench the fluorescence emission of compound **FL1** including 2,4-DNT, PA, 3-NP and 4-NP as seen in **Figure 3.2.6a**. Upon the addition of PA, it showed quenching ratio of (I_0/I)-1 39 folds while 2,4-DNT, 3-NP and 4-NP have lower quenching efficiency and less than 5 folds of quenching ratio (I_0/I)-1 (**Figure 3.2.6b**).

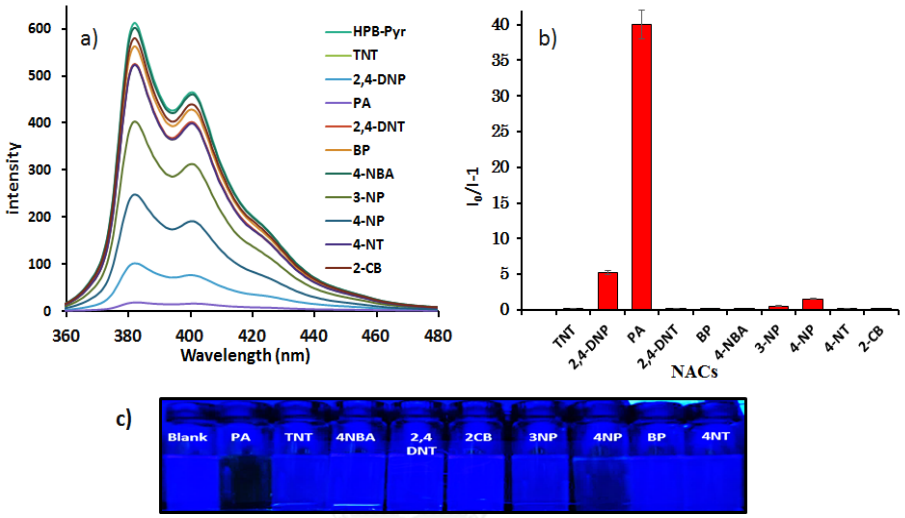

Figure 3.2.6 a) Fluorescence spectra b) ratio of fluorescence intensity c) photograph under illumination of a UV lamp of **FL1** (0.5 μM) in absence and presence of different nitroaromatic compounds in 6:4 (v/v) H_2O/THF at λ_{ex} = 346 nm

3.2.4 Stern-Volmer plot

In order to determine the sensitivity of compound **FL1** for PA detection, the fluorescent signals of fixed concentration of compound **FL1** solution with various concentrations of PA were measured as seen in **Figure 3.2.7a.** Then the plot between I_0/I and the concentration of PA were plotted and slope was corresponded to the Stern-Volmer constants (K_{sv}) as equation:

$$I_0/I = 1 + K_{sv}[PA]$$

The Stern–Volmer plots of compound **FL1** are linear and give quenching constants (K_{sv}) of 4.845 × 10^4 M^{-1}(**Figure 3.2.7b**). Moreover, the detection limit was found to be 0.88 μM calculated by 3**σ**/K when K is a slope of linear equation [44].

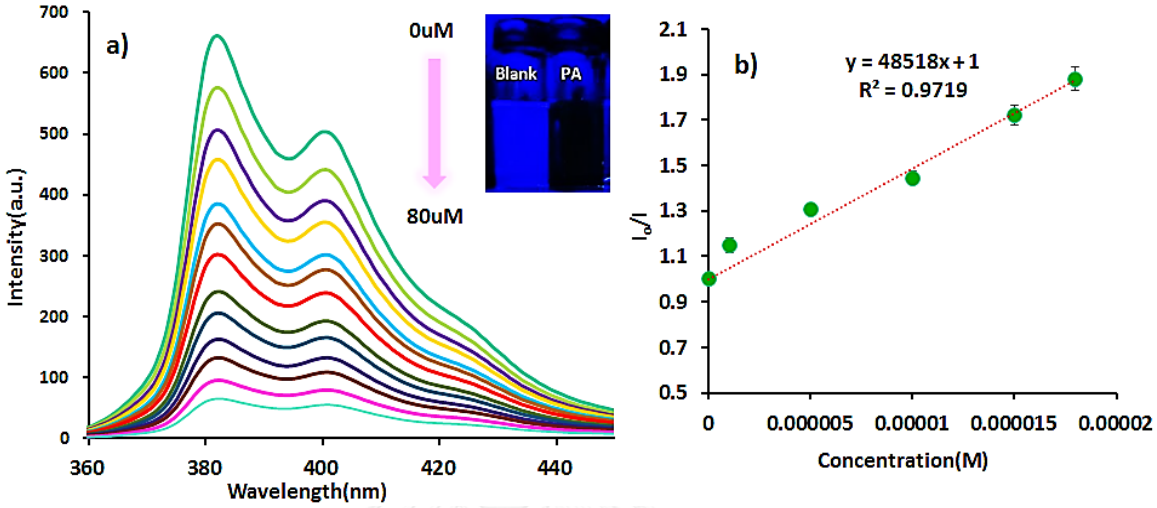

Figure 3.2.7 a) Change in the fluorescence of **FL1** (0.5 μM) upon the addition of PA (80 μM) in H_2O/THF, (60:40); **λ**ex = 346 nm. Inset: difference in the fluorescence of **FL1** before and after the addition of PA b) Stern–Volmer plot of the percent quenching of **FL1** versus the concentration of PA (M)

3.2.5 Proposed quenching mode for detection of PA using compound FL1

The possible quenching mechanism in this case could be 1) energy transfer[45] 2) charge transfer [29] and 3) competitive absorption process [46] between donor and acceptor molecules. To gain more insight of quenching mechanism, we therefore plotted the absorption of PA and the emission of compound **FL1** showing significant overlaps as seen in red region in **Figure 3.2.8a**. These observations indicate that the main quenching mechanism for PA is energy transfer between the emissions of compound **FL1** to absorption of PA. In addition, when plotted the absorption of PA and compound **FL1**, it displays overlaps between two spectra between 250-370 nm as seen in red region in **Figure 3.2.8b**.Therefore it

is possible that in high concentration of PA, the competitive between two probes might occur. We conclude that detection PA by compound **FL1** is governed by two mechanisms including energy transfer process and competitive absorption.

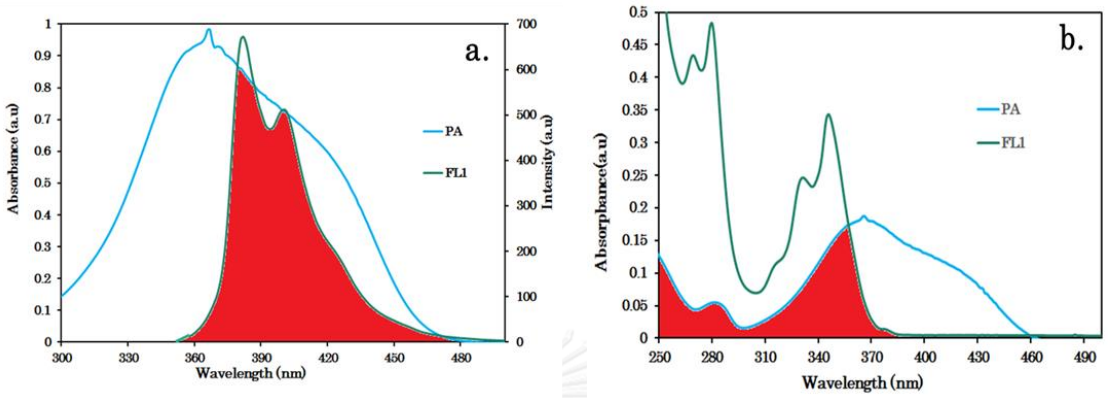

Figure 3.2.8 a) Normalized overlay plot of a) absorption of PA vs. emission of **FL1** b) absorption of PA vs. **FL1**

3.3 Synthesis and characterization of hexaphenylbenzene derivatives containing imine moiety SW (2-6) and their application in metal sensing.

3.3.1 Synthesized of hexaphenylbenzene derivatives containing imine moiety SW2-6.

Our sensors **SW2-6** were designed to possess hexaphenylbenzene (HPB) as flurophore and imine moiety as receptor for metal ion as depicted in **Scheme 3.3.** Initially, **SW1** was obtained from [4+2] cycloaddition reaction between tetraphenylcyclopenta-2,4-dienone (**3**) and diphenylacetylene (**2**) in 51% yield as a white solid after recrystallization from methanol. The biphenyl acetylene (**2**) was obtained from iodination of salicylaldehyde (**1**) followed by Sonogashira coupling reaction with phenylacetylene in 79% yield. Then the targets **SW2-6** were synthesized in excellent yields from **SW1** via the imine formation with the

corresponding amines such as 2-aminophenol, aniline, 2-aminoethanol, *N*, *N*-dimethylethylenediamine and *n*-propylamine respectively.

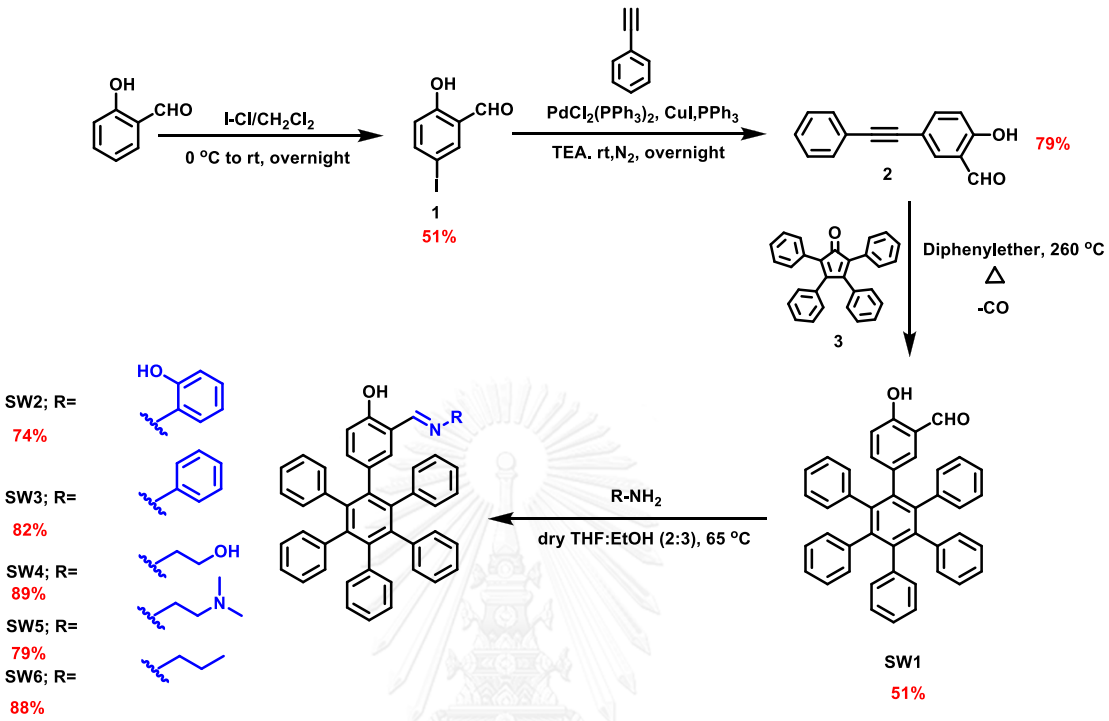

Scheme 3.3 Synthesis of **SW2-6**

3.3.2 Characterization

The ^{1}H NMR spectra of **SW1** and **SW2-6** are presented in **Figure 3.3.1.** All signals were assigned to all protons in each corresponding compound structure. As the starting substrate, **SW1** possesses singlet signal at 10.31 and 9.91 corresponding to its phenolic proton and aldehyde proton respectively. As evidence of HPB moiety in **SW1**, the multiplet group of aromatic protons can be seen at around 6.5-7.0 ppm. For ^{1}H NMR of **SW2-6**, the phenolic proton shifted toward downfield while the aldehyde peak at 9.43 ppm disappeared. Moreover, new peaks in **SW2-6** appeared at 8.53, 8.53, 8.12, 7.91 and 7.86 ppm, respectively. Those peaks can be assigned as the imine proton suggesting that the imine formation is successful. In addition, molecular weights of all synthesized compounds were confirmed by HRMS as seen in **Figure S.32**.

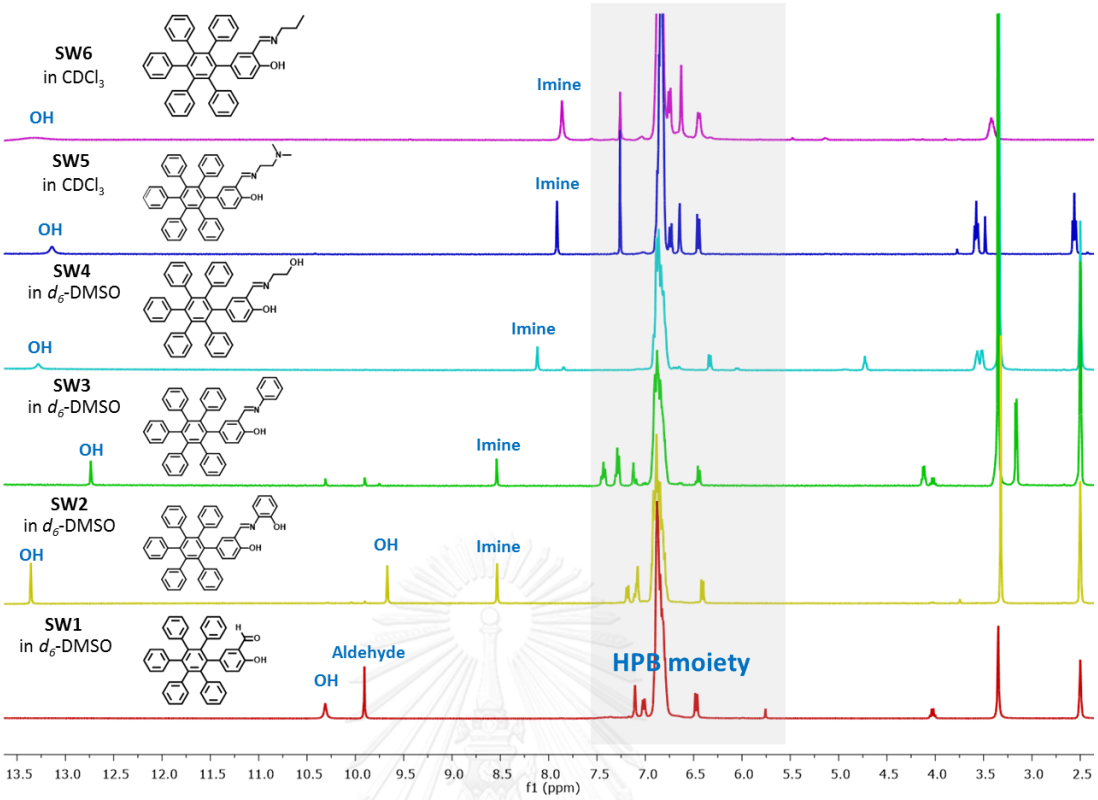

Figure 3.3.1 ^{1}H NMR (400) MHz of **SW (1-6)**

3.3.3 Photophysical properties studies

The photophysical properties of **SW2-6** were investigated by the spectrofluorometer and UV-Vis spectrophotometer (**Table 3.1**). **SW2-6** exhibited the wavelength of maximum absorbance (λ_{max}) around 250 nm with the two shoulder peaks at 280 and 330 nm (**Figure 3.3.2a**). Molar extinction coefficient (ε) of prepared compounds was found at between 5,110 and 10,529 $M^{-1}cm^{-1}$. When excited 280 nm, SW2 emitted 366 nm while SW3-SW6 showed red shift emission band at 459-470 nm as seen in **Figure 3.3.2a**

Table 3.1 Photophysical properties of **SW 2-6** in THF [a]

Compounds	Absorption		Emission
	λ_{max} (nm)	ε (M/cm^{-1})	λ_{max} (nm)
SW2	280	5,110	366
SW3	280	-	459
SW4	280	17,148	470
SW5	290	10,529	460
SW6	280	5,726	460

[a] 20 μM of **SW2-6** in THF was used.

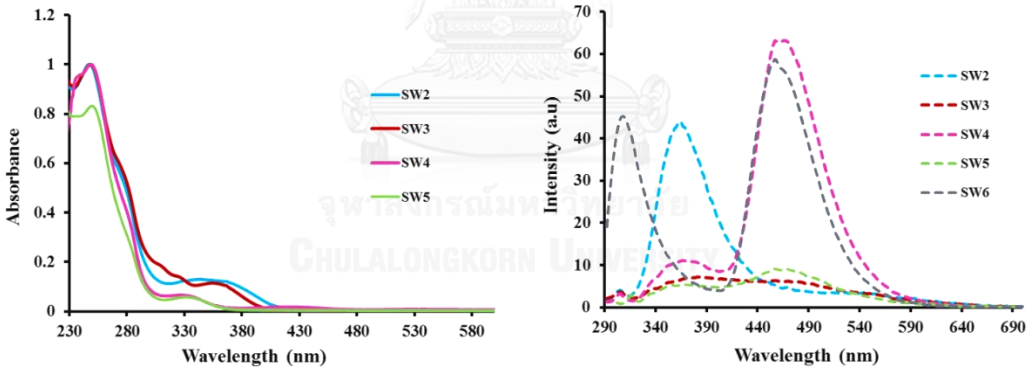

Figure 3.3.2 a) Absorption spectra b) fluorescence spectra of **SW2-6** 20 μM in THF

3.3.4. Effect of water content on photophysical properties

The **HPB** derivatives are well-known flurophores that can exhibit aggregation induced emission (AIE) due to their restricted intramolecular rotations behaviors (**RIR**) [21]. Therefore, we began the investigation of the AIE effect on our flurophore **SW2** and **SW3** by studying the relationship between the amounts of water in THF solution

toward the relative fluorescence intensity. In case of **SW2**, it showed an obvious fluorescence enhancement upon increasing the ratio of water from 0 to 60%, suggesting the AIE effect (**Figure 3.3.3**). However, the addition of water higher than 60% led to a decrease in the emission intensity. This result may be attributed to the low solubility of **SW2** in the solvent mixture, leading to a decrease in the number of emissive molecules per unit volume. For **SW3**, it exhibited this effect similar to **SW2**. The AIE of both **SW2** and **SW3** possibly arose from the restriction of intramolecular rotation (RIR). The single bond rotation and C=N double bond isomerization of imine moiety [16] in compounds **SW2** and **SW3** are mainly responsible for dominant non-radiative decay. Therefore if both processes were suppressed, fluorescence intensity will regain. We propose the self-assembly hydrogen bonding intermolecular of both aggregate **SW2** and **SW3** as shown in **Figure 3.3.4**. These will not only be the cause for RIR but also dismissing excited-state intramolecular proton transfer (ESPT) between –OH and C=N in **SW2** and **SW3**.

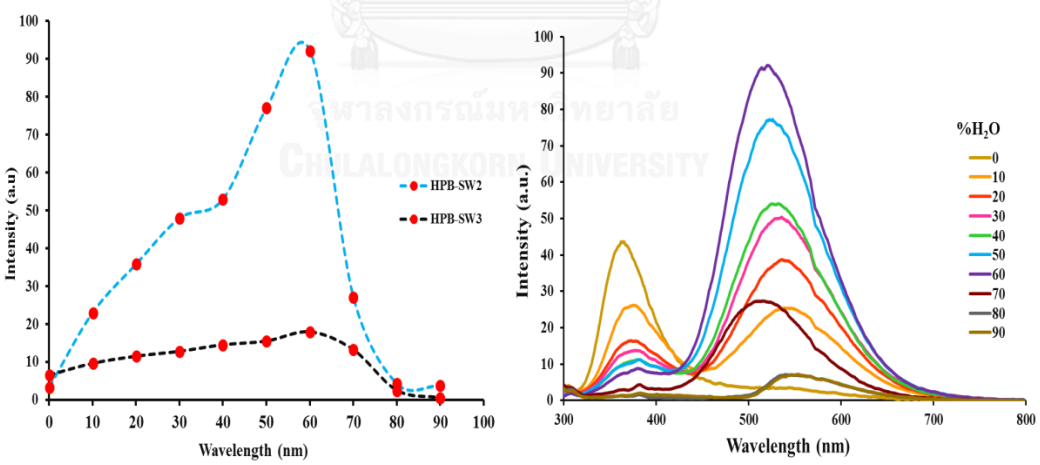

Figure 3.3.3 a) Fluorescence intensity b) Plot of maximum emission of **SW2** (λ_{em} 524 nm**)** and **SW3** (λ_{em} 416 nm**)** 20 μM in THF: H_2O mixtures at different water contents. All compounds were excited at 280 nm.

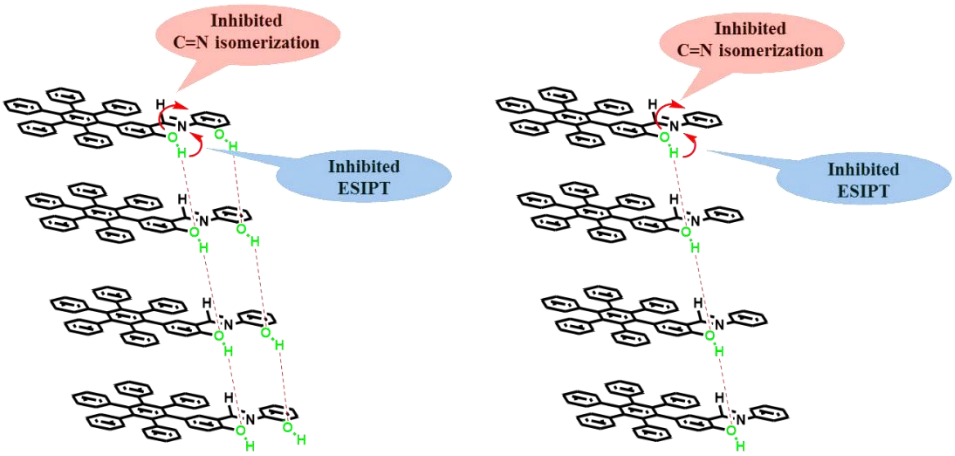

Self-assembly of SW2 Self-assembly of SW3

Figure 3.3.4 Proposed structure of self-assembly in aggregate state of **SW2** and **SW3**

On the other hand, the fluorescence intensity of **SW4**, **SW5** and **SW6** gradually decreased as the fraction of THF in the mixed THF/water solution decrease (100:0 to 10:90 v/v) (**Figure 3.3.5**). These properties differ from **SW2** and **SW3**. The strong emission of **SW4**, **SW5** and **SW6** in 100%THF may be attributed to nonaggregated molecules. In contrast, the decreasing fluorescence intensity of **SW4**, **SW5** and **SW6** along with a slight red shift from 455 to 500 nm was observed upon addition of water fraction in THF solution. To the best of our knowledge, these are the first example of **HPB** derivatives that have no AIE effect but exhibited aggregate caused quenching (ACQ) instead. We hypothesized that the free rotation of aliphatic imine linkage induces C=N isomerization and ESIPT process resulting in non-radiative decay of **SW4-6** even in their aggregates as shown in **Figure 3.3.6**. Therefore, flurophore **SW4**, **SW5** and **SW6** should be suitable for the design of “turn-on” fluorescence sensor.

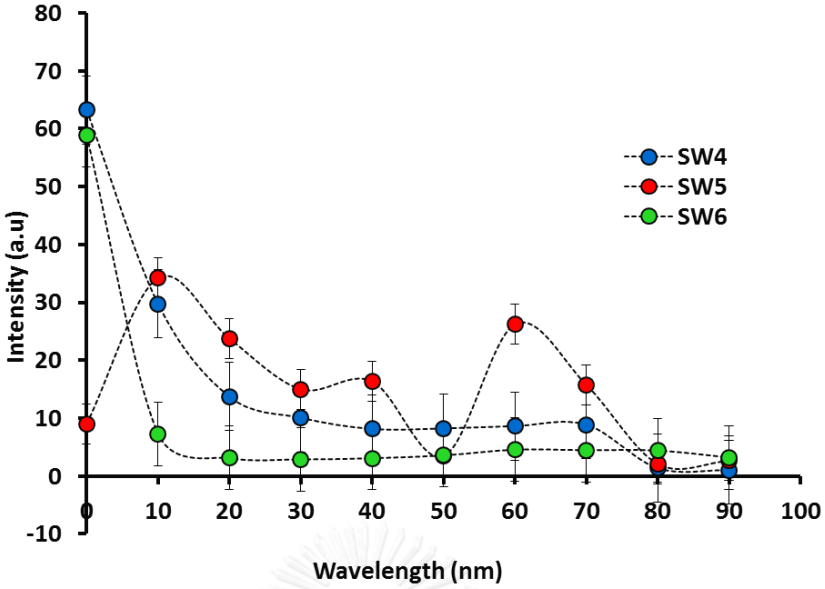

Figure 3.3.5 Fluorescence intensity of **SW4** (λ_{em} 460 nm, λ_{ex} =280 nm), **SW5** (λ_{em} 470 nm, λ_{ex} =290 nm) and **SW6** (λ_{em} 470 nm, λ_{ex} =280 nm) (20 μM) in THF: H_2O mixtures at different water contents.

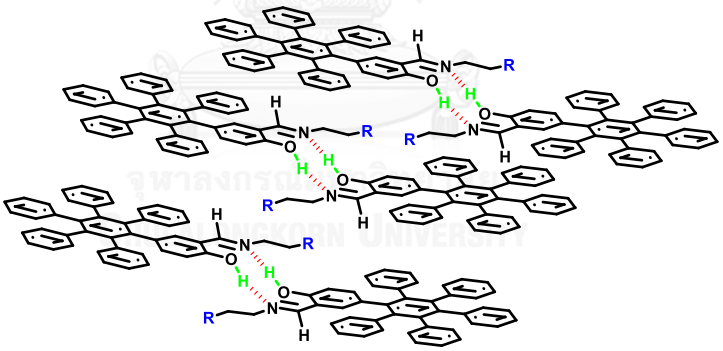

Self-assembly

SW4, R = -OH; **SW5**, R= -$N(CH_3)_2$; **SW6**, R= -CH_3

Figure 3.3.6 Proposed structure of self-assembly in aggregate state of **SW4-6**

3.3.5 Metal ion sensing ability

3.3.5.1 Selectivity of SW2 and SW3 toward metal ions

We began our study by testing the sensing ability of hexaphenylbenzene containing moiety aromatic imine **SW2** and **SW3**. The fluorescence responses of compound **SW2 and SW3** to various metal ions such as Cr^{3+}, Al^{3+}, Zn^{2+}, Ni^{2+}, Co^{2+}, Ag^{+}, Ba^{2+}, Pb^{2+}, Ca^{2+}, Cu^{2+}, Cd^{2+}, Hg^{2+}, Mg^{2+}, Na^{+}, K^{+}, Fe^{3+} and Fe^{2+} were presented in **Figure 3.3.7.** The compound **SW2** and **SW3** alone displayed a very weak emission band at 366 and 457 nm, respectively when excited at 280 nm in H_2O/THF solution (6:4, v/v). Upon the addition of 10 equiv. of metal ions to both flurophores, **SW3** showed insignificant fluorescence change. However, the **SW2** demonstrated selective turn-on fluorescence with Al^{3+}, whereas other metal ions revealed a negligible change in fluorescence. A fluorescence maximum was observed at 457 nm showing almost 1.3-fold increase in fluorescence intensity (**Figure 3.3.7**).

Figure 3.3.7 Fluorescence responses of **SW2** and **SW3** 20μM in H_2O/THF solution (6:4, v/v) upon addition of various cation 10 equiv. λ_{ex} 280 nm

3.3.5.2 Selectivity of SW4, SW5 and SW6 toward metal ion

Then we turned our attention to hexaphenylbenzene (HPB) **SW4**, **SW5** and **SW6** having alkyl imine substituents in order to investigate the effect of substituents toward metal sensing ability of HPB. The weak emission bands of **SW4-6** alone were observed at 457 nm in **FigureS44-S46.** The addition of 1 equiv. of each metal ion to solution of **SW6** gave the same fluorescence intensity as the initial state, while **SW4** displayed a small fluorescence enchantment (I/I_0-1) with only Zn^{2+} around 0.83-folds. On the other hand, **SW5** showed an exclusive strong fluorescence enchantment up to 23.93-fold, upon the addition of 1 equiv. of Zn^{2+} **Figure 3.3.8a**. This significant fluorescence amplification can also be observed visually by black light as seen in **Figure 3.3.8b.**

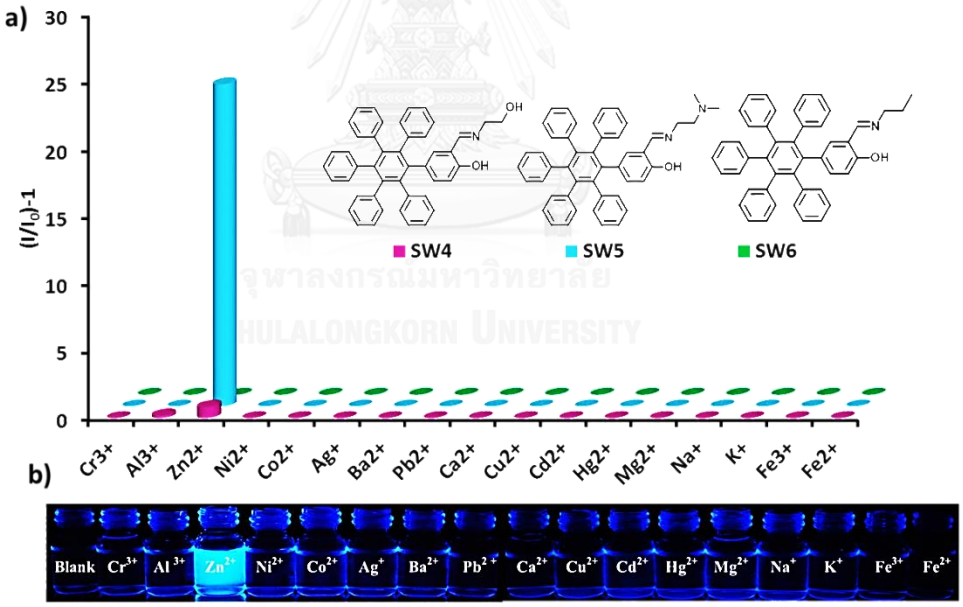

Figure 3.3.8 a) Bar graph representing the change of the relative emission intensity of **SW4** (THF: H_2O; 1:1, v/v, λ_{ex} 280 nm), **SW5** (THF: H_2O; 7:3, v/v, λ_{ex} 290 nm) and **SW6** (THF: H_2O; 1:1, v/v λ_{ex} 280 nm) upon mixing with different other metal ions 1eq. 10 μM of **SW4-6** were used. b) Photographs of **SW5** (50 μM) upon mixing with different other metal cation (10eq) in THF/H_2O (7:3, v/v) under black light

Based on above results, we can conclude that the flurophore **SW5** is the best choice for Zn^{2+} detection and **SW4** is also the potential one. Therefore, we further investigated flurogenic sensing ability of compound **SW4** and compared with **SW6** in higher concentration of flurophore (20μM) and metal (100μM) as seen in **Figure 3.3.9.** Only Zn^{2+} induced instantly a noticeable intensity enhancement while other metal ions showed either no or slight change in the emission spectra relative to the free **SW4** and **SW6**. Obviously, **SW4** clearly showed better fluorescence respond toward Zn^{2+} compared with **SW6.** Thus, the order of sensing ability of HPB series is in order as followed **SW5** > **SW4** > **SW6**. The effect heteroatoms in **SW** toward Zn^{2+} binding efficiency will be further studied and discussed in the next section. Based on these results, we will focus on **SW4** and **SW5** as Zn^{2+} sensors and their sensitivity, binding ability and interference will also be investigated due to their higher selectivity than other prepared flurophores.

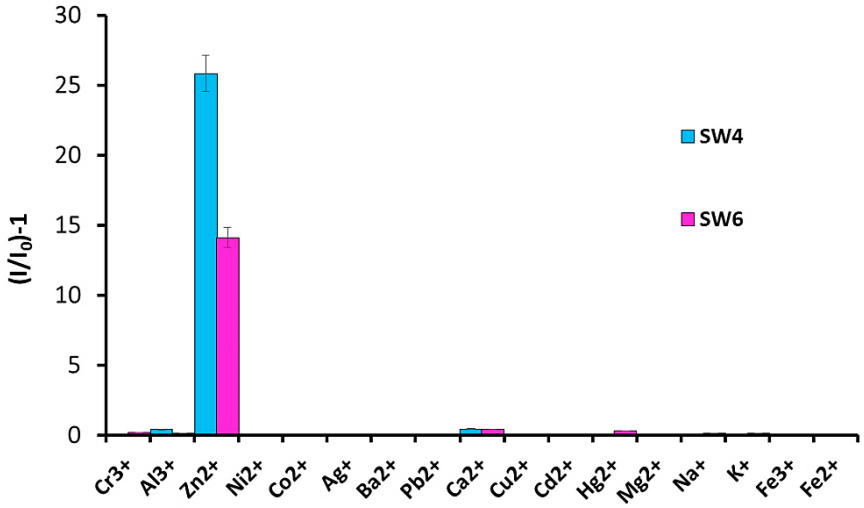

Figure 3.3.9 Bar graph selectivity of **SW (4, 6)** (20 μM) upon mixing with different other metal cations (10eq) in THF/H_2O (1:1, v/v) λ_{ex} 280 nm

3.3.6 Sensitivity of SW4 and SW5 toward metal ions

3.3.6.1 Fluorescence titration of SW4 and SW5

The quantitative fluorescence titration experiments were carried out using 20μM of **SW4** in the presence of different concentrations of Zn^{2+} from 0 to 10.0 equiv. On the other hand we used only 0 to 1.5 equiv. of Zn^{2+} to titrate with **SW5** (10 μM). The difference amount of flurophores and Zn^{2+} in each experimental is due to higher sensitivity of **SW5** toward Zn^{2+}. The emission intensity of **SW4** and **SW5** gradually increased upon the addition of Zn^{2+} and saturated at 10.0 equiv. and 1.5 equiv. respectively as shown in **Figure 3.3.10** and **Figure 3.3.11,** respectively. The quantum yields (Φ) of **SW5** could not be determined due to their poor fluorescence emission. Upon addition of Zn^{2+} 10 equiv. to **SW5**, the quantum yield increase up to 17%. Moreover, the plot between concentration and fluorescence intensity revealed the large linear relationship between 5×10^{-6} to 1×10^{-4} M for **SW4** in **Figure 3.3.10 b**) and 3×10^{-7} to 9×10^{-6} M for **SW5** as seen in **Figure 3.3.11 b**). The detection limit of **SW4** and **SW5** were evaluated to be as low as 0.160 μM and 0.035 μM respectively, which are far below the World Health Organization guideline (76 μM) [47].

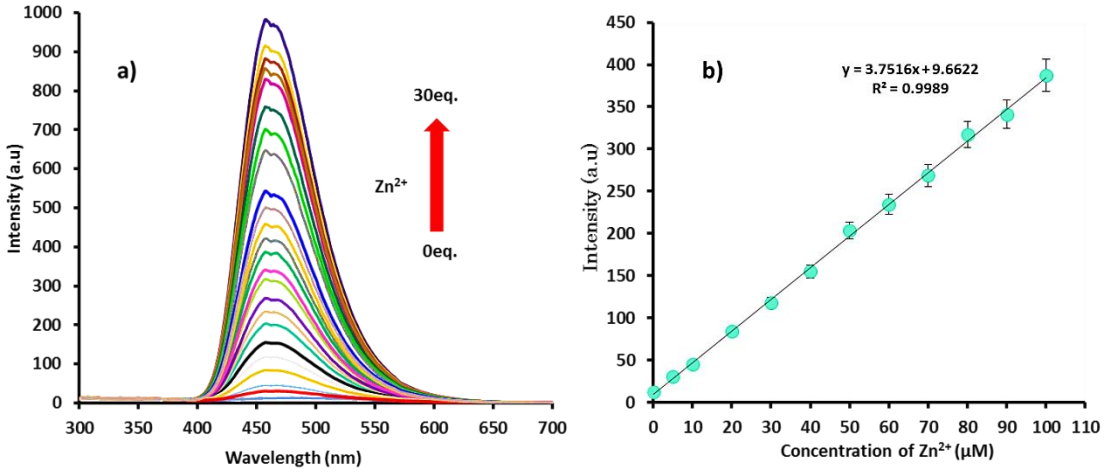

Figure 3.3.10 a) Change in the fluorescence spectra b) The plot between concentration and fluorescence intensity revealed of **SW4** (20 μM) upon a gradual increase in the concentration of Zn^{2+} in THF/H_2O (1:1, v/v) λ_{ex} 280 nm

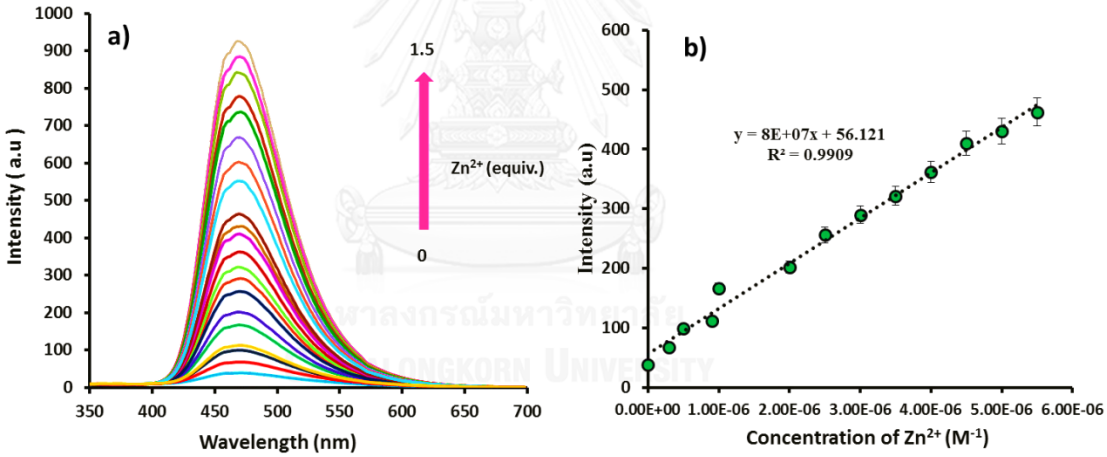

Figure 3.3.11 a) Change in the fluorescence spectra b) The plot between concentration and fluorescence intensity revealed of **SW5** (10 μM) upon a gradual increase in the concentration of Zn^{2+} in THF/H_2O (7:3, v/v) λ_{ex} 290 nm

3.3.6.2 Time dependent with Zn^{2+} of SW4 and SW5

Next, we realized that fluorescence enhancement of **SW4** and **SW5** toward Zn^{2+} might be time-dependent. Therefore it is very important to find the optimal time for measurement. We recorded the fluorescence intensity of both flurophore with Zn^{2+} from 1-30 minutes as depicted in **Figure 3.3.12**. It showed that the fluorescence intensity was exponentially increased within 1-2 min after the addition of Zn^{2+}. For **SW4**, the fluorescence intensity remained the same while **SW5** shown a small decrease in fluorescence intensity. This observation could be due to the fact that C=N double bond of imine moiety might be hydrolyzed in aqueous condition also and the decomplexation between flurophores and metal might be occurred [48]. However, in the first 5 minutes, there was no significant change in the intensity and it gave the maximum enhancement suggesting that our flurophores are suitable for rapid and sensitive Zn^{2+} detection.

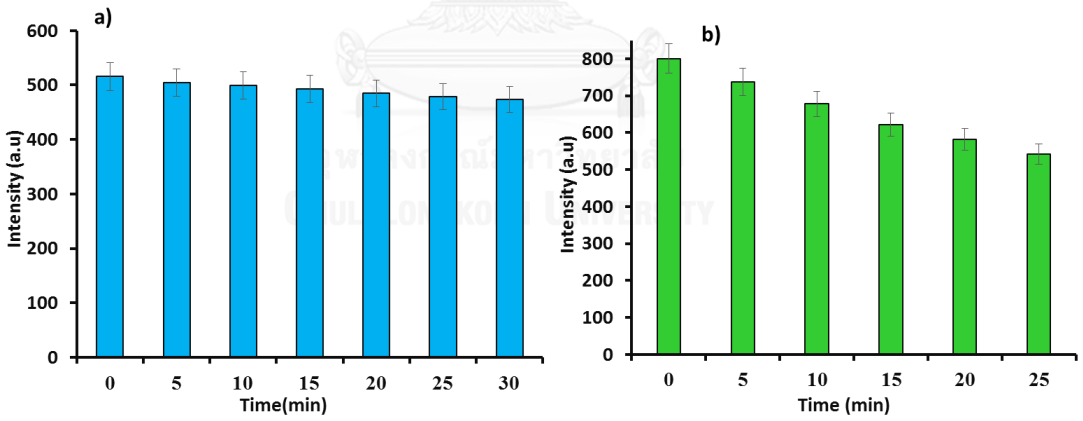

Figure 3.3.12 Bar graph time-dependent changes in the fluorescence intensity a) **SW4** 20 μM upon addition of Zn^{2+} 10 equiv. in THF/H_2O (1:1, v/v), λ_{ex} 280 nm b) **SW5** 20 μM) upon addition of Zn^{2+} 1.5 equiv. in THF/H_2O (7:3, v/v), λ_{ex} 290 nm.

3.3.6.3 Solvent effect of water fraction in THF

We also investigated the effect of water fraction in THF toward the sensitivity of flurophores **SW4** and **SW5** as seen in **Figure 3.3.13**. **SW4** exhibited the maximum fluorescence at 1:1 v/v ratio while **SW5** was 3:7 v/v ratios of water and THF. However, within the range between 30-60 fractions, both flurophores displayed an acceptable fluorescence enchantment upon addition of Zn^{2+} between 12-14 folds and 12-19 folds for **SW4** and **SW5**, respectively.

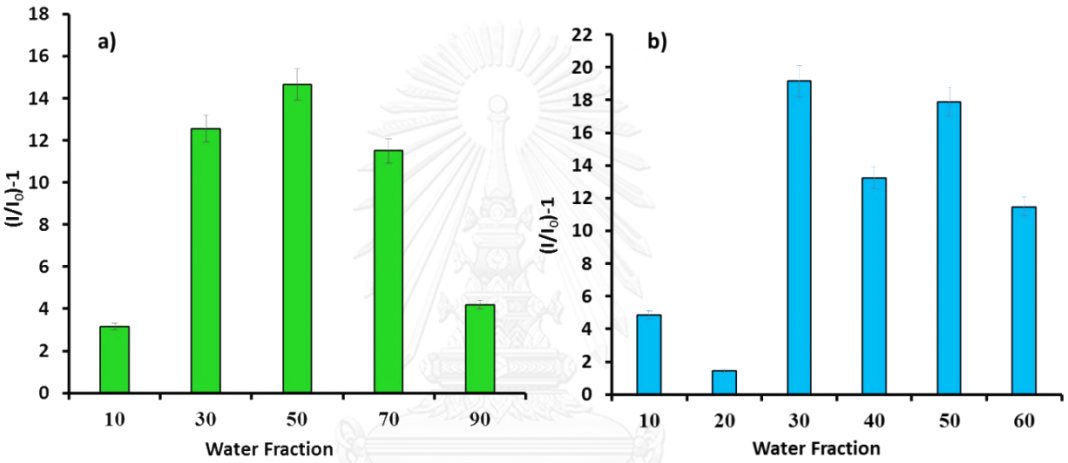

Figure 3.3.13 Bar graph water fraction changes in the fluorescence intensity a) **SW4** 20 μM upon addition of Zn^{2+} 10 equiv. in THF/H_2O (1:1, v/v) λ_{ex} 280 nm b) **SW5** 20 μM) upon addition of Zn^{2+} 1.5 equiv. in THF/H_2O (7:3, v/v) λ_{ex} 290 nm

3.3.6.4 The effect of pH on SW5 for zinc ion detection

To investigate the pH working range of **SW5,** the fluorescent intensity of **SW5** in the absence and presence of Zn^{2+} were studied at different pH values, as shown in **Figure 3.3.14. SW5** showed nearly no fluorescence in the pH range of 3-11(black circles). In the presence of 1.5 equiv. of Zn^{2+}, there were no significant change in fluorescence intensity in high acidic condition (pH = 3-6) and highly basic condition (pH= 10-11). The low sensitivity under strong acidic condition is caused by the

protonation of the N atoms at imine and 3^0 amine of **SW5** leading to the weak coordination capability with Zn^{2+} [49]. On the other hand, the addition of hydroxide to imine moiety of **SW5** could occur under high basic condition. Interestingly, remarkable fluorescence enchantment upon addition of Zn^{2+} was observed in pH range 7-9 with maximum value at pH = 8.0 (I/I_0=76)

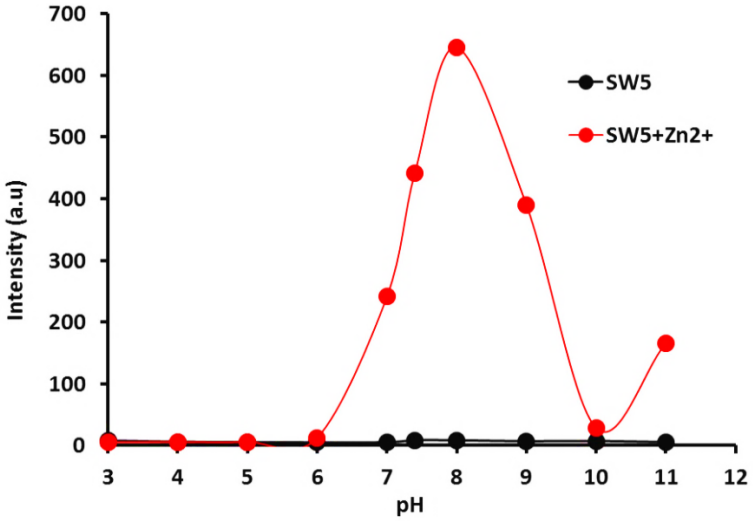

Figure 3.3.14 Fluorescence intensity of **SW5** (10 μM) at various pH values in 7:3 v/v THF: Water in the absence and presence of Zn^{2+} 1.5 equiv.

3.3.7 Investigation of the binding mode

3.3.7.1 Job's plot experiment

In order to explore the binding stoichiometry between **SW4** and **SW5** with Zn^{2+}, a Job's plot experiment was conducted as shown in **Figure 3.3.15a** and **Figure 3.3.16**, respectively. The fluorescence intensities at maximum emission were plotted against the molar fractions of Zn^{2+} by keeping their total concentration constantly. In the case of **SW4**, Job's plot indicated that the coordination between Zn^{2+} and probe has 1:1 stoichiometry. To obtain insight into binding efficiency of probes **SW4** toward Zn^{2+}, the associations were determined. The association constant (K_a) of **SW4** was calculated to be 1.33×10^3 from a Benesi–Hildebrand [35] shown in **Figure 3.3.15b.** Moreover, the result from Job's plot of **SW5-Zn^{2+}** indicated a much stronger

complexation showing a 2:1 stoichiometry. It confirmed that the amino group in **SW5** plays a vital role in the coordination with Zn^{2+}.

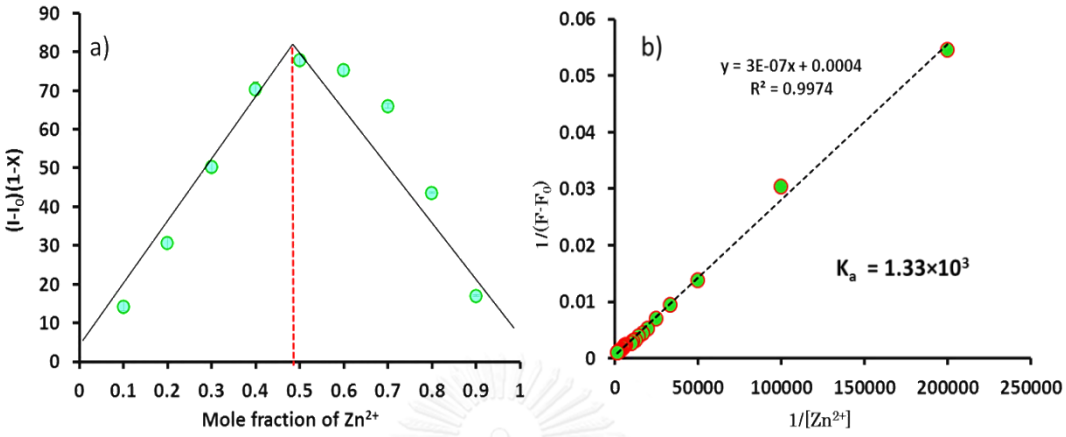

Figure 3.3.15 a) Job's plot of the **SW4-Zn**$^{2+}$ complexes in THF: H_2O (1:1, v/v) solution, keeping the total concentration of **SW4** and Zn^{2+} at 0.1 mM. b) Benesi–Hildebrand plot of **SW4** with Zn^{2+} in THF: H_2O (1:1, v/v) solution. λex 280 nm and the observed wavelength was 457 nm.

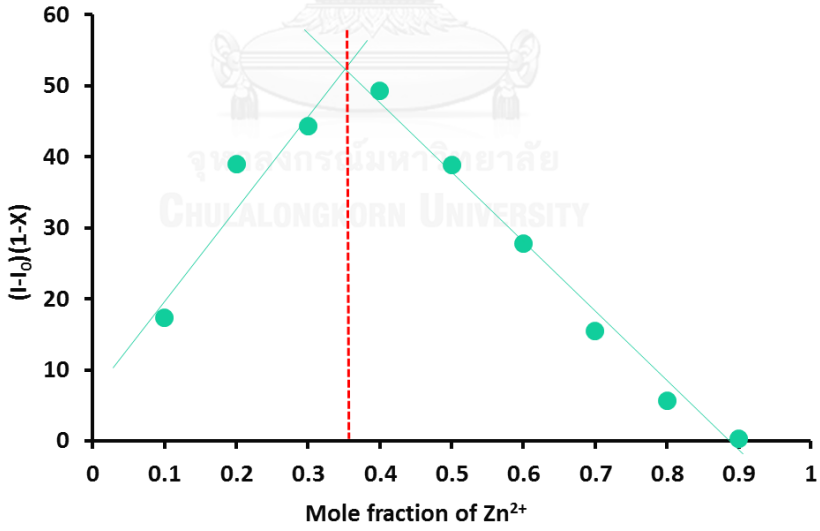

Figure 3.3.16 Job's plot of the **SW5-Zn**$^{2+}$ complexes in THF: H_2O (7:3, v/v) solution. λex 290 nm, keeping the total concentration of **SW5** and Zn^{2+} at 10 μM the observed wavelength was 470 nm.

3.3.7.2 ^{1}H NMR experiment

To gain more information for the binding site of **SW5** with zinc ion, we designed to perform the ^{1}H NMR titration between **SW5** and Zn $(CH_3COO)_2$ as shown in Figure **3.3.17.** Initially, **SW5** displayed hydroxyl proton (H_h) at 12.82 ppm, imine proton (H_d) at 8.00 ppm and *N*-methyl (*N*-CH_3) proton (H_a) at 2.20 ppm. Upon the addition of Zn^{2+}, the hydroxyl proton peak (h) decreased gradually and totally disappeared when 0.75 eq. of Zn^{2+}ion was added. Moreover, the imine proton peak (d) at 8.00 ppm decreased along with the rise of a new peak at 7.95 ppm. Similarly, the *N*-methyl (*N*-CH_3) proton (H_a) peak at 2.20 ppm decreased and formed a new peak at 2.38 ppm. Importantly, a downfield shift trend was observed in all of aromatic protons in **HPB** moiety. This suggested that the hetero atoms in **SW5** such as N atoms in imine and amine moieties as well as O atom in phenolic group are indeed the binding site for zinc ion.

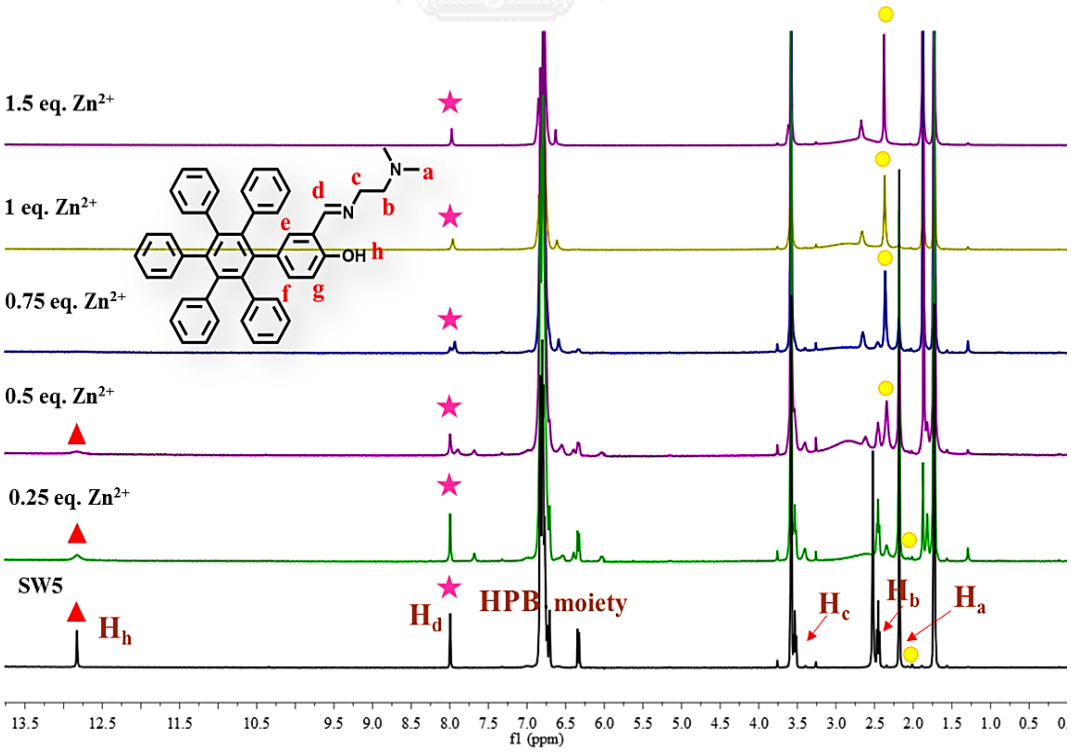

Figure 3.3.17 ^{1}H NMR titration of **SW5** (20 mM) with Zn $(CH_3COO)_2$ in d_8-THF

3.3.7.3 Morphology investigation

Dynamic light scattering (DLS) studies of **SW5** (50μM) in a mixed aqueous media 7:3 THF: water suggested that the average particle size decreased from 1000 nm to ≈3 nm upon the addition of 1.5 equiv. (**Figure 3.3.18a** and **b**). When amount of Zn^{2+} were changed from 1.5 equiv. to 10 equiv. (500μM), the particles size remain unchanged (**Figure 3.3.18c**). We believe that the saturation of complex in the ratio 2:1 between **SW5** and Zn^{2+} based on Job's plot (**Figure 3.3.16.**)

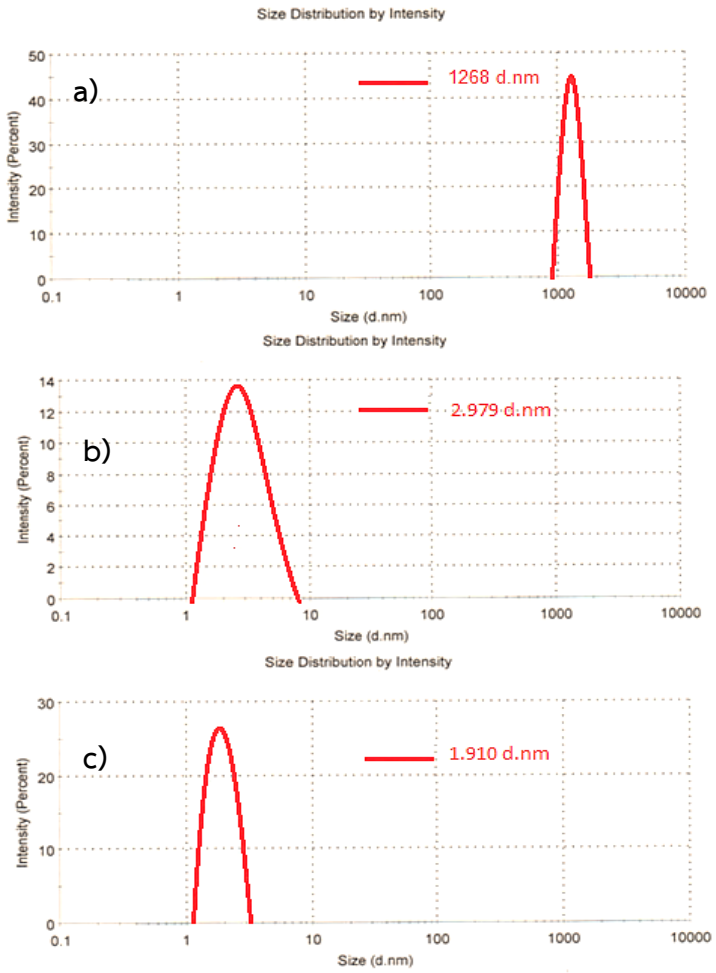

Figure 3.3.18. DLS-based particle size analysis of **SW5** in a) the THF: H_2O (7:3, v/v) solution**.** b) presence of 1.0 equivalent of Zn^{2+} and c) presence of 10.0 equivalent of Zn^{2+} to **SW5**.

The SEM images of **SW5** alone show large irregular shaped aggregates as seen in **Figure 3.3.19a** while the adding of 10 equiv. of Zn^{2+} results in the formation of small rice-like aggregate (**Figure 3.3.19b**). These results suggest that interaction between aggregates of **SW5** and Zn^{2+} responds for modulation of aggregates structure of **SW5**. We believe that in the presence of water as co-solvent **SW5**, it forms large aggregates via intermolecular hydrogen bonding as descripted in **Figure 3.3.6**. Upon addition of Zn^{2+}, it destroys such structure and forms smaller nanoaggregates.

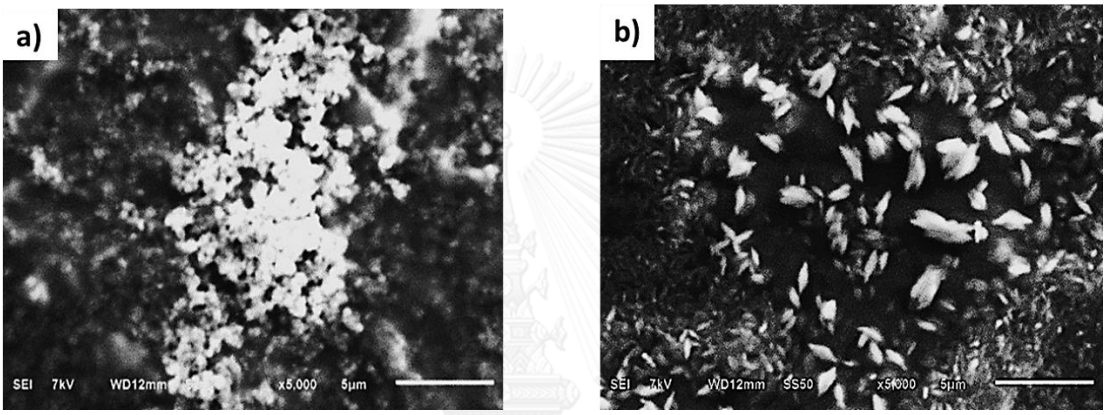

Figure 3.3.19 Photographs of SEM images of compound **SW5** a) showing the irregular shaped aggregates b.) Upon addition Zn^{2+} showing the regular shaped aggregates, in THF: H_2O (7:3, v/v) solution

3.3.7.4 Proposed binding of complex

Therefore, based on the above studies including fluorescence titration spectra, Job's plots coordination chemistry, ^1H NMR titration experiment, dynamic light scattering (DLS) and scanning electron microscopic (SEM) analysis, we proposed a mechanism for fluorescence turn-on of **SW5** toward Zn^{2+}**.** It may be assumed that along with the formation of **SW5** aggregates**,** it formed large aggregates in mixture media at 30% water in THF (%v/v) due to intermolecular hydrogen bonding which exhibited aggregate caused quenching (ACQ) as shown in **Figure 3.3.20**. Interestingly, Most HPB derivative exhibit AIE effect but our HPB show reverses effect which has

never been reported before. We hypothesized that the free rotation of aliphatic imine linkage induce C=N isomerization and ESIPT process results in non-radiative decay. Upon the addition of Zn^{2+}, the large aggregation of **SW5** was deaggregates into smaller aggregates [50] as seen by the DLS (**Figure 3.3.18**) and SEM analysis (**Figure 3.3.19**). These smaller aggregates show strong emission in solution. The lone pair electrons of N and O atoms in HPB contribute as receptor for chelation with Zn^{2+} ion resulting in destroying hydrogen bonding intermolecular force. Therefore, the quenching behavior from intramolecular rotation (RIR), C=N isomerization, single rotation and ESIPT of **SW5** was removed and gave the fluorescence enhancement. Moreover, the formation small of nanoaggregates of **SW5** and Zn^{2+} gave stronger fluorescence emission due to the less shielding effect from the surface of aggregates which block inner molecules to emit [21].

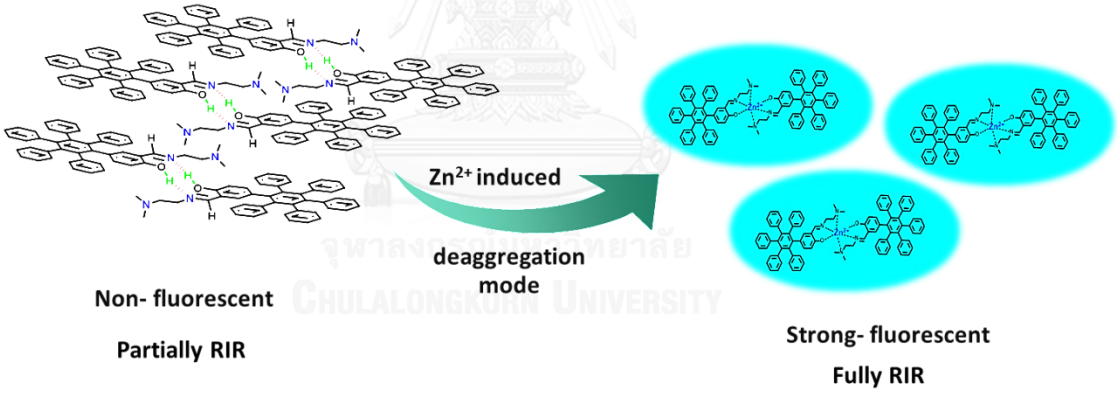

Figure 3.3.20 Schematic illustration of the increase in fluorescence achieved by inhibiting C=N isomerization and single bond rotation

3.3.8 Interference of other metal ions toward the detection of zinc with SW5

To examine the selectivity for Zn^{2+} in a complex background of potentially competing species, the fluorescence enhancement of **SW5** with Zn^{2+} was investigated in the presence of other metal ions. When **SW5** was treated with 1.5 equiv. of Zn^{2+} in the presence of equal other metal ions in THF/H_2O, the emission

spectra were almost identical in the case of Ag^{+}, Ba^{2+}, Ca^{2+}, Mg^{2+}, Na^{+}, K^{+} suggesting a slight interference in the detection of Zn^{2+} under these metals as seen in **Figure 3.3.21**. However other metal ions including Cr^{3+}, Al^{3+}, Cu^{2+}, Fe^{3+} and Fe^{2+} almost quenched the emission of **SW5-Zn^{2+}**. This phenomenon is due to the displacement of Zn^{2+} by these cations. Interestingly, when the experiments were conducted in THF/water in HEPES buffer (pH = 8.0), there was a little interference from most other ions except for Cu^{2+} which showed almost no emission as seen in **Figure 3.3.22** Therefore, this observation confirmed that the optimal condition for Zn^{2+} detect using **SW5** is in buffer pH = 8. This improvement is perhaps governed by the strong complexation between **SW5-Zn^{2+}** under the studied condition. However Cu^{2+} ion exists at very low concentration in normal biological sample so our sensor **SW5** showed a promising selective fluorescence sensor for Zn^{2+} in the presence of other metal ions.

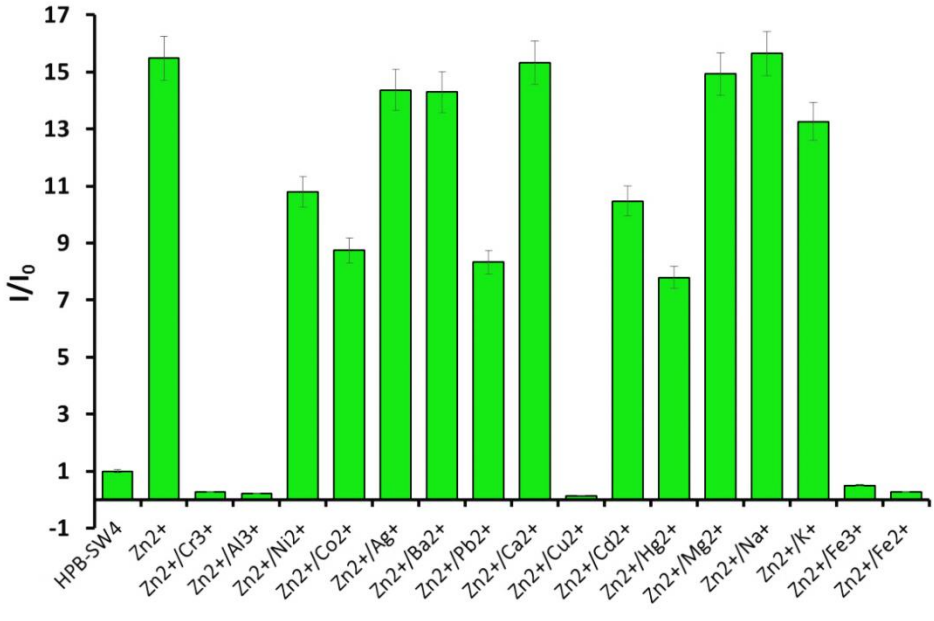

Figure 3.3.21 Bar graph representing the change of competitive selectivity of **SW5** toward Zn^{2+} in the present of other metal ions (1eq.) in THF: H_2O (7:3, v/v) solution with an emission of 470 nm

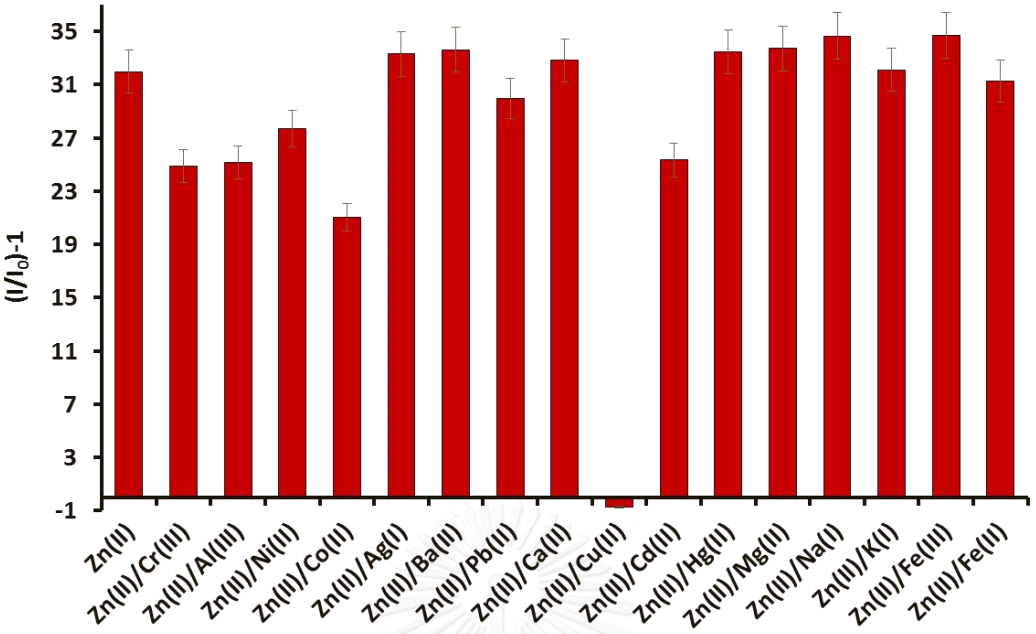

Figure 3.3.22 Bar graph representing the change of competitive selectivity of **SW5** toward Zn^{2+} in the present of other metal ions (1eq.) in THF/H_2O (7:3, v/v) buffer pH = 8.0 (10mM HEPES) λex 290 nm with an emission of 470 nm

3.3.9. Application of flurophores for Zn^{2+} detection

3.3.9.1 Quantitative analysis of Zn^{2+} in mineral water

We have investigated the ability of SW5 probe in sensing Zn^{2+} in mineral water. In Mont Fleur ™ mineral water, we spiked Zn^{2+} concentration between 2.0–10 μM followed by addition of **SW5** and the fluorescence measurement were performed (**Figure 3.3.23**). Each concentration was repeated three times. The fluorescence response was linear with respect to the concentration showing R^2= 0.9557. We found 1.14 μM of Zn^{2+} in mineral water. Accordingly, **SW5** would be useful as a quantitative detect Zn^{2+} sensor in real water samples.

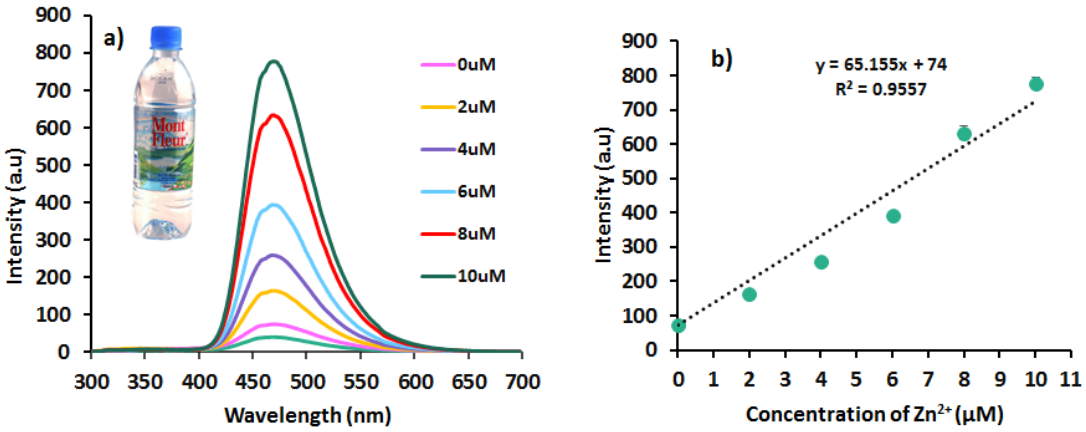

Figure 3.3.23 a) Change in the fluorescence spectra **SW5** (10 μM) **b)** Plot of fluorescence intensity of **SW5** (10 μM) in THF: H_2O (7:3, v/v) solution upon addition of spiked Zn^{2+} (2.0–10 mM) in mineral water samples

3.3.9.2 Cell imaging

We have investigated the potential of the application of **SW5** for sensing Zn^{2+} in living cells. The images of cells were obtained using an Olympus DP71 microscope digital camera with an objective lens x40. When Kasky cell was incubated with **SW5** (50 μM) for 1 hr. at room temperature, it showed nearly no fluorescence (**Figure 3.3.24c and d**). After the treated cells were incubated with Zn^{2+} (0.5 mM) in the culture medium for 1 hr. at room temperature, a bright blue fluorescence was observed (**Figure 3.3.24e and f**). Importantly, the cell morphology remained in good condition after intake of **SW5**. This indicated the great cytocompatibility and low toxicity of the probe **SW5**. Therefore, the **SW5** probe has cell membrane permeability and could be applied in the detection of Zn^{2+} within living cells.

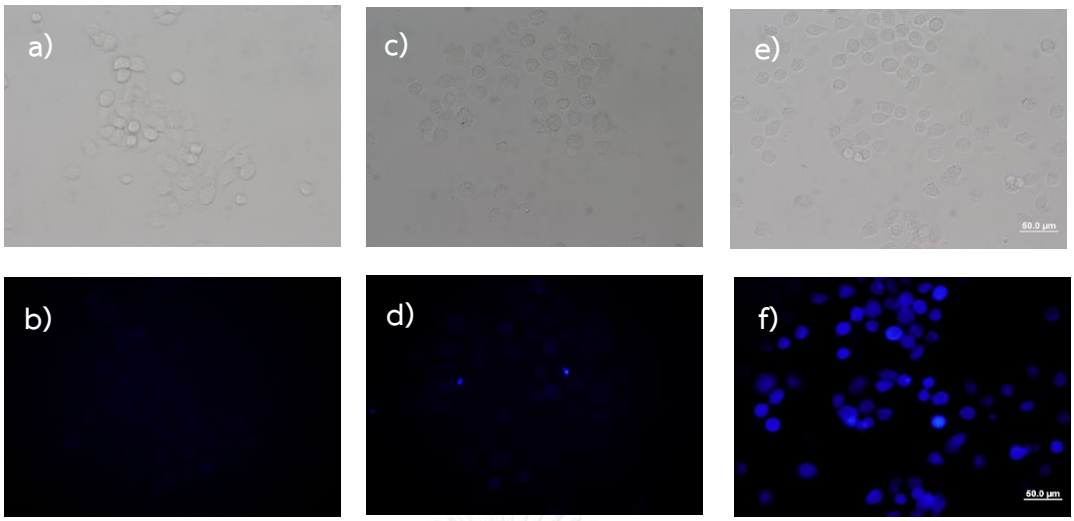

Figure 3.3.24 Above bright field image and **Below** fluorescent (under blue light) image of Kasky cells for (a, b) Blank Kasky cells (c, d) cells treated with 50 μM of **SW5** (e, f) addition 50 μM of **SW5** and 10eq. of Zn^{2+}. Scale bar for the images is 50 μm

3.3.9.3 The sensing behavior of SW4-Zn^{2+} complex toward anions

It is conceivable that Zn^{2+} containing complex of **SW4** is labile and thus an anion binding to the metal center would displace the neutral ligand resulting in the change or recovery of its spectroscopic behavior. This coordination complex-based displacement approach has been used for detection of certain anionic species[34]. The secondary sensing behavior of the *in situ* generated highly fluorescent **SW4-Zn^{2+}** (20 μM and 200 μM) complex toward different anionic species (10 equiv.) including CN^-, HCO_3^-, $H_2PO_4^{2-}$, AcO^-, N_3^-, SCN^-, SO_3^{2-}, Cl^-, I^-, Br^-, SO_4^{2-}, AMP, ADP and ATP were investigated as shown in **Figure 3.3.25**. It displayed little fluorescence quenching with $H_2PO_4^{2-}$ while AMP, ADP and ATP gave completely fluorescence quenching. It must be noted that the other anions revealed no noticeable changes in fluorescence intensity with **SW4-Zn^{2+}** complex.

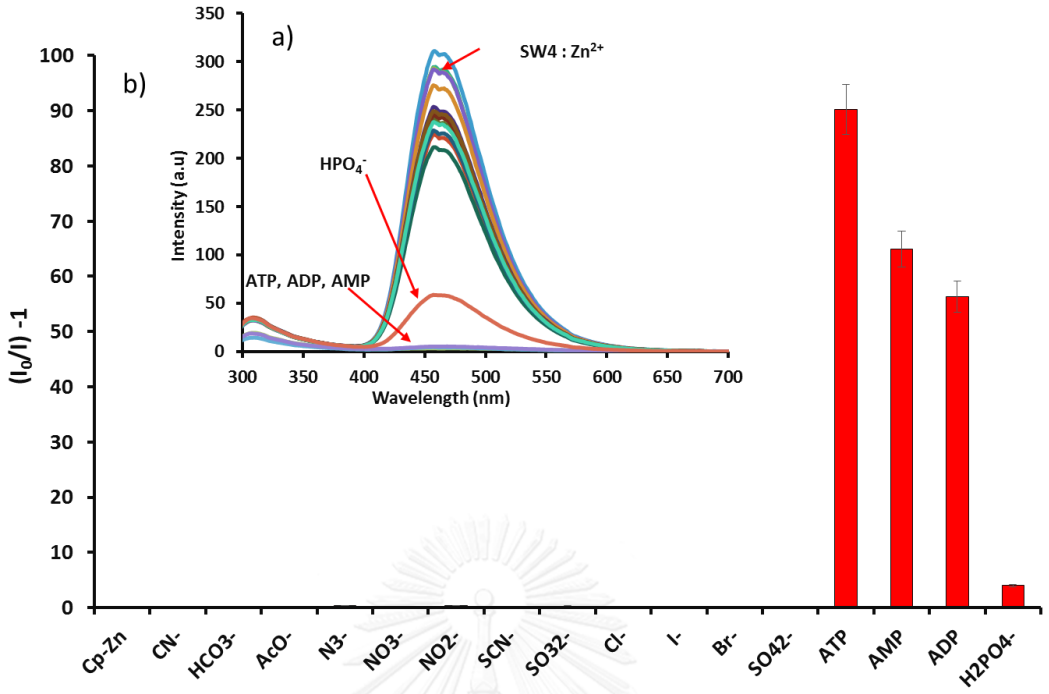

Figure 3.3.25 a) Fluorescence spectra and b) bar graph of fluorescence enchantment ratio of **SW4-Zn**$^{2+}$ complex 20 μM (water/THF, 1:1) toward addition of various anions, ATP, ADP and AMP (10 equiv.)

3.3.9.4 Sensing of pesticides with a SW5-Zn^{2+} complex

Pesticides play an important role in contemporary agricultural operations by increasing crop yield while stabilizing global food supply through the protection of plant from diseases and pests. Pesticide control thus has been widely recognized to be important for public health. Conventional detection methods relied on potentiometry, [51] gas chromatography and mass spectrometry [52] which require expensive instrument and highly skilled operators. In recent year, zinc complex as chemosensor for detected organophosphate in biomolecules sensing such as PPi, AMP, ADP and ATP [53, 54]. However there was no report on using metal complex to detect organophosphate in pesticides. Therefore we planned to use emissive **SW5-Zn**$^{2+}$ ensemble for detection of pesticides by using fluorescence technique. Among a

number of pesticides, we selected eight chemicals such as diazinon, EPN, phosalone, fenvalerate, aldicarbsulfone, endosolfansulfate, methidathion and monocrotophos as shown in **Figure 3.3.26** which are commonly pesticides in insecticides used for pest control in rice and vegetables.

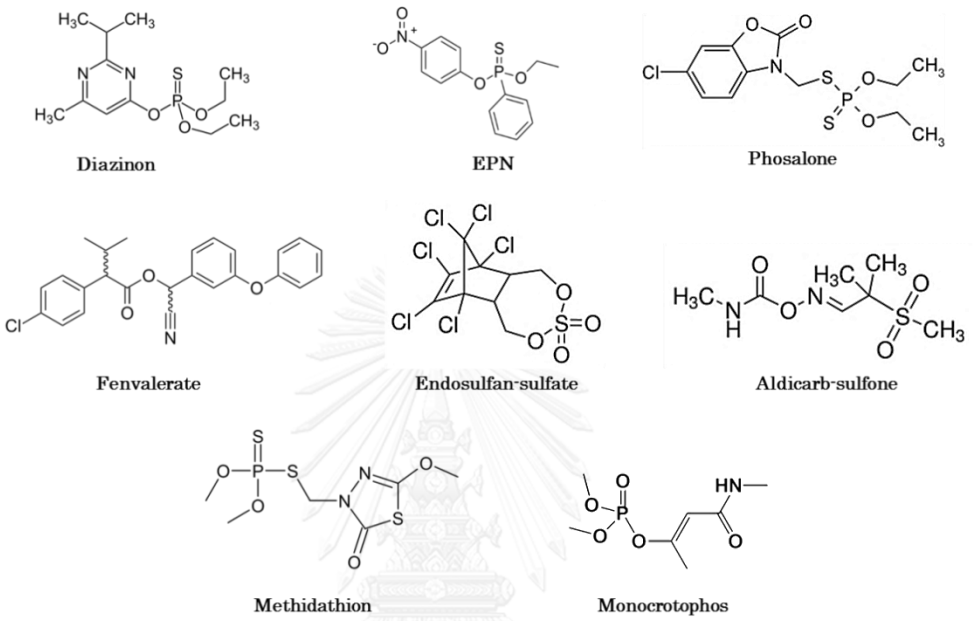

Figure 3.3.26 Structure of investigated pesticides

The sensing ability of **SW5-Zn**$^{2+}$ ensemble toward various pesticides was evaluated further by fluorescence spectroscopic measurements. The **SW5-Zn**$^{2+}$ complex (10μM with 0.5equiv. of Zn^{2+}) was prepared in *situ* and treated with eight pesticides at 50 ppm concentration as shown in **Figure 3.3.27.** It clearly demonstrated that **SW5-Zn**$^{2+}$ is highly sensitive to diazinon. The emission intensity of the **SW5-Zn**$^{2+}$ ensemble decreased instantly upon the addition of diazinon showing 41-folds quenching ratio while the other pesticides give slight or no fluorescence changes. The remarkable selectivity of **SW5-Zn**$^{2+}$ toward Diazinon sensing is due to the strong complexation between Zn^{2+} and heteroatoms (N and S atoms) in Diazinon leading to the

decomplexation of **SW5-Zn**$^{2+}$. Therefore, our sensor system is capable of selectively sensing Diazinon over other organophosphate pesticides.

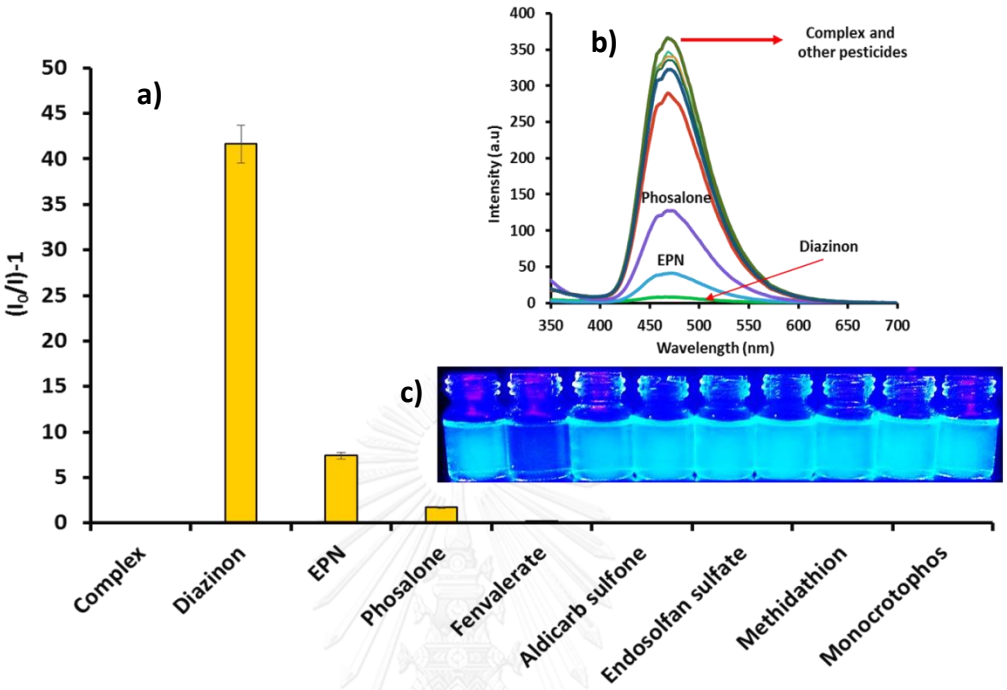

Figure 3.3.27 a) Fluorescence intensity ration $(I/I_0)-1$, b) fluorescence spectra of **SW5-Zn**$^{2+}$ (10 μM and 5 μM) and c) photographs under black light of **SW5-Zn**$^{2+}$ (50 μM and 25μM) in water: THF 3:7 v/v toward addition of pesticides (50ppm) at λ_{ex} 290 nm and λ_{em} 470 nm

In order to determine the sensitivity of compound **SW5-Zn**$^{2+}$ for Diazinon detection, the fluorescent signals of fixed concentration of **SW5-Zn**$^{2+}$ solution with various concentrations of Diazinon were measured as seen in **Figure 3.3.28**. It demonstrated the fluorescence quenching upon increase of Diazinon concentration as seen in **Figure 3.3.28a**.Then the plot between I_0/I and the concentration of Diazinon were plotted and slope was corresponded to the Stern-Volmer constants (K_{sv}) (**Figure 3.3.28b**). The detection limit was found to be 2 ppm.

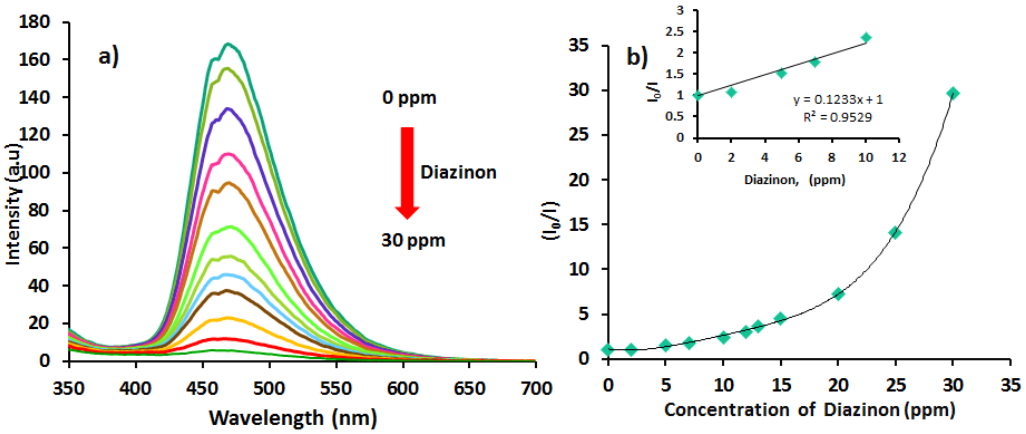

Figure 3.3.28 a) Change in the fluorescence intensities upon the addition of Diazinon (30 ppm) **SW5-Zn**$^{2+}$ (10 μM and 5 μM) in water: THF 3:7 v/v; λ_{ex} = 290 nm. **b**) Stern–Volmer plot of the percent quenching of **SW5-Zn**$^{2+}$ versus the concentration of Diazinon (ppm).

CHAPTER IV
CONCLUSION

4.1 Conclusion

In summary, three objectives were successfully investigated. In term of the effect of substituent of hexaphenylbenzene (HPB) derivatives, the donating groups showed the ability on induced fluorescence intensity whereas the withdrawing groups are less governed on aggregation state. In term of an oligophenylene-based pyrene derivatives (**FL1** and **FL2**), we have successfully synthesized the compounds by Diels-Alder reaction. **FL1** displayed AIE effect upon addition 60% water into THF solution while **FL2** showed no significant fluorescence enhancement. **FL1** showed better sensing ability in comparison with **FL2** toward nitroaromatic compounds, specifically picric acid, which has quenching constants (Ksv) of 4.845×10^{4} M^{-1} and the detection limit was found to be 0.88 μM. The fluorescence quenching upon addition of PA was governed by energy transfer process and competitive absorption. As for the hexaphenylbenzene (HPB) containing imine moiety **SW (2-6)** for metal chemosensor, they were successfully synthesized in 4 steps. The compound **SW2** and **SW3** exhibited ACQ effect while **SW (4-6)** showed AIE effect upon increasing of water fraction in THF solution. This result suggested that the types of imine moiety have an important role toward emission under aggregate condition. For the sensing ability of aggregate of flurophores toward difference metal ions, **SW2** showed selectivity toward Al^{3+} resulting in the strong enhancement as blue fluorescence emission while the **SW (4-6)** showed selective turn-on fluorescence toward Zn^{2+} ion. The detection limit of **SW4** and **SW5** were calculated to be 0.160 μM and 0.0353 μM for Zn^{2+}. Moreover**, SW5** was able to detect Zn^{2+} in living cell and the emissive **SW5-Zn^{2+}** complex can detect organophosphate pesticides.

REFERENCES

[1] Hong, Y., Lam, J.W.Y., and Tang, B.Z. Aggregation-induced emission: phenomenon, mechanism and applications. Chemical Communications (29) (2009): 4332-4353.

[2] B.T. Fedoroff, O.E.S. Encyclopedia of Explosives and Related Items. USDepartment of Commerce Springfield, Virginia, 1962.

[3] Pimienta, V., Etchenique, R., and Buhse, T. On the Origin of Electrochemical Oscillations in the Picric Acid/CTAB Two-Phase System. The Journal of Physical Chemistry A 105(44) (2001): 10037-10044.

[4] Toal, S.J. and Trogler, W.C. Polymer sensors for nitroaromatic explosives detection. Journal of Materials Chemistry 16(28) (2006): 2871-2883.

[5] Zhaoxiong Yan, Z.X., Wanju Zhang, Shengfang Zhao, Yu Xu. A Novel Electrochemical Nitrobenzene Sensor Based on NiCu Alloy Electrode. International Journal of ELECTROCHEMICAL SCIENCE 7 (2012): 2938 - 2946.

[6] Zhou, H.-C., Long, J.R., and Yaghi, O.M. Introduction to Metal–Organic Frameworks. Chemical Reviews 112(2) (2012): 673-674.

[7] Choi, Y.W., et al. A single schiff base molecule for recognizing multiple metal ions: A fluorescence sensor for Zn(II) and Al(III) and colorimetric sensor for Fe(II) and Fe(III). Sensors and Actuators B: Chemical 194(0) (2014): 343-352.

[8] Cronan, C.S., Walker, W.J., and Bloom, P.R. Predicting aqueous aluminium concentrations in natural waters. Nature 324(6093) (1986): 140-143.

[9] Leary, D.A.S.J.J. Principles of Instrumental Analysis. 3 ed. Saunders College Publishing, Holt, Rinehart and Winston, USA, 1985.

[10] [Online]. Available from: http://de.wikipedia.org/wiki/Stokes-Verschiebung

[11] Arimori, S., Bosch, L.I., Ward, C.J., and James, T.D. Fluorescent internal charge transfer (ICT) saccharide sensor. Tetrahedron Letters 42(27) (2001): 4553-4555.

[12] Joyce, L.A., Shabbir, S.H., and Anslyn, E.V. The uses of supramolecular chemistry in synthetic methodology development: examples of anion and

neutral molecular recognition. Chemical Society Reviews 39(10) (2010): 3621-3632.

[13] Chen, K.-Y. and Tsai, H.-Y. Synthesis, X-ray Structure, Spectroscopic Properties and DFT Studies of a Novel Schiff Base. International Journal of Molecular Sciences 15(10) (2014): 18706-18724.

[14] Yang, G., Morlet-Savary, F., Peng, Z., Wu, S., and Fouassier, J.-P. Triplet-triplet absorption of 2-(2′-hydroxyphenyl) benzoxazole (HBO) in polar solvents. Chemical Physics Letters 256(4–5) (1996): 536-542.

[15] Li, Z. and Wu, S. The effect of molecular structure on the photophysical behavior of substituted styryl pyrazine derivatives. Journal of Fluorescence 7(3) (1997): 237-242.

[16] Wu, J., Liu, W., Ge, J., Zhang, H., and Wang, P. New sensing mechanisms for design of fluorescent chemosensors emerging in recent years. Chemical Society Reviews 40(7) (2011): 3483-3495.

[17] An, B.-K., Gierschner, J., and Park, S.Y. **π**-Conjugated Cyanostilbene Derivatives: A Unique Self-Assembly Motif for Molecular Nanostructures with Enhanced Emission and Transport. Accounts of Chemical Research 45(4) (2012): 544-554.

[18] Thomas, S.W., Joly, G.D., and Swager, T.M. Chemical Sensors Based on Amplifying Fluorescent Conjugated Polymers. Chemical Reviews 107(4) (2007): 1339-1386.

[19] Sapsford, K.E., Berti, L., and Medintz, I.L. Materials for Fluorescence Resonance Energy Transfer Analysis: Beyond Traditional Donor–Acceptor Combinations. Angewandte Chemie International Edition 45(28) (2006): 4562-4589.

[20] Tang, B.Z., Zhan, X., Yu, G., Sze Lee, P.P., Liu, Y., and Zhu, D. Efficient blue emission from siloles. Journal of Materials Chemistry 11(12) (2001): 2974-2978.

[21] Hong, Y., Lam, J.W.Y., and Tang, B.Z. Aggregation-induced emission. Chemical Society Reviews 40(11) (2011): 5361-5388.

[22] Dong, Y., et al. Aggregation-induced emissions of tetraphenylethene derivatives and their utilities as chemical vapor sensors and in organic light-emitting diodes. Applied Physics Letters 91(1) (2007): 011111.

[23] Kumar, M., Vij, V., and Bhalla, V. Vapor-Phase Detection of Trinitrotoluene by AIEE-Active Hetero-oligophenylene-Based Carbazole Derivatives. Langmuir 28(33) (2012): 12417-12421.

[24] Bhalla, V., Pramanik, S., and Kumar, M. Cyanide modulated fluorescent supramolecular assembly of a hexaphenylbenzene derivative for detection of trinitrotoluene at the attogram level. Chemical Communications 49(9) (2013): 895-897.

[25] Pramanik, S., Bhalla, V., and Kumar, M. Mercury assisted fluorescent supramolecular assembly of hexaphenylbenzene derivative for femtogram detection of picric acid. Analytica Chimica Acta 793(0) (2013): 99-106.

[26] Sahoo, S.K., Sharma, D., Bera, R.K., Crisponi, G., and Callan, J.F. Iron(iii) selective molecular and supramolecular fluorescent probes. Chemical Society Reviews 41(21) (2012): 7195-7227.

[27] Potter, R.G. and Hughes, T.S. Synthesis of Heterosubstituted Hexaarylbenzenes via Asymmetric Carbonylative Couplings of Benzyl Halides. Organic Letters 9(7) (2007): 1187-1190.

[28] Bhalla, V., Vij, V., Kumar, M., Sharma, P.R., and Kaur, T. Recognition of Adenosine Monophosphate and H2PO4– using Zinc Ensemble of New Hexaphenylbenzene Derivative: Potential Bioprobe and Multichannel Keypad System. Organic Letters 14(4) (2012): 1012-1015.

[29] Bhalla, V., Kaur, S., Vij, V., and Kumar, M. Mercury-Modulated Supramolecular Assembly of a Hexaphenylbenzene Derivative for Selective Detection of Picric Acid. Inorganic Chemistry 52(9) (2013): 4860-4865.

[30] Wade, L.G. Organic chemistry. 8 ed. USA, 2013.

[31] Wu, J.-S., et al. Fluorescence Turn On of Coumarin Derivatives by Metal Cations: A New Signaling Mechanism Based on C=N Isomerization. Organic Letters 9(1) (2007): 33-36.

[32] Lin, H.-Y., Cheng, P.-Y., Wan, C.-F., and Wu, A.-T. A turn-on and reversible fluorescence sensor for zinc ion. Analyst 137(19) (2012): 4415-4417.

[33] Choi, J.Y., Kim, D., and Yoon, J. A highly selective “turn-on” fluorescent chemosensor based on hydroxy pyrene–hydrazone derivative for Zn^{2+}. Dyes and Pigments 96(1) (2013): 176-179.

[34] Zhang, M., et al. A simple and effective fluorescent chemosensor for the cascade recognition of Zn^{2+} and $H_2PO_4^-$ ions in protic media. Tetrahedron 70(4) (2014): 1011-1015.

[35] Xiao, H., et al. A highly selective turn-on fluorescent probe for Al(iii) based on coumarin and its application in vivo. Analyst 139(8) (2014): 1980-1986.

[36] Chuentragool, P., Vongnam, K., Rashatasakhon, P., Sukwattanasinitt, M., and Wacharasindhu, S. Calcium carbide as a cost-effective starting material for symmetrical diarylethynes via Pd-catalyzed coupling reaction. Tetrahedron 67(42) (2011): 8177-8182.

[37] Kawano, N., Okigawa, M., Hasaka, N., Kouno, I., Kawahara, Y., and Fujita, Y. Atropisomerism of biphenyl compounds. An Important role of o-substituted methoxy groups and fluorine atoms. The Journal of Organic Chemistry 46(2) (1981): 389-392.

[38] Tang, B.Z., et al. Processible Nanostructured Materials with Electrical Conductivity and Magnetic Susceptibility: Preparation and Properties of Maghemite/Polyaniline Nanocomposite Films. Chemistry of Materials 11(6) (1999): 1581-1589.

[39] Keshtov, M.L., et al. Synthesis and photo- and electrophysical properties of conjugated copolyfluorenes with 7,8,10-triarylfluoranthene fragments in the main chain. Doklady Chemistry 442(2) (2012): 23-29.

[40] Kumar, S., Venkatramaiah, N., and Patil, S. Fluoranthene Based Derivatives for Detection of Trace Explosive Nitroaromatics. The Journal of Physical Chemistry C 117(14) (2013): 7236-7245.

[41] Kartha, K.K., Babu, S.S., Srinivasan, S., and Ajayaghosh, A. Attogram Sensing of Trinitrotoluene with a Self-Assembled Molecular Gelator. Journal of the American Chemical Society 134(10) (2012): 4834-4841.

[42] Bhalla, V., Gupta, A., and Kumar, M. Fluorescent Nanoaggregates of Pentacenequinone Derivative for Selective Sensing of Picric acid in Aqueous Media. Organic Letters 14(12) (2012): 3112-3115.

[43] Wang, J., et al. Hyperbranched polytriazoles with high molecular compressibility: aggregation-induced emission and superamplified explosive detection. Journal of Materials Chemistry 21(12) (2011): 4056-4059.

[44] Ma, Y., Li, H., Peng, S., and Wang, L. Highly Selective and Sensitive Fluorescent Paper Sensor for Nitroaromatic Explosive Detection. Analytical Chemistry 84(19) (2012): 8415-8421.

[45] Gao, D., Wang, Z., Liu, B., Ni, L., Wu, M., and Zhang, Z. Resonance Energy Transfer-Amplifying Fluorescence Quenching at the Surface of Silica Nanoparticles toward Ultrasensitive Detection of TNT. Analytical Chemistry 80(22) (2008): 8545-8553.

[46] Pinrat, O., Boonkitpatarakul, K., Paisuwan, W., Sukwattanasinitt, M., and Ajavakom, A. Glucopyranosyl-1,4-dihydropyridine as a new fluorescent chemosensor for selective detection of 2,4,6-trinitrophenol. Analyst 140(6) (2015): 1886-1893.

[47] Kumar, Y.P., King, P., and Prasad, V.S.R.K. Zinc biosorption on Tectona grandis L.f. leaves biomass: Equilibrium and kinetic studies. Chemical Engineering Journal 124(1–3) (2006): 63-70.

[48] Tsay, O.G., Manjare, S.T., Kim, H., Lee, K.M., Lee, Y.S., and Churchill, D.G. Novel Reversible Zn2+-Assisted Biological Phosphate “Turn-On” Probing through Stable Aryl-hydrazone Salicylaldimine Conjugation That Attenuates Ligand Hydrolysis. Inorganic Chemistry 52(17) (2013): 10052-10061.

[49] Goswami, S., et al. Ratiometric and absolute water-soluble fluorescent tripodal zinc sensor and its application in killing human lung cancer cells. Analyst 138(16) (2013): 4593-4598.

[50] Pramanik, S., Bhalla, V., and Kumar, M. Hexaphenylbenzene-Based Fluorescent Aggregates for Ratiometric Detection of Cyanide Ions at Nanomolar Level: Set–Reset Memorized Sequential Logic Device. ACS Applied Materials & Interfaces 6(8) (2014): 5930-5939.

[51] Stein, K. and Schwedt, G. Comparison of immobilization methods for the development of an acetylcholinesterase biosensor. Analytica Chimica Acta 272(1) (1993): 73-81.

[52] Steiner, W.E., Klopsch, S.J., English, W.A., Clowers, B.H., and Hill, H.H. Detection of a Chemical Warfare Agent Simulant in Various Aerosol Matrixes by Ion Mobility Time-of-Flight Mass Spectrometry. Analytical Chemistry 77(15) (2005): 4792-4799.

[53] Chen, W.-H., Xing, Y., and Pang, Y. A Highly Selective Pyrophosphate Sensor Based on ESIPT Turn-On in Water. Organic Letters 13(6) (2011): 1362-1365.

[54] Datta, B.K., Mukherjee, S., Kar, C., Ramesh, A., and Das, G. Zn^{2+} and Pyrophosphate Sensing: Selective Detection in Physiological Conditions and Application in DNA-Based Estimation of Bacterial Cell Numbers. Analytical Chemistry 85(17) (2013): 8369-8375.

APPENDIX

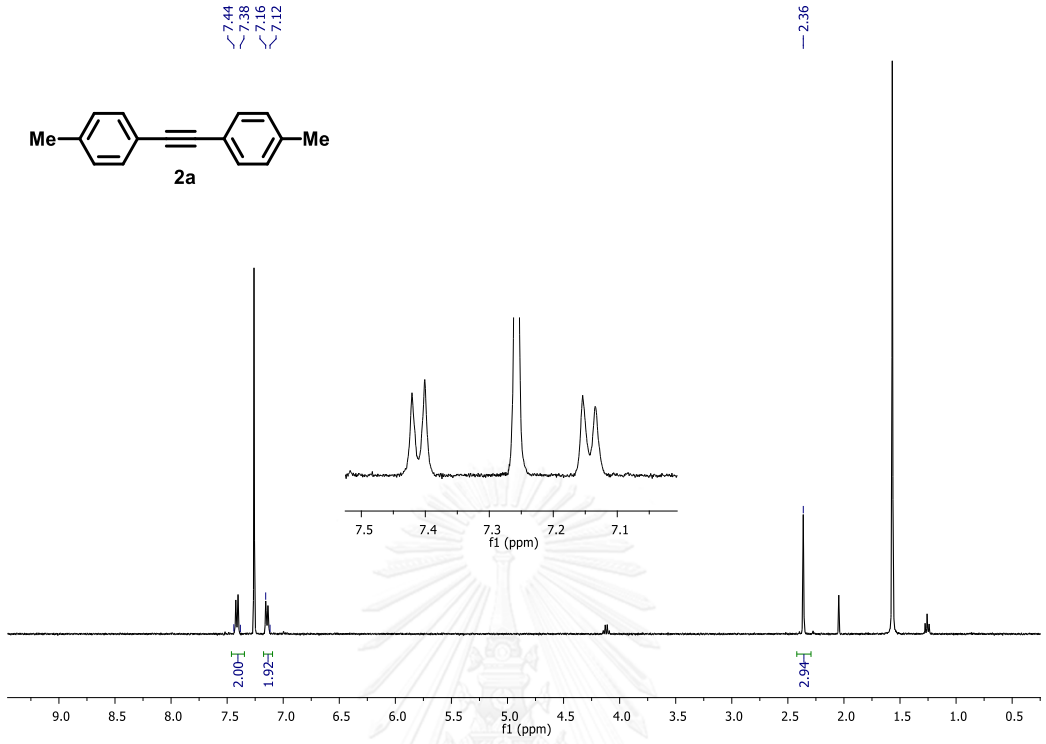

Figure S.1 ^{1}H-NMR spectrum of 1,2-di-p-tolylethyn (**2a**)

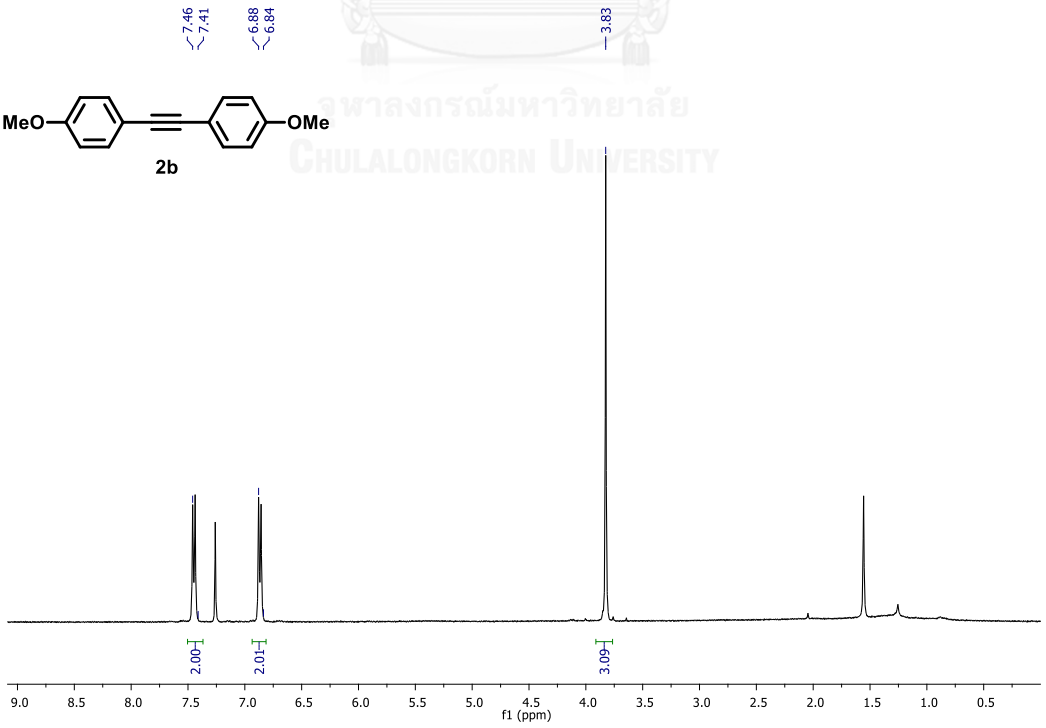

Figure S.2 ^{1}H-NMR spectrum of 1,2-bis(4-methoxyphenyl)ethyne (**2b**)

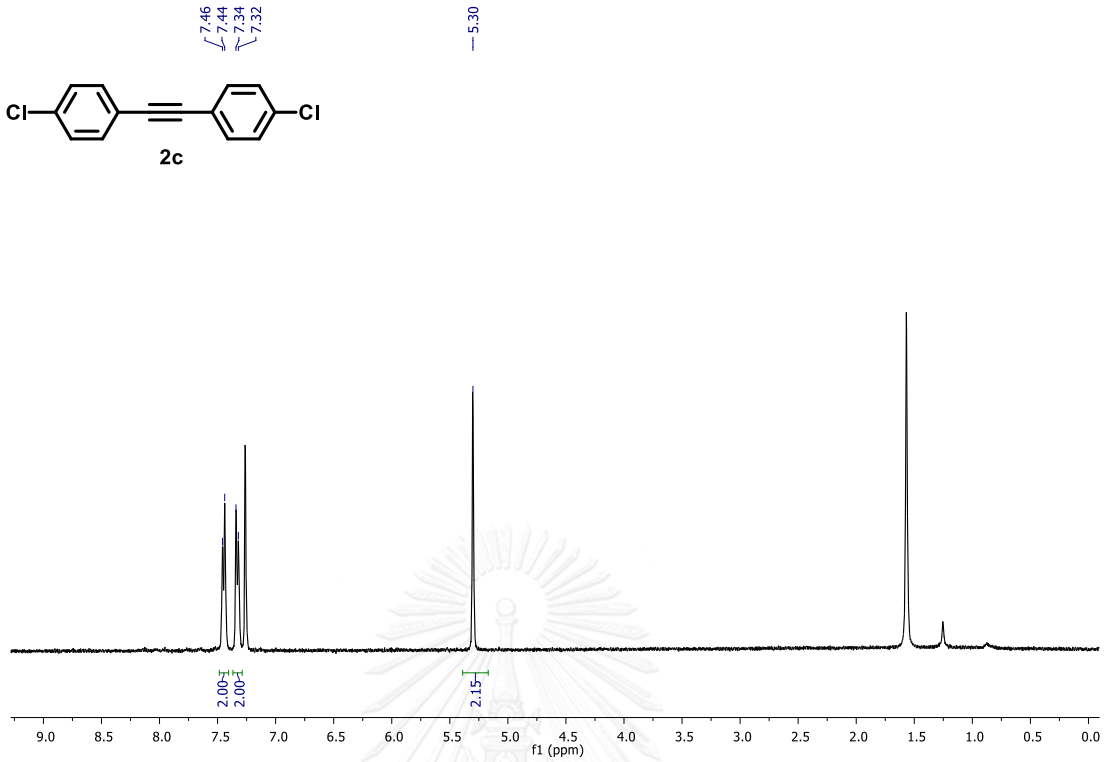

Figure S.3 ^{1}H-NMR spectrum of 1,2-bis(4-chlorophenyl)ethyne (**2c**)

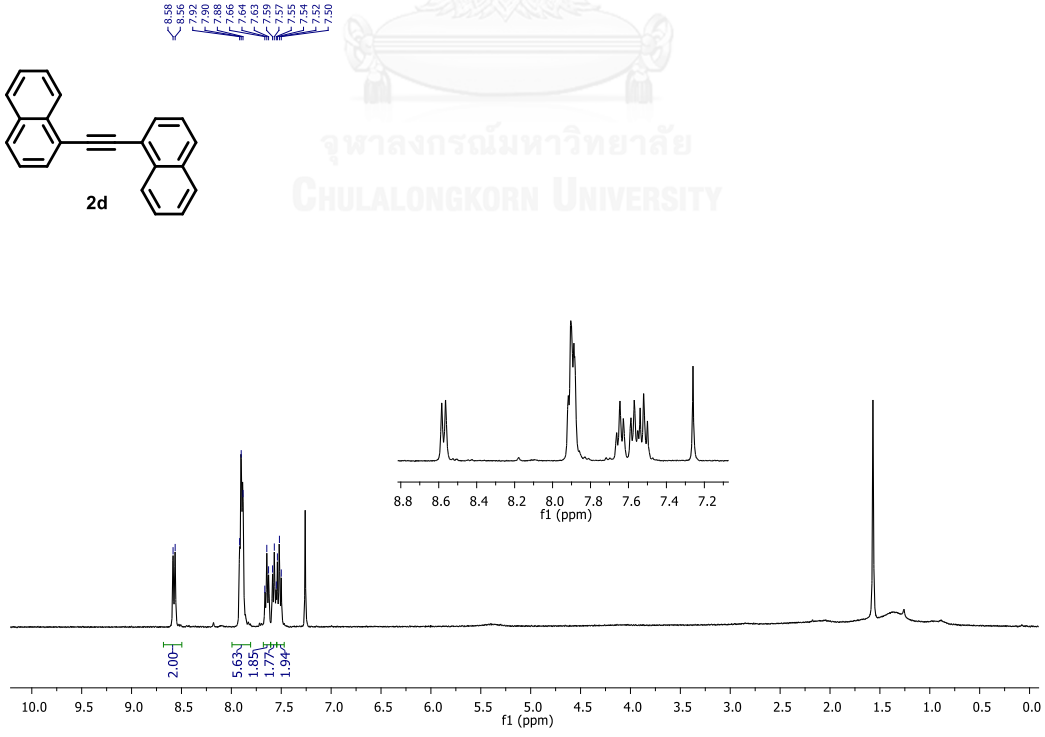

Figure S.4 ^{1}H-NMR spectrum of 1,2-di(naphthalen-1-yl)ethyne (**2d**)

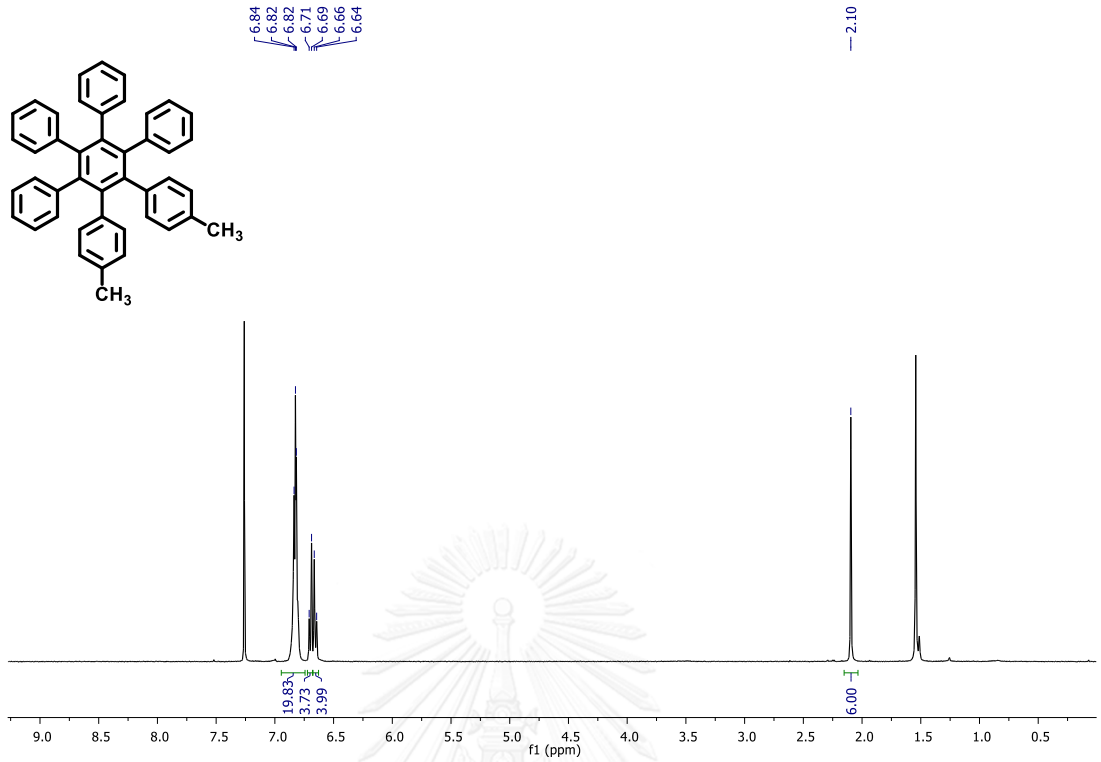

Figure S.5 ^{1}H-NMR spectrum of **HPB-2Me**

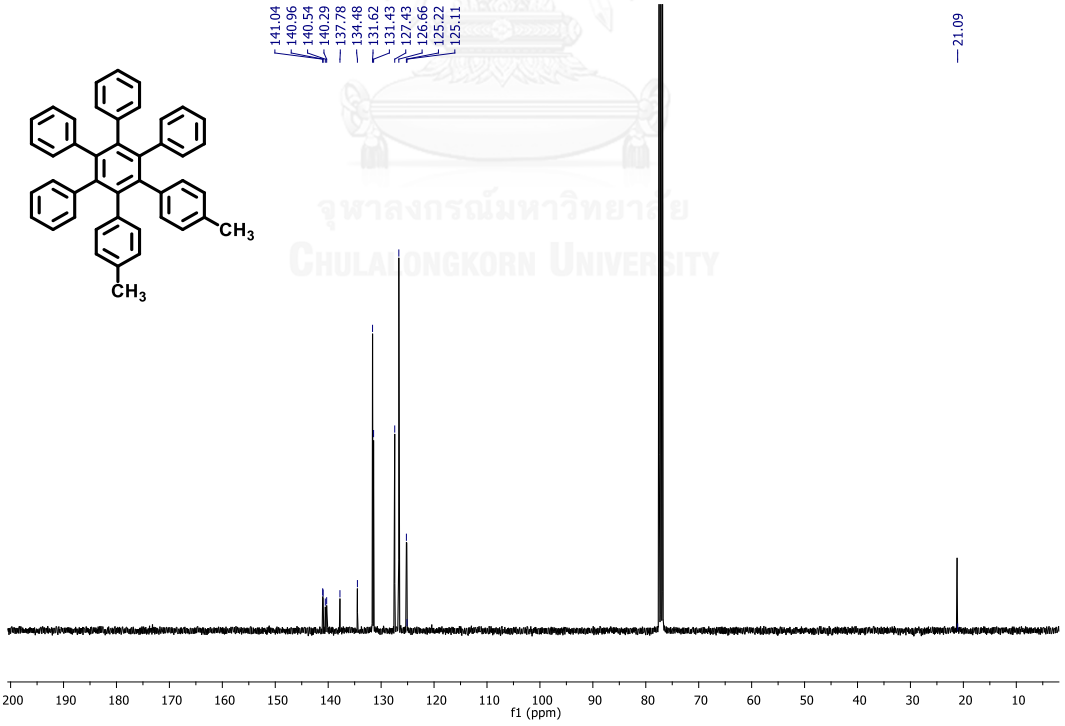

Figure S.6 ^{13}C-NMR spectrum of **HPB-2Me**

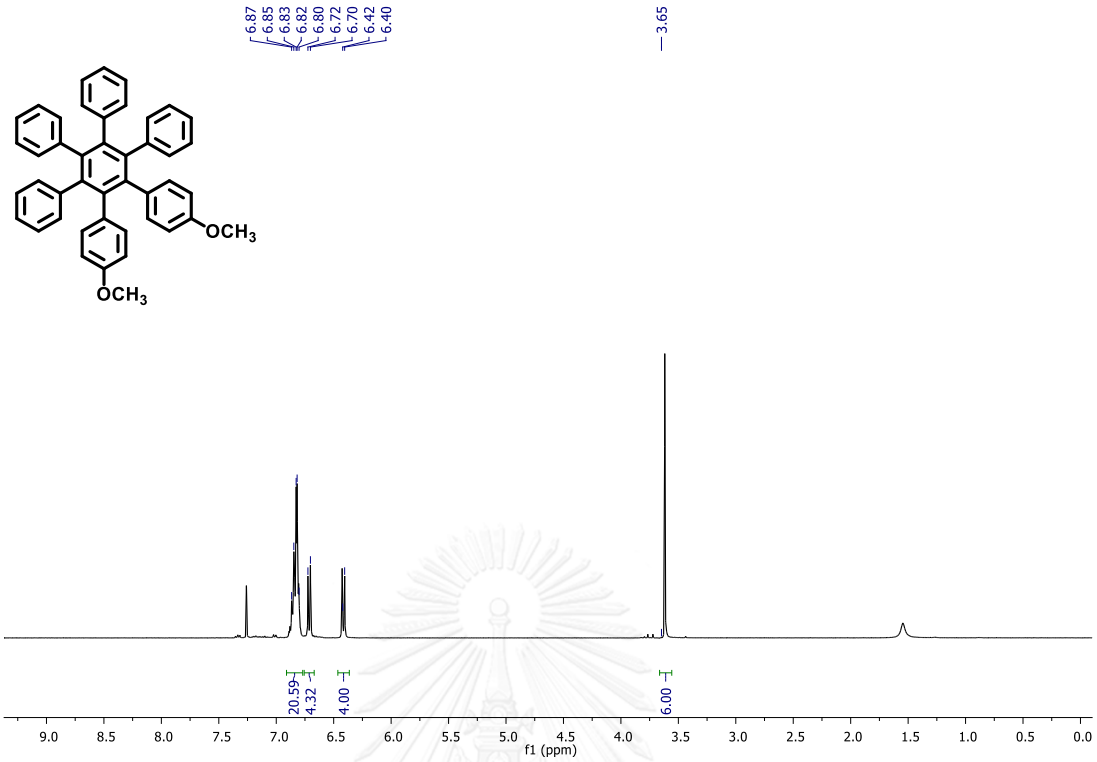

Figure S.7 ^{1}H-NMR spectrum of **HPB-2OMe**

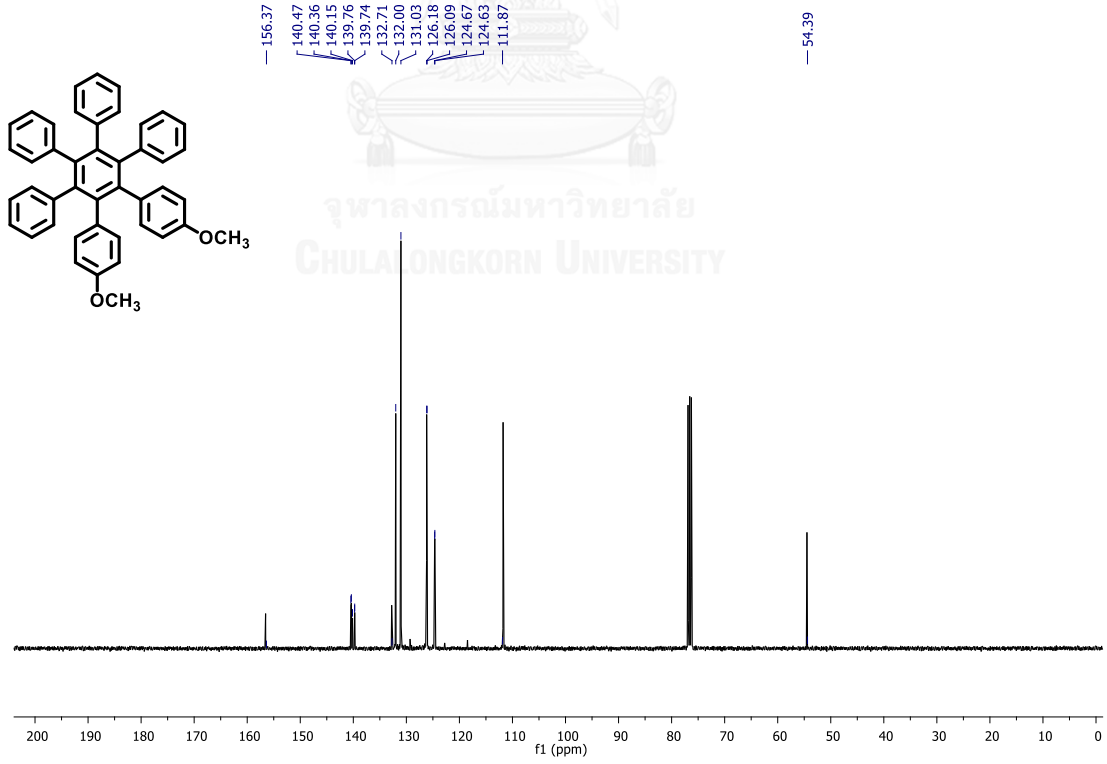

Figure S.8 ^{13}C-NMR spectrum of **HPB-2OMe**

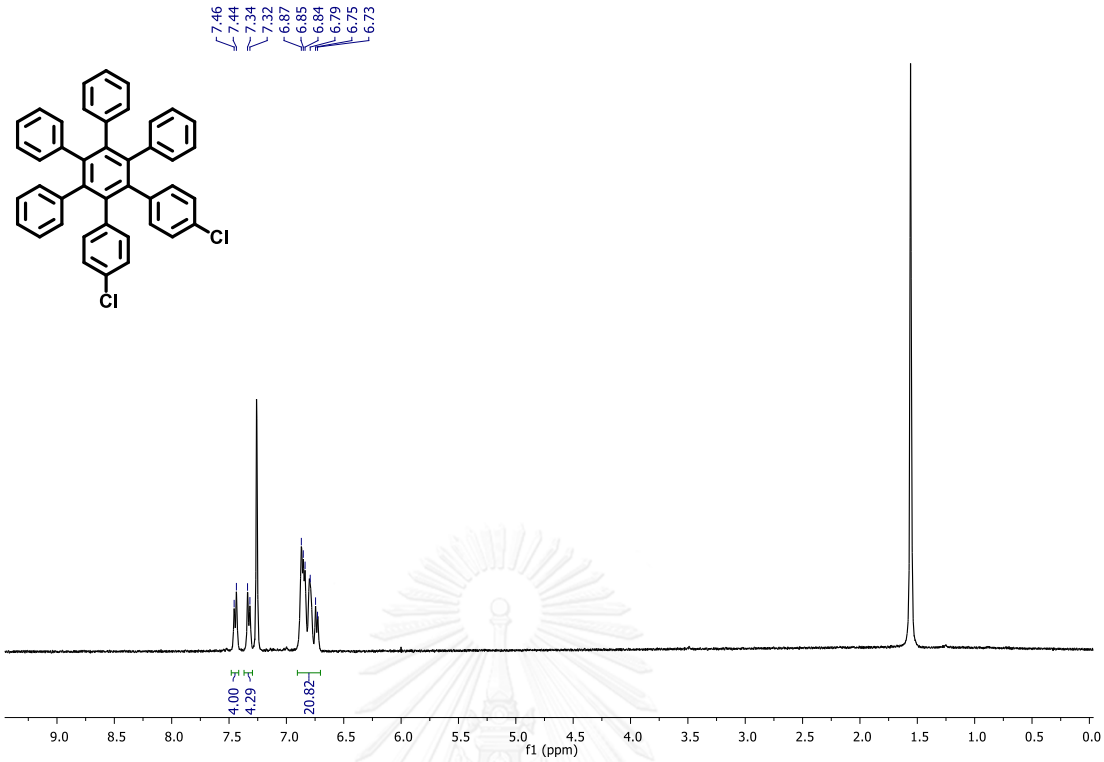

Figure S.9 ^{1}H-NMR spectrum of **HPB-2Cl**

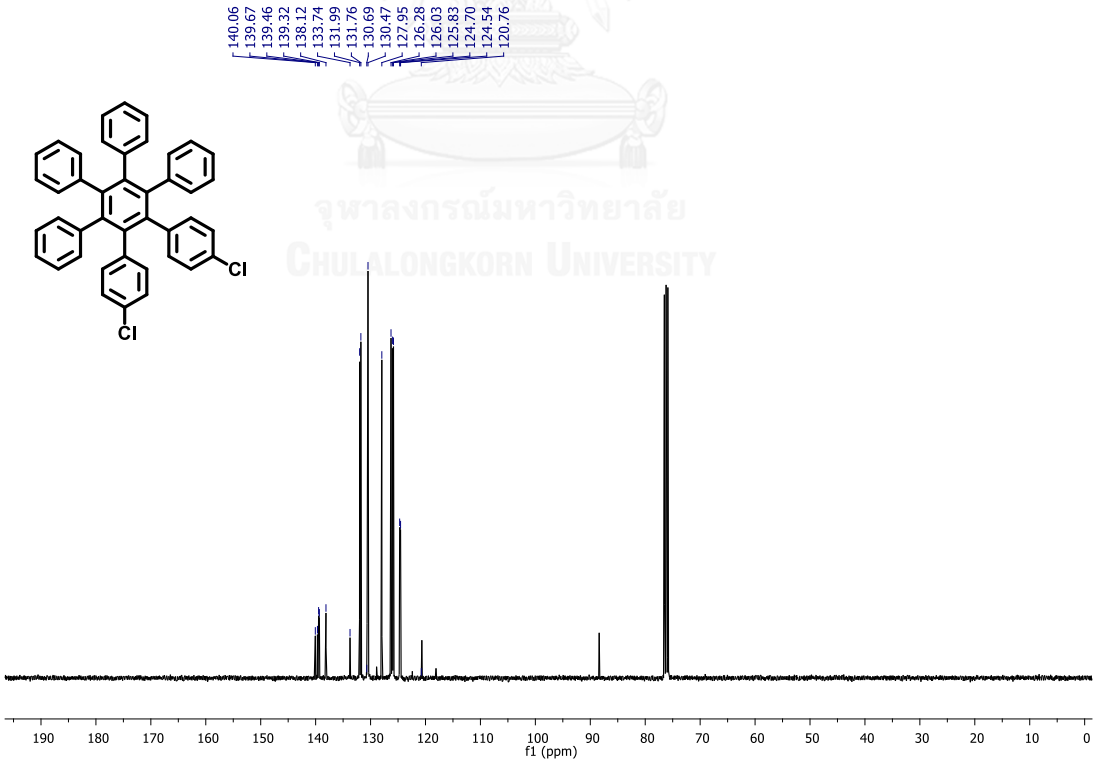

Figure S.10 ^{13}C-NMR spectrum of **HPB-2Cl**

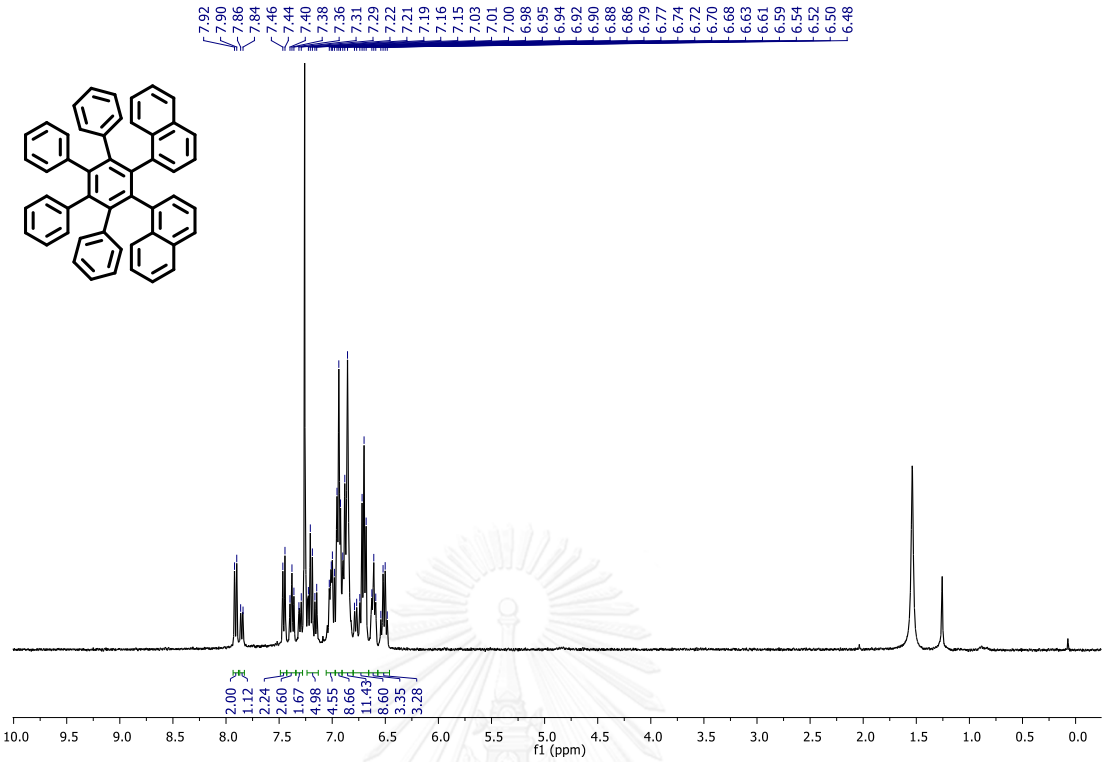

Figure S.11 ^{1}H-NMR spectrum of HPB-2NAP

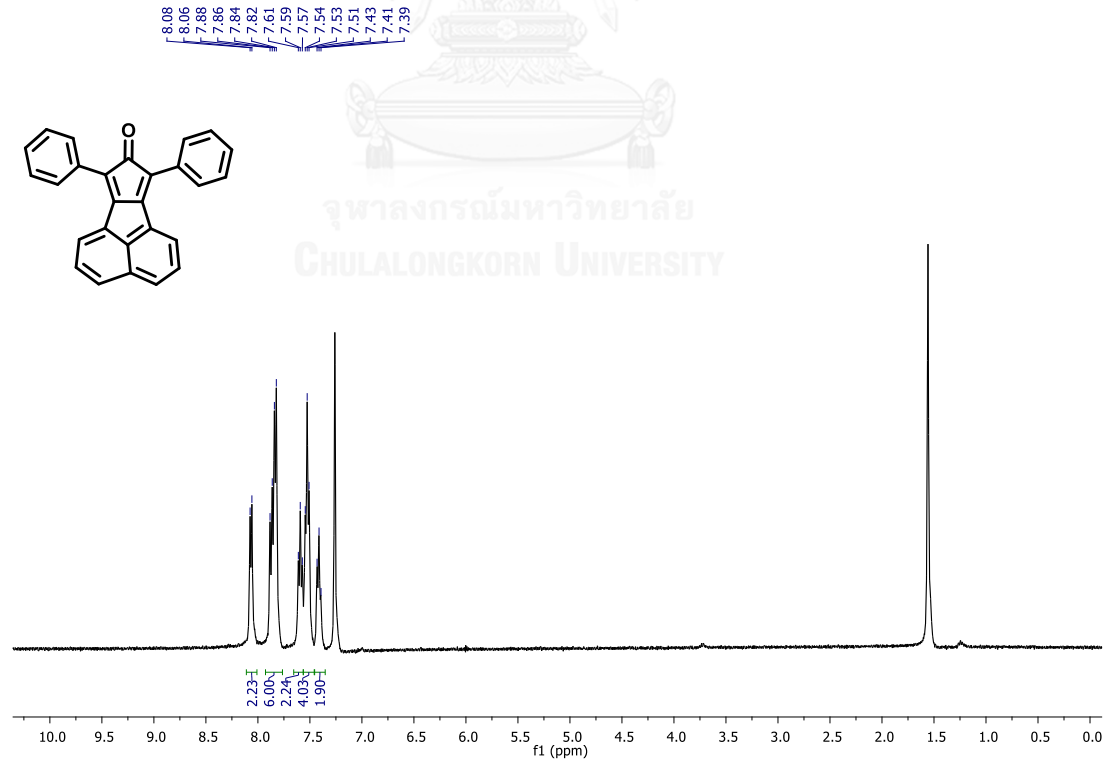

Figure S.12 ^{1}H-NMR spectrum of 7, 9-diphenyl-8H-cyclopenta[l]acenaphthylen-8-one

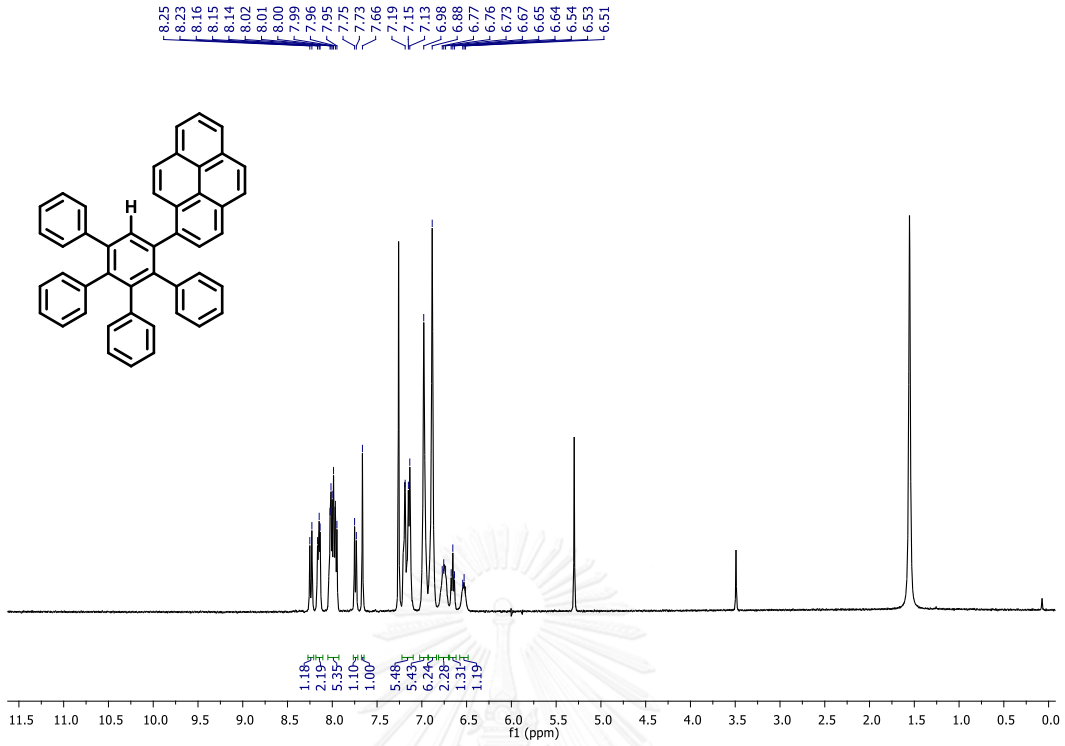

Figure S.13 ^{1}H-NMR spectrum of **FL1**

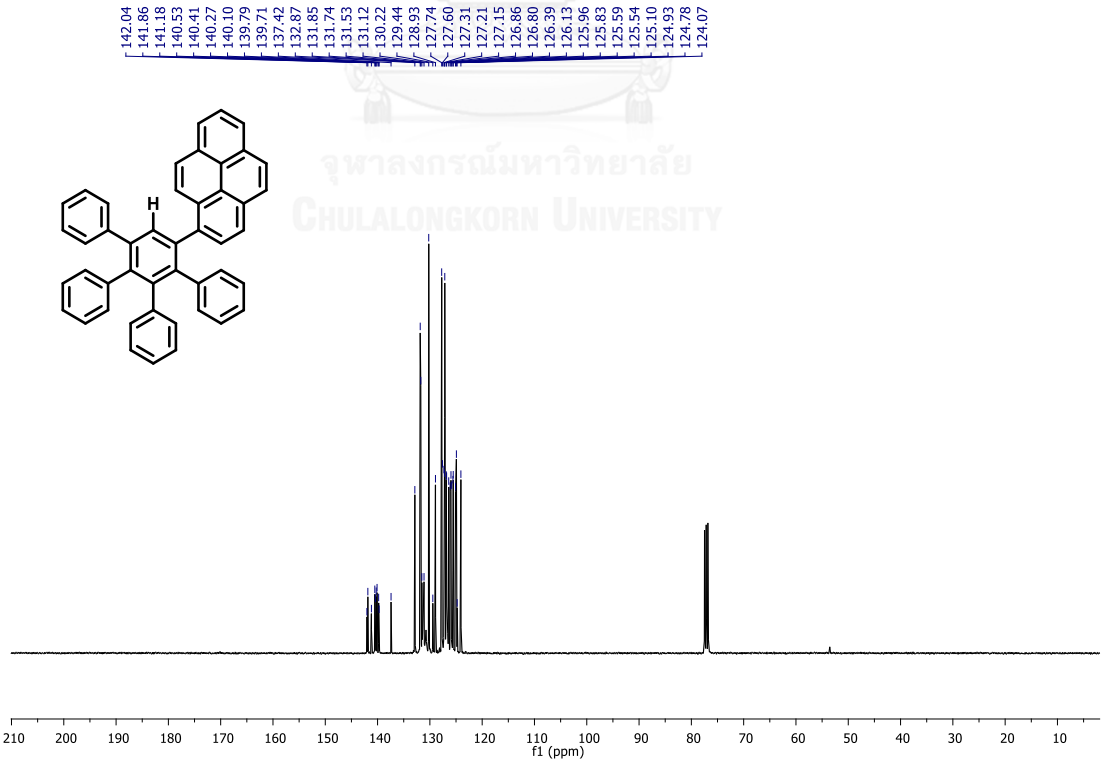

Figure S.14 ^{13}C-NMR spectrum of **FL1**

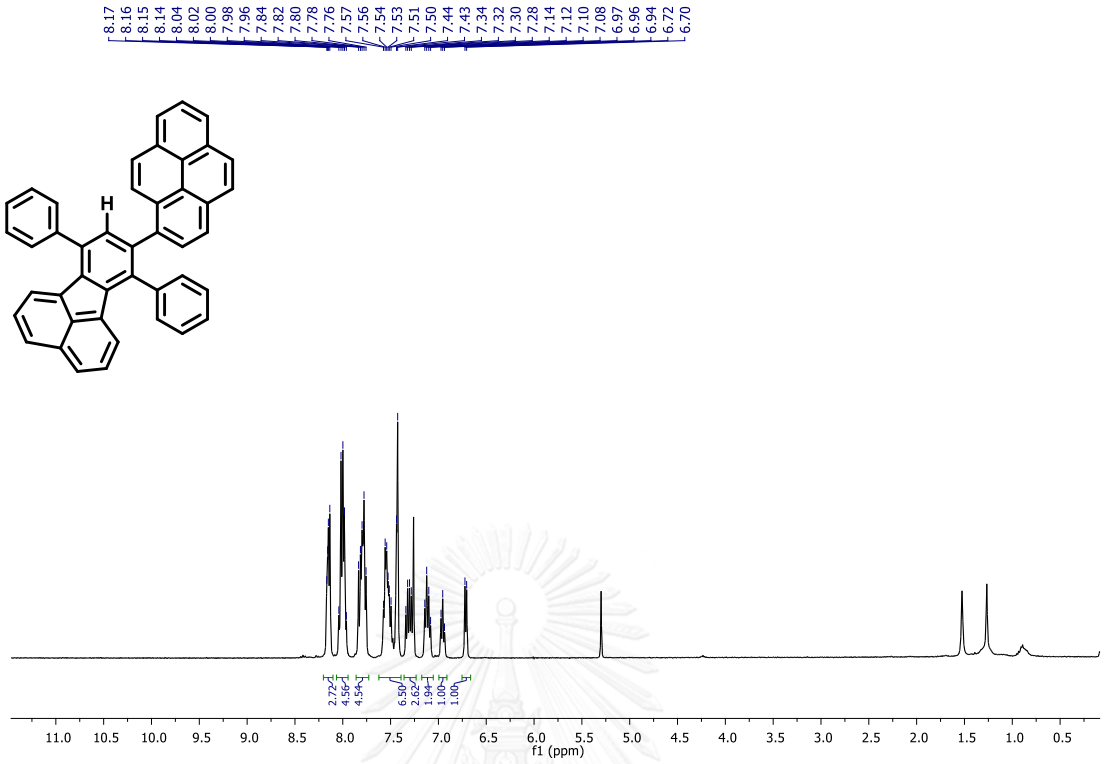

Figure S.15 ^{1}H-NMR spectrum of **FL2**

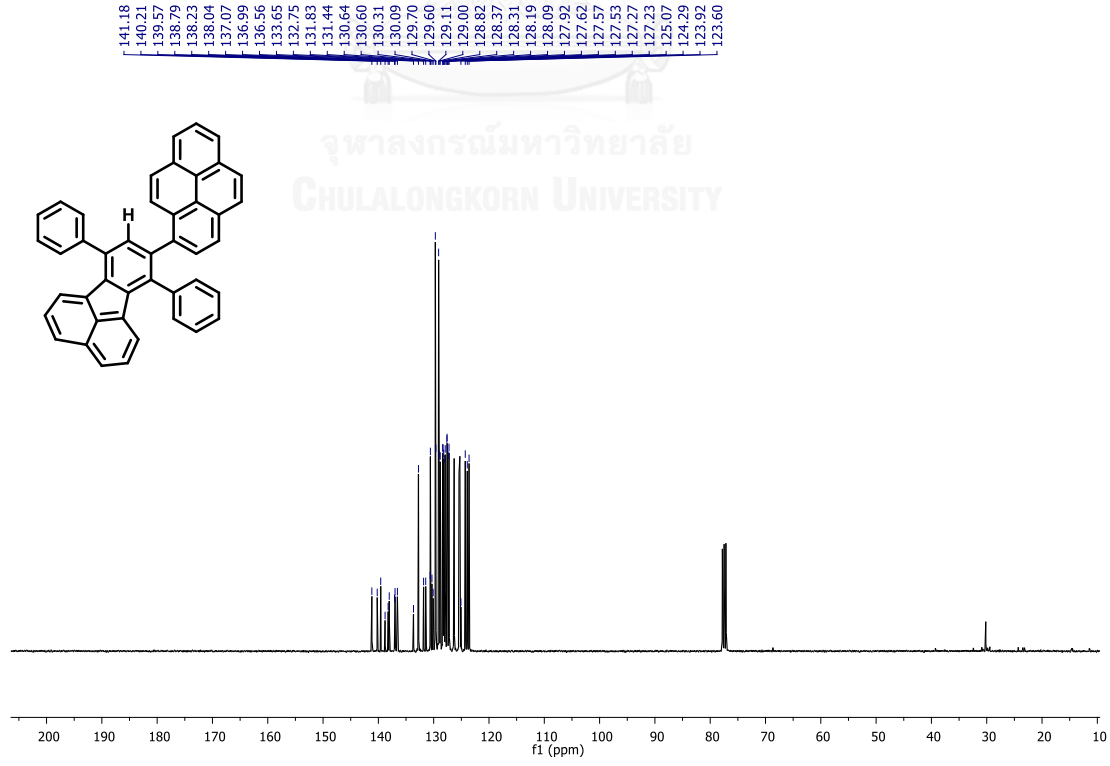

Figure S.16 ^{13}C-NMR spectrum of **FL2**

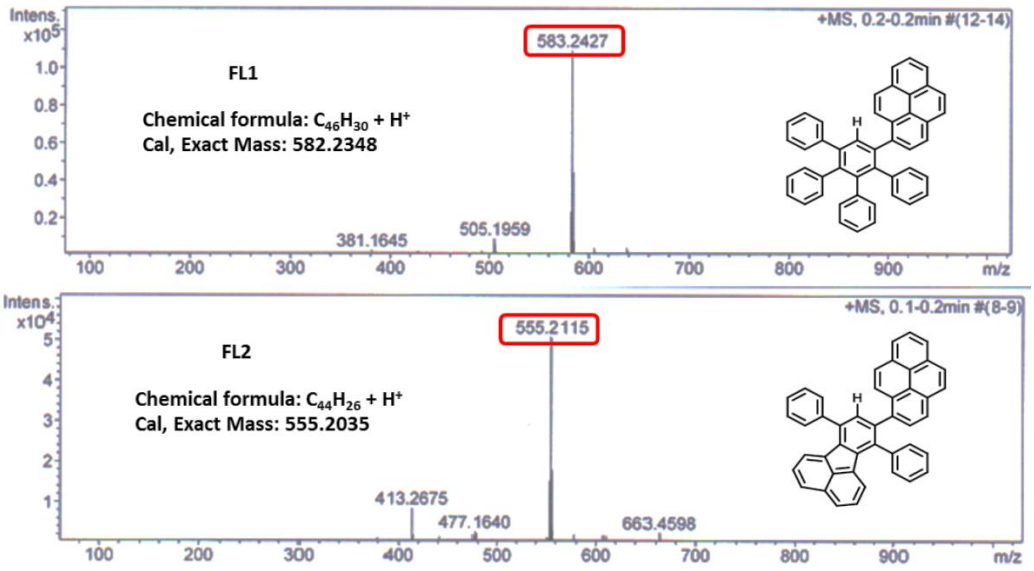

Figure S.17 the HRMS of **FL1** and **FL2**

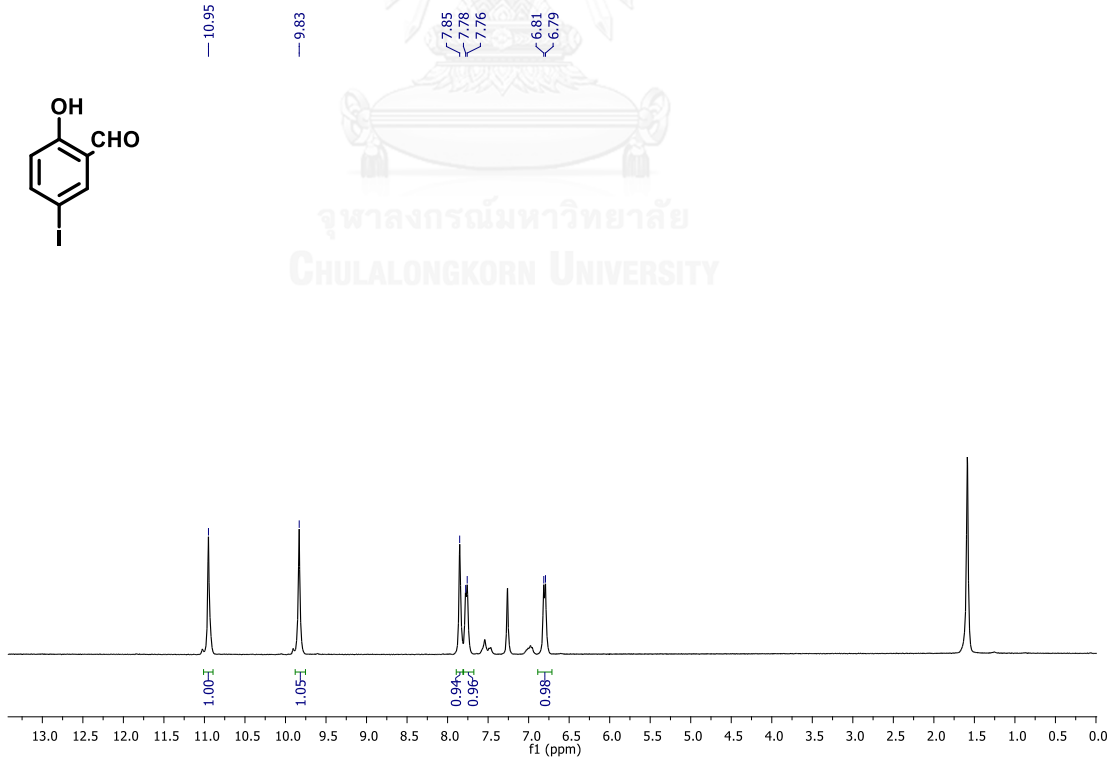

Figure S.18 ^{1}H-NMR spectrum of compound 1

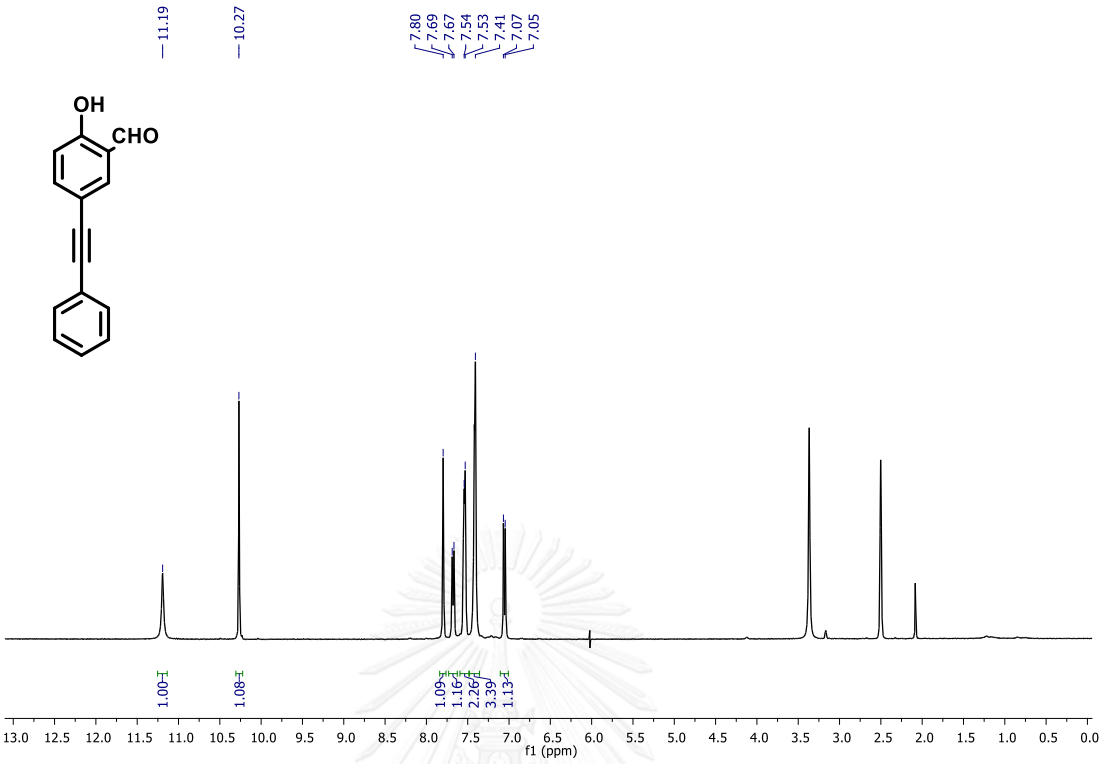

Figure S.19 ^{1}H-NMR spectrum of compound 2

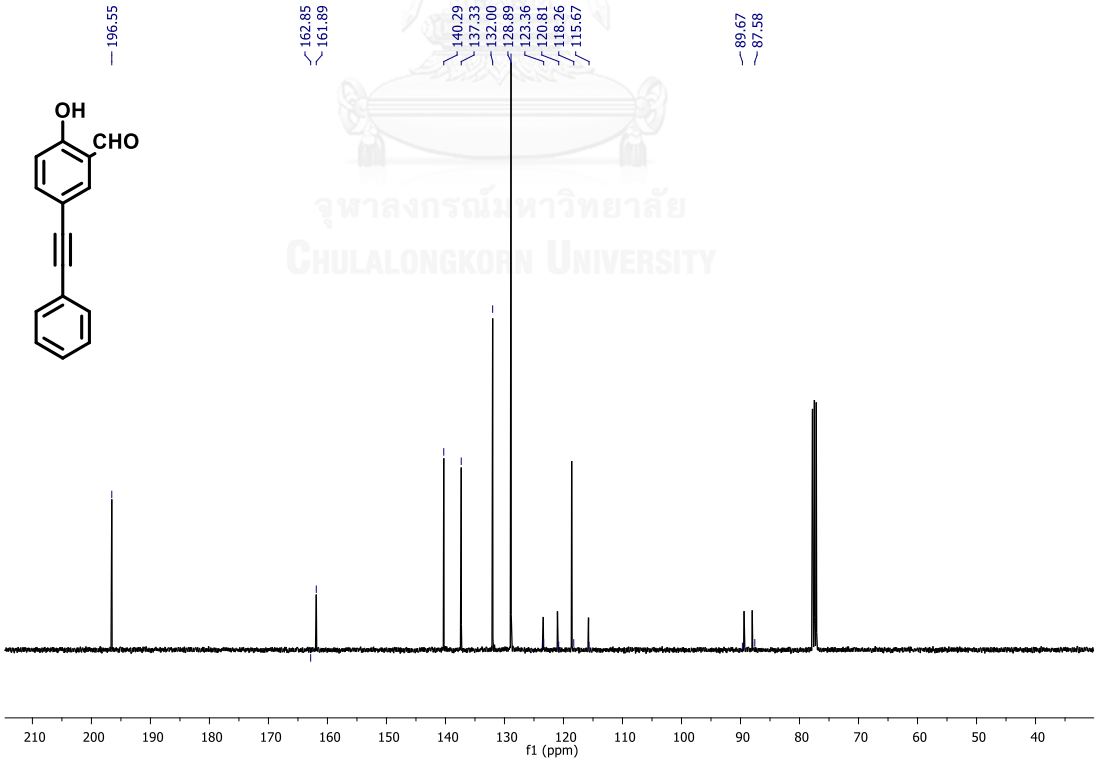

Figure S.20 ^{13}C-NMR spectrum of compound 2

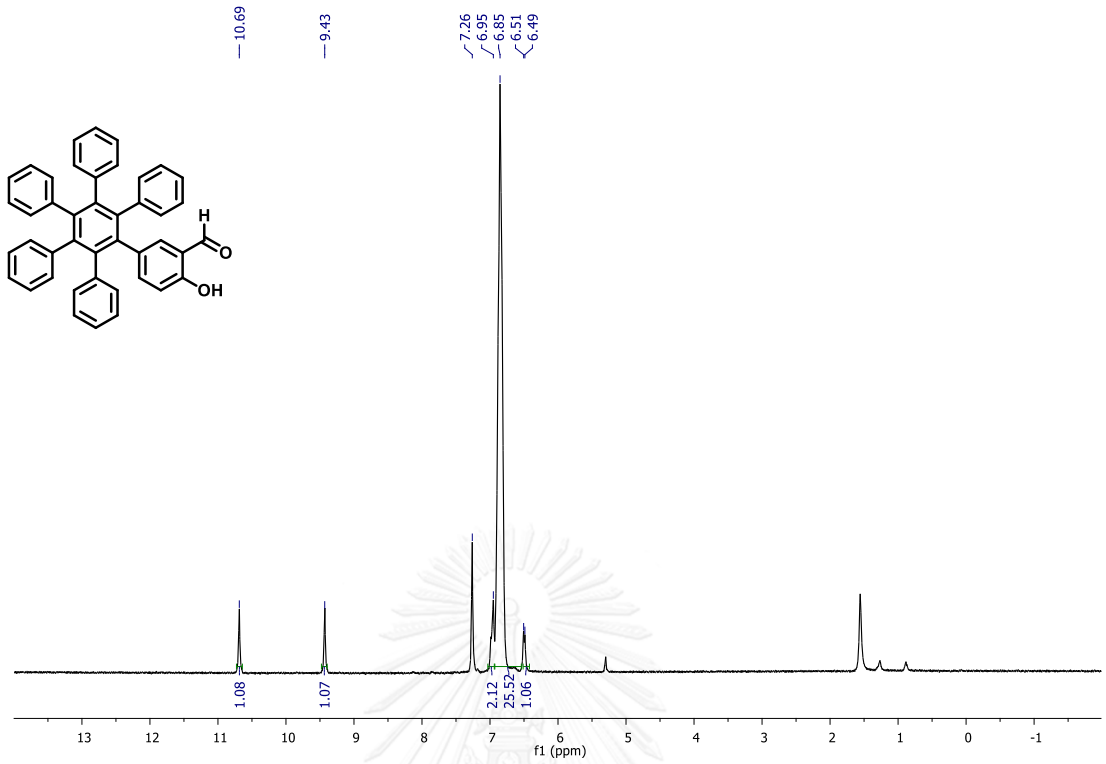

Figure S.21 ^{1}H-NMR spectrum of SW1

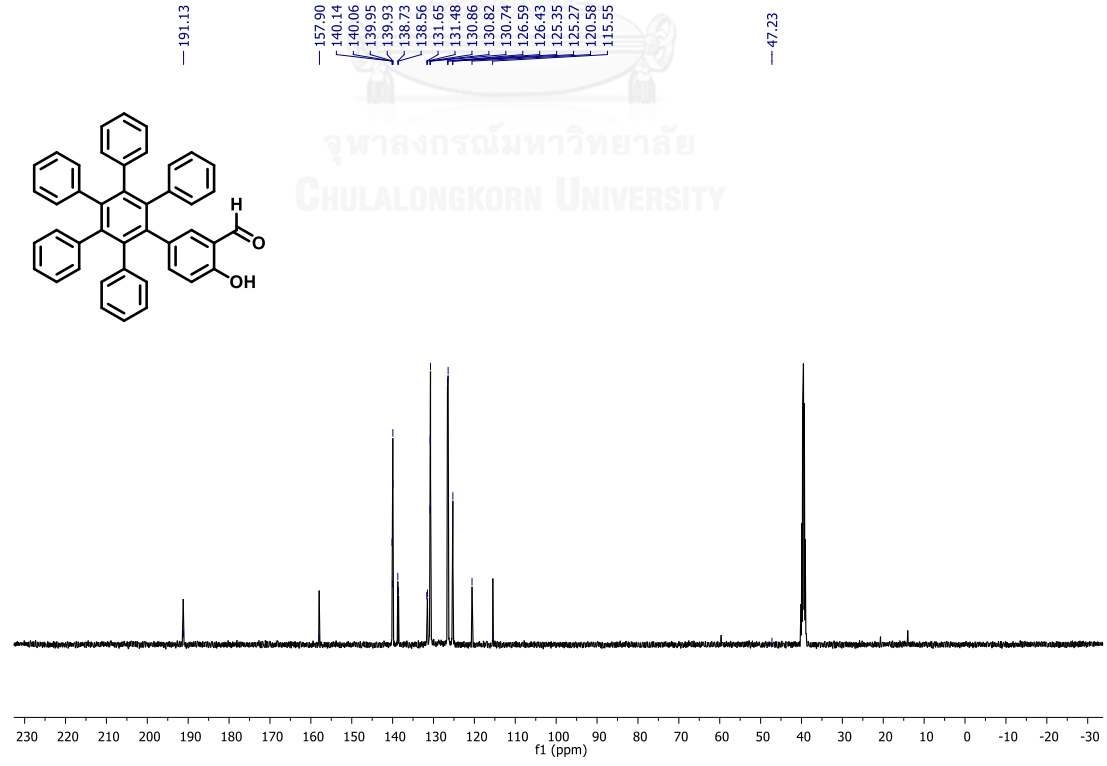

Figure S.22 ^{13}C-NMR spectrum of SW1

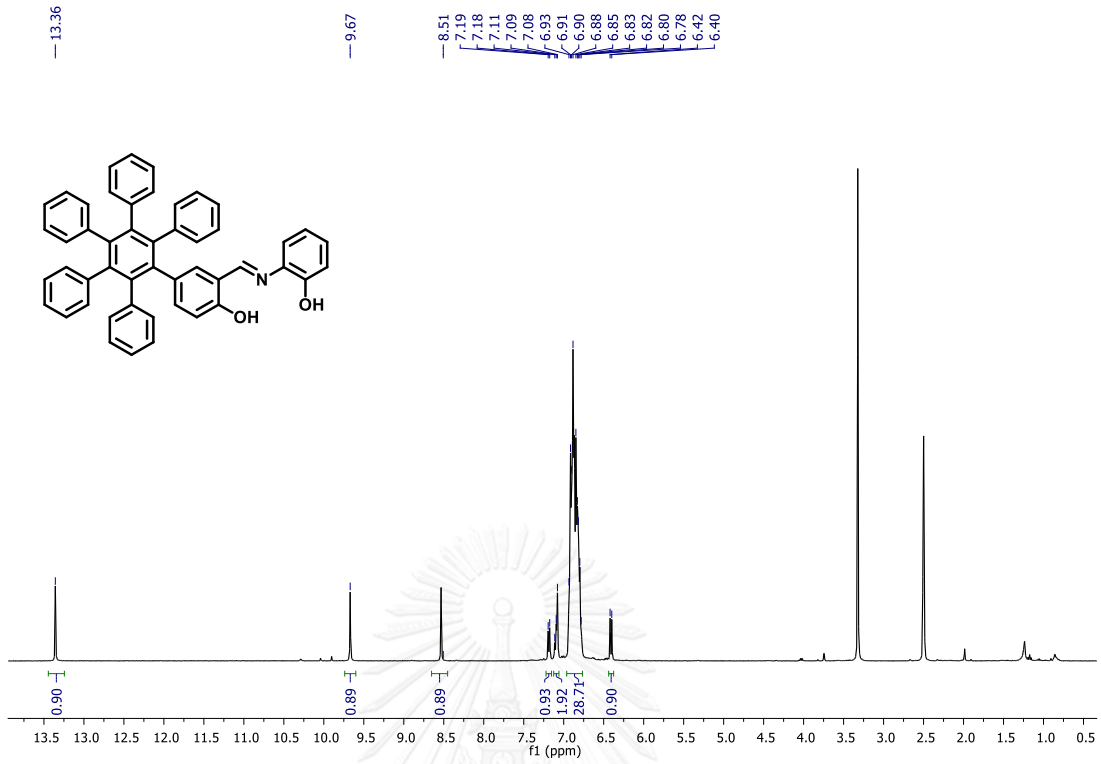

Figure S.23 ^{1}H-NMR spectrum of SW2

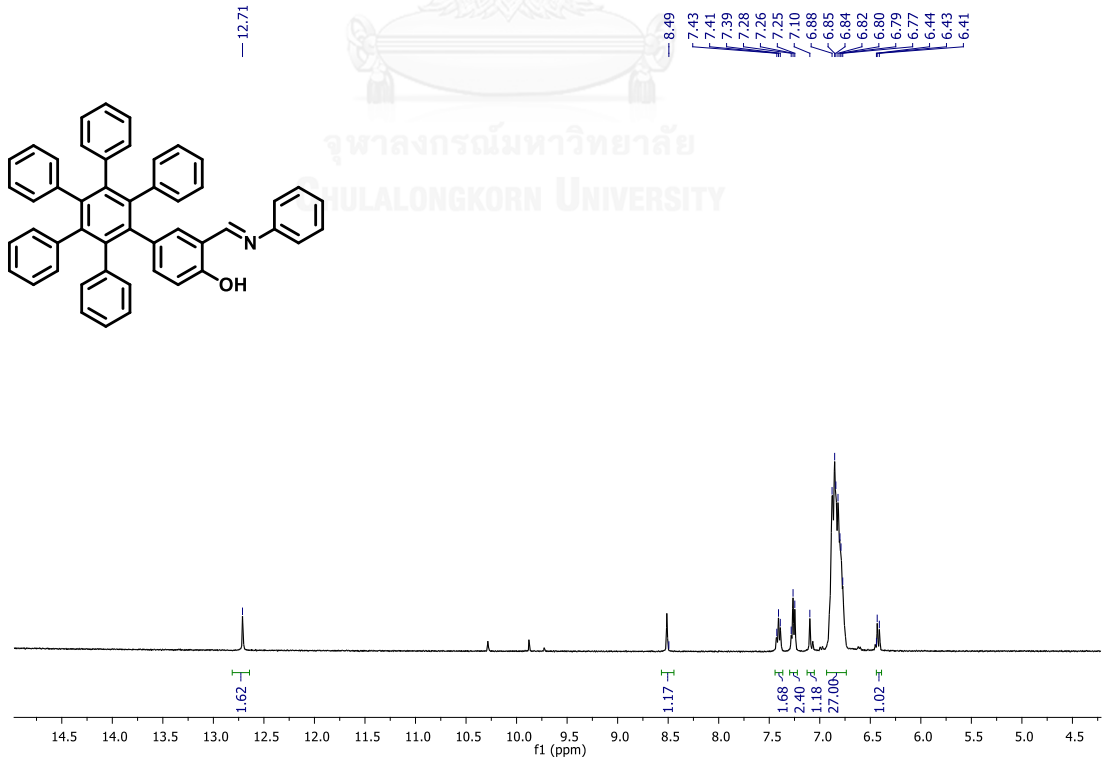

Figure S.24 ^{1}H-NMR spectrum of SW3

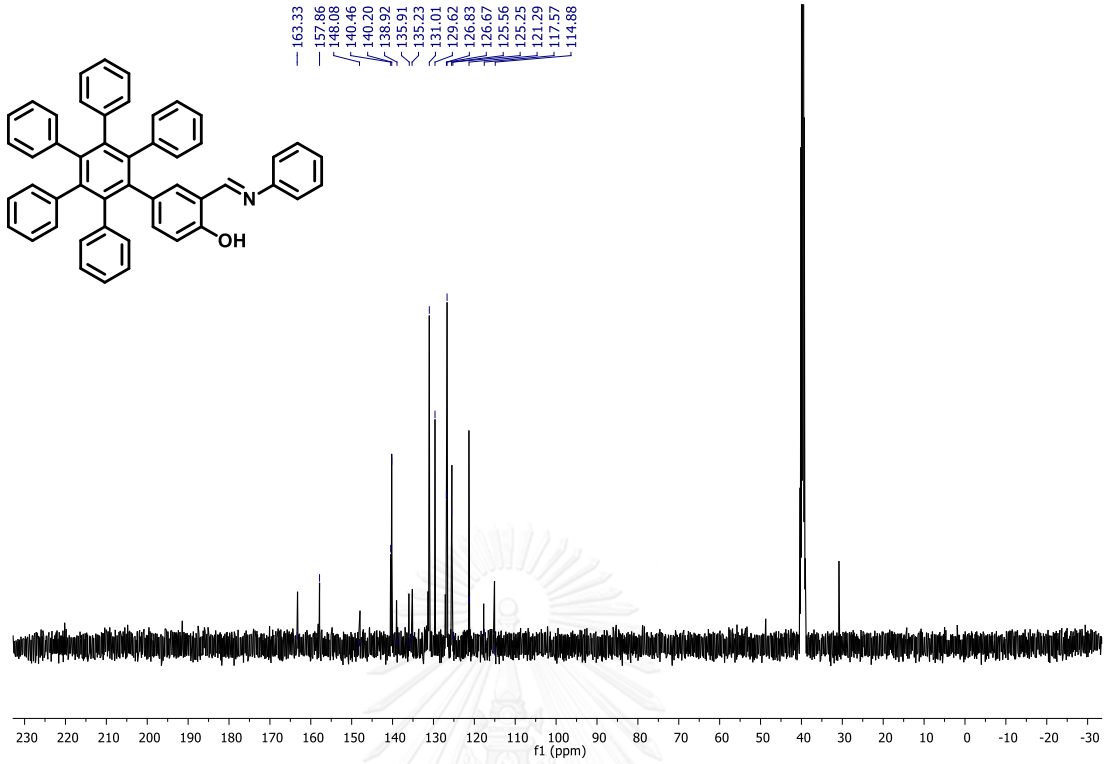

Figure S.25 ^{13}C-NMR spectrum of SW3

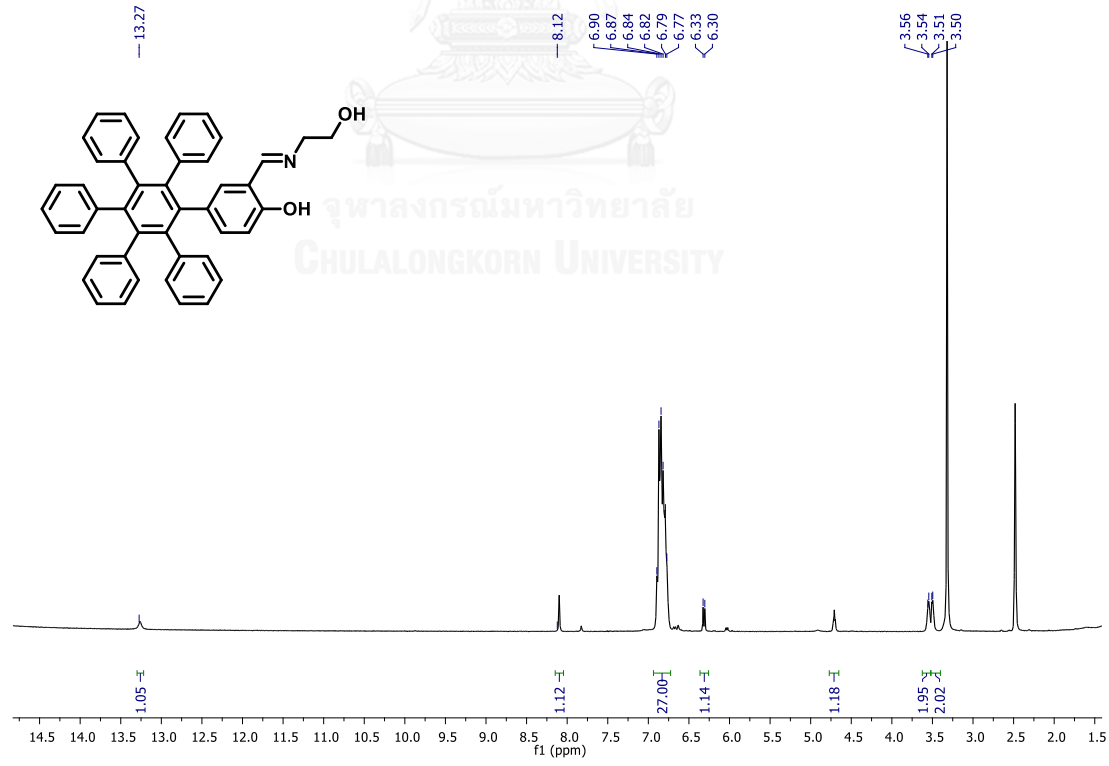

Figure S.26 ^{1}H-NMR spectrum of SW4

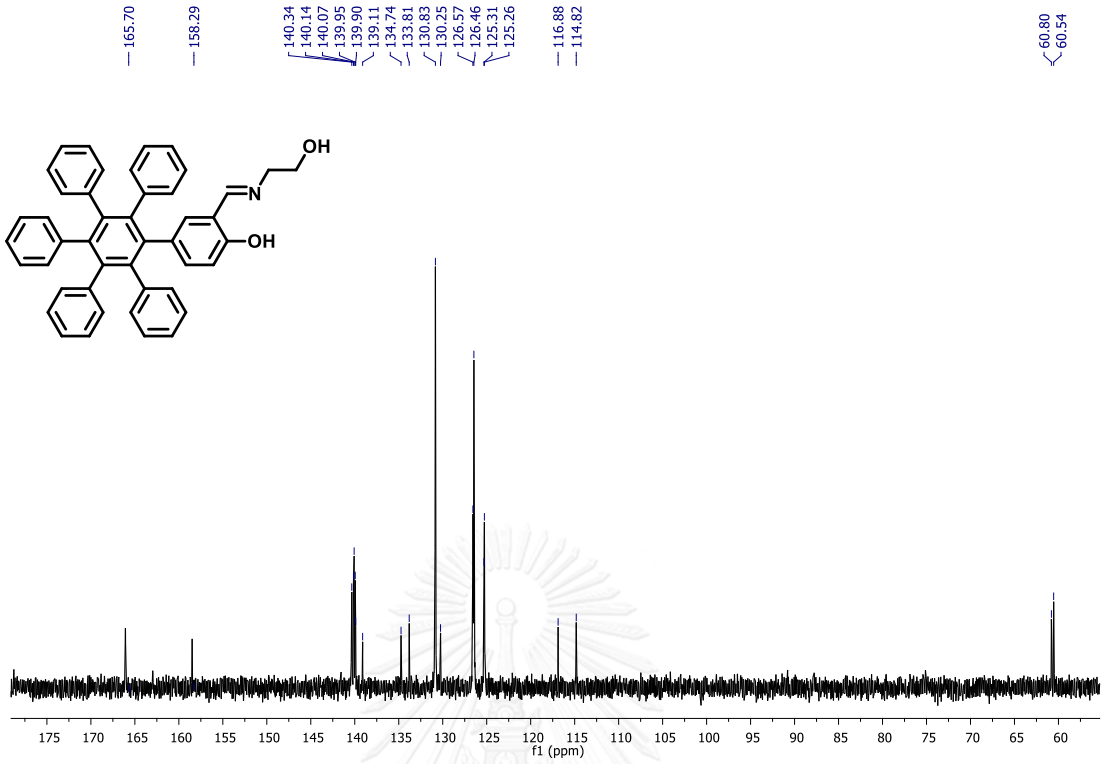

Figure S.27 ^{13}C-NMR spectrum of SW4

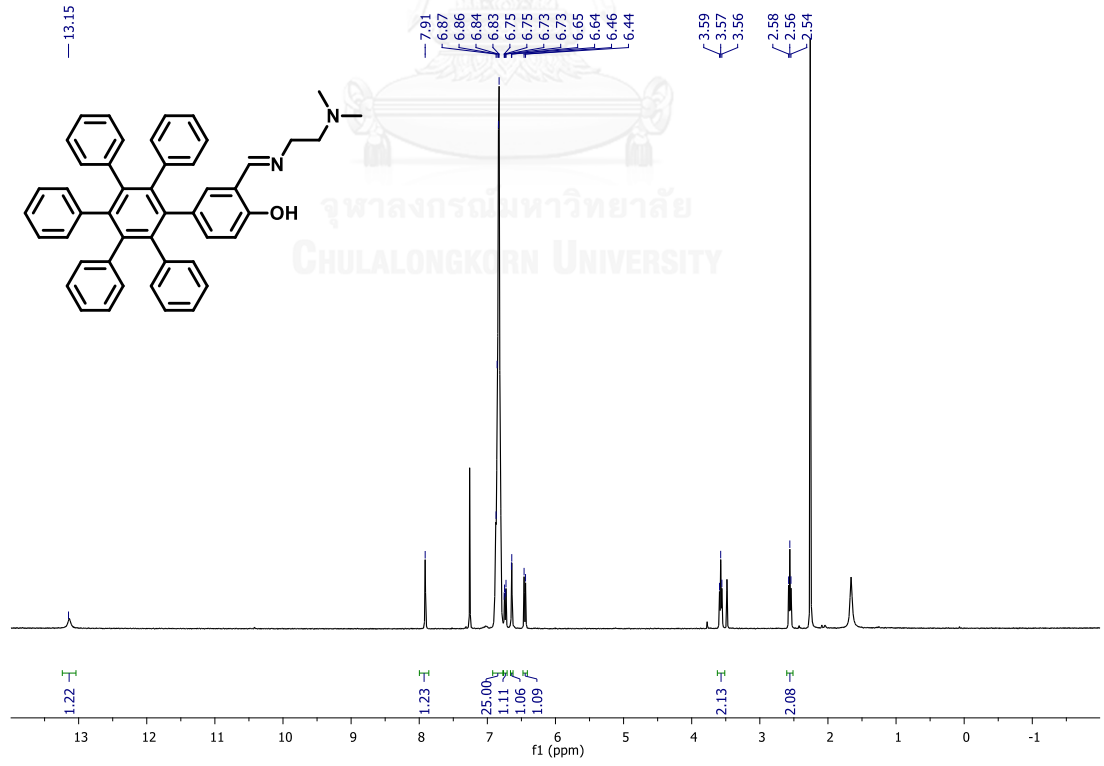

Figure S.28 ^{1}H-NMR spectrum of SW5

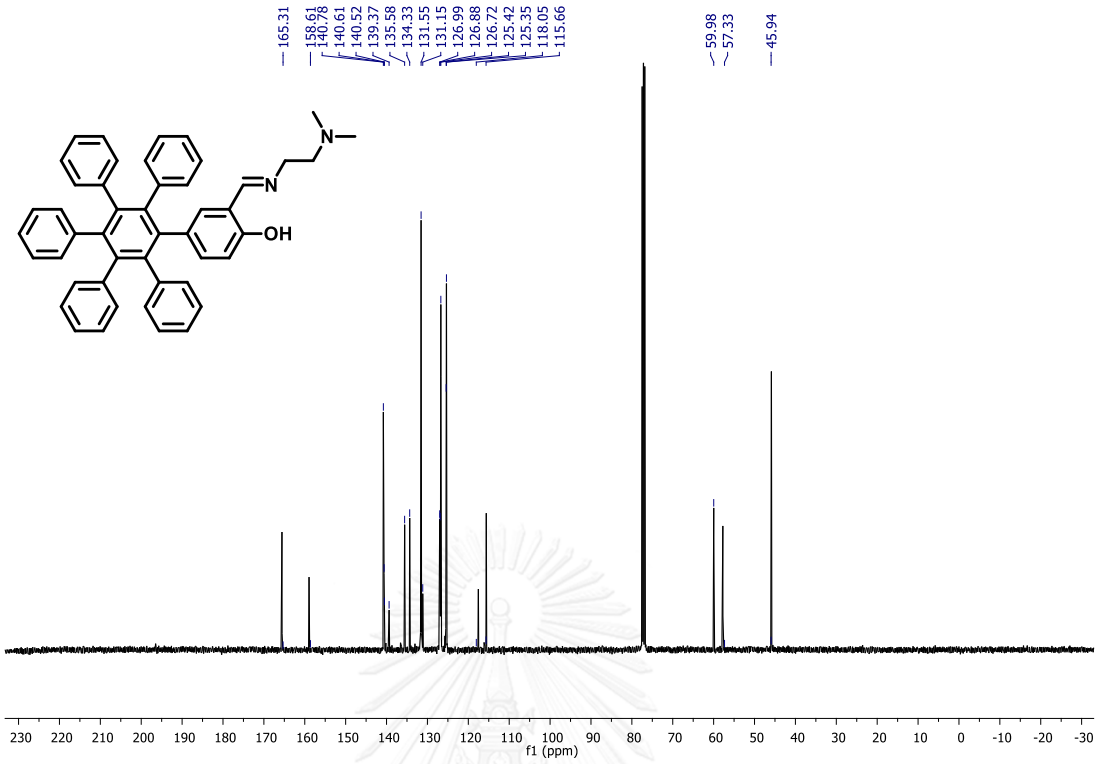

Figure S.29 ^{13}C-NMR spectrum of SW5

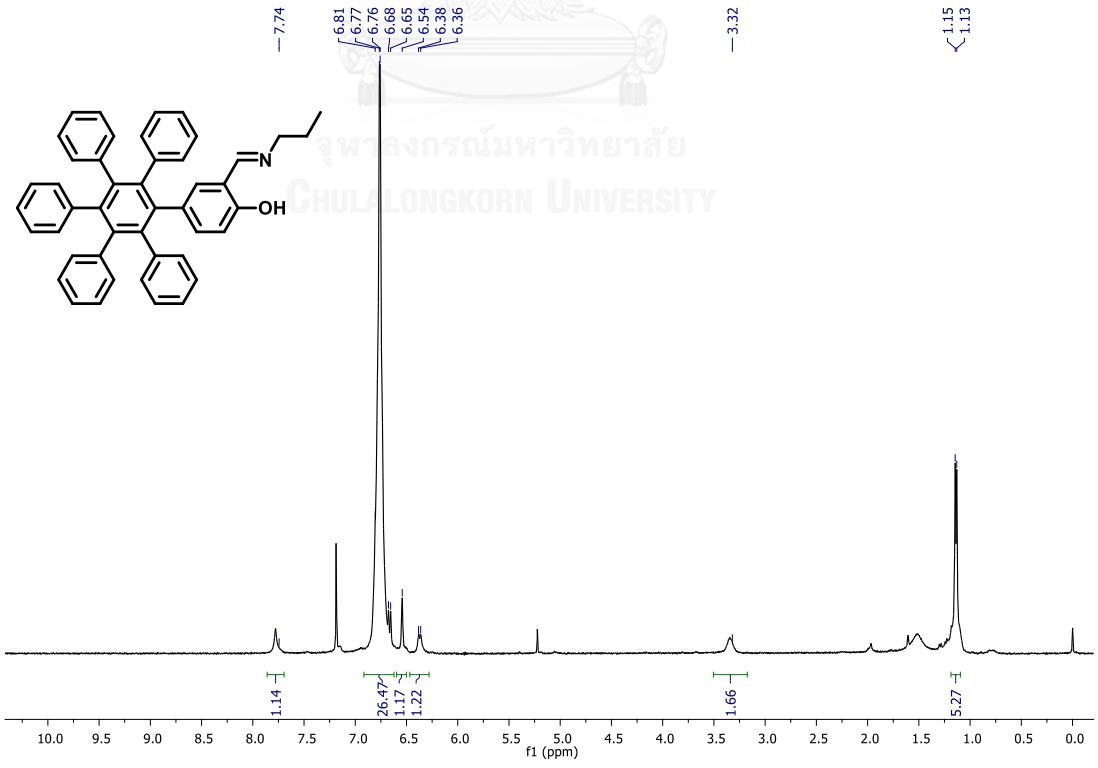

Figure S.30 ^{1}H-NMR spectrum of SW6

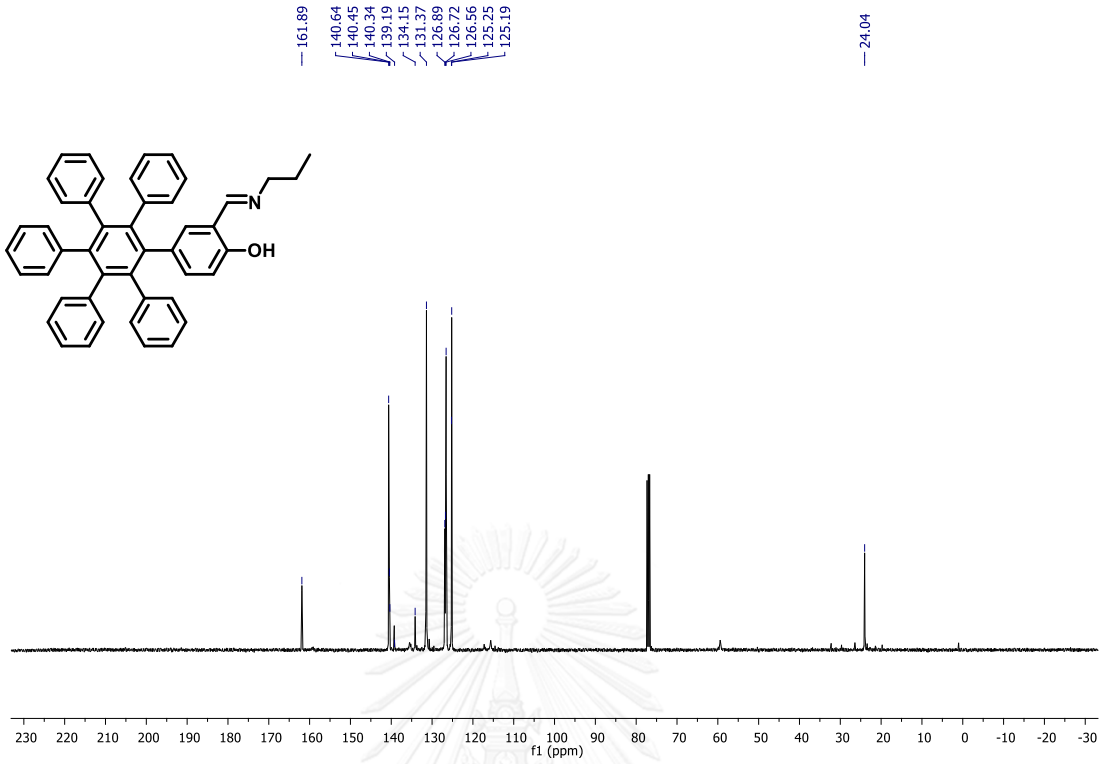

Figure S.31 ^{13}C-NMR spectrum of SW6

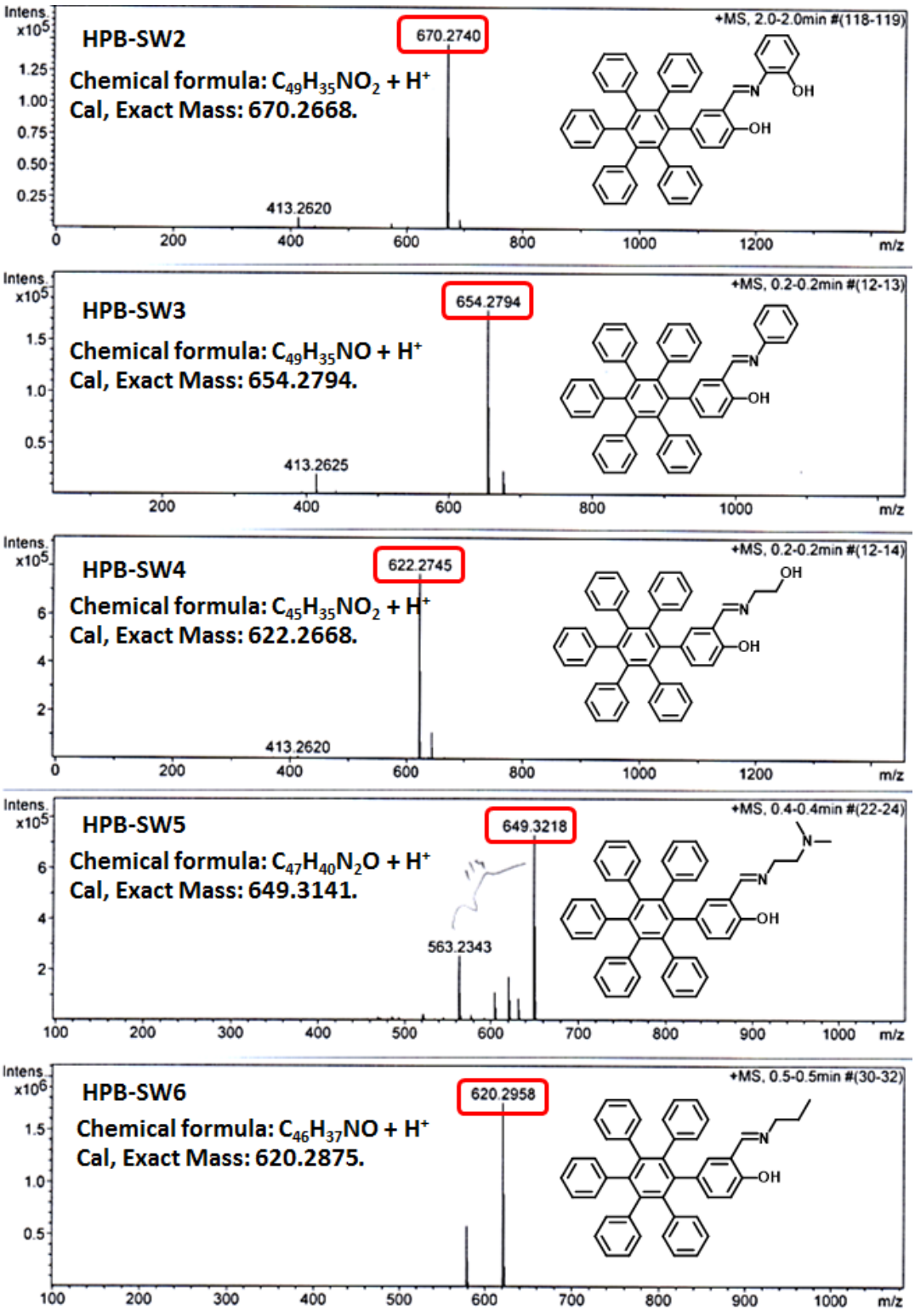

Figure S.32 the HRMS of **SW (2-6)**

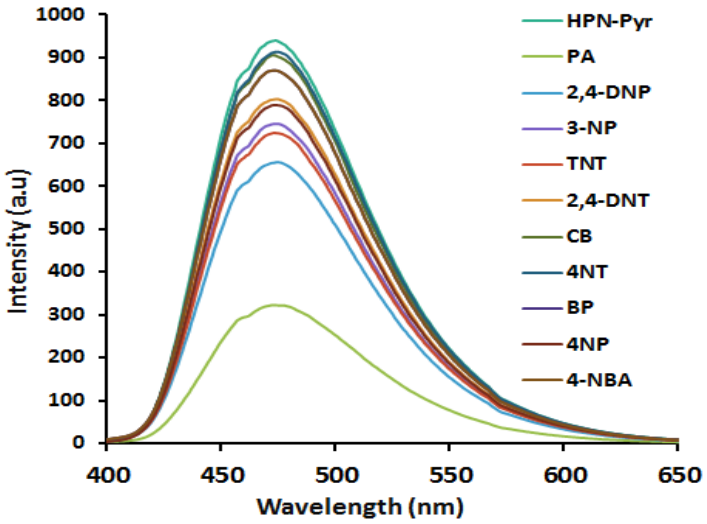

Figure S.33 fluorescence emission spectra of HNB-Pyr in different nitroaromatic compounds in THF at λex = 346 nm.

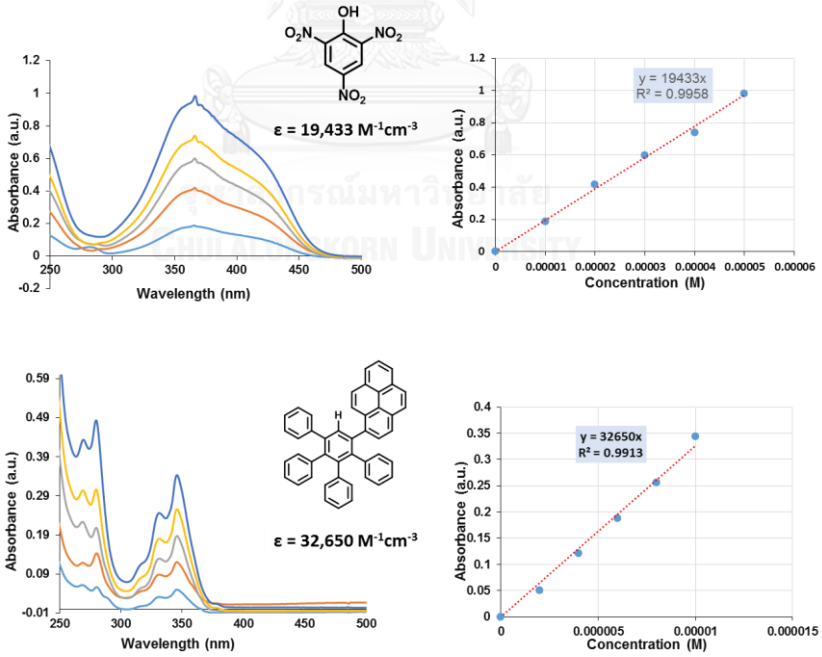

Figure S.34 molar absorptivity of **FL1**

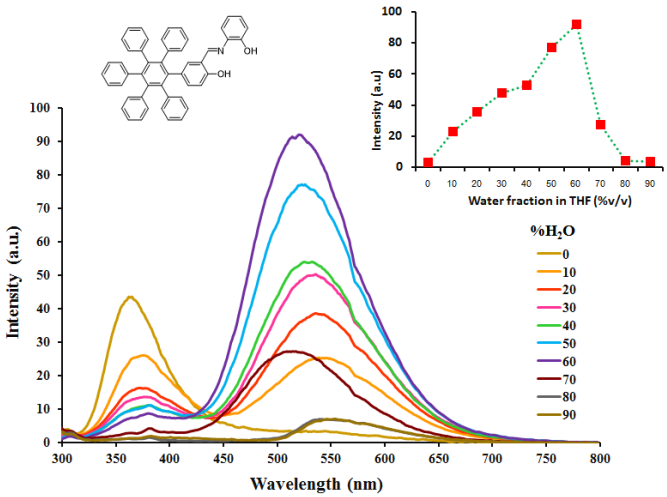

Figure S.35 fluorescence emission spectra of **SW2** (20μM) in variable H_2O: THF λex 280 nm

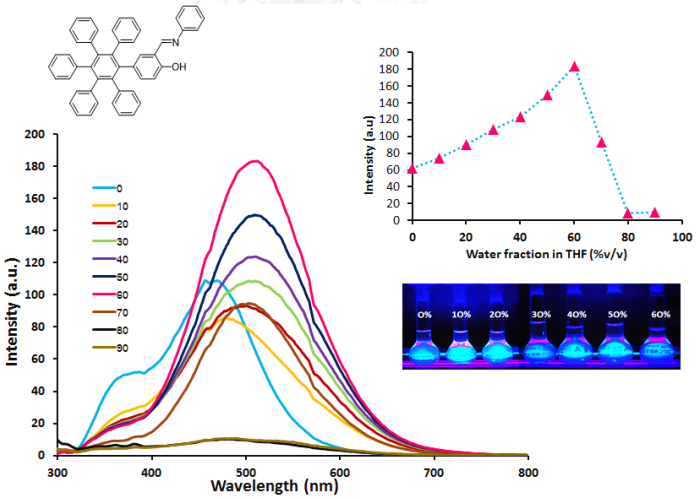

Figure S.36 fluorescence emission spectra of **SW3** (20μM) in variable in variable H_2O: THF λex 280 nm

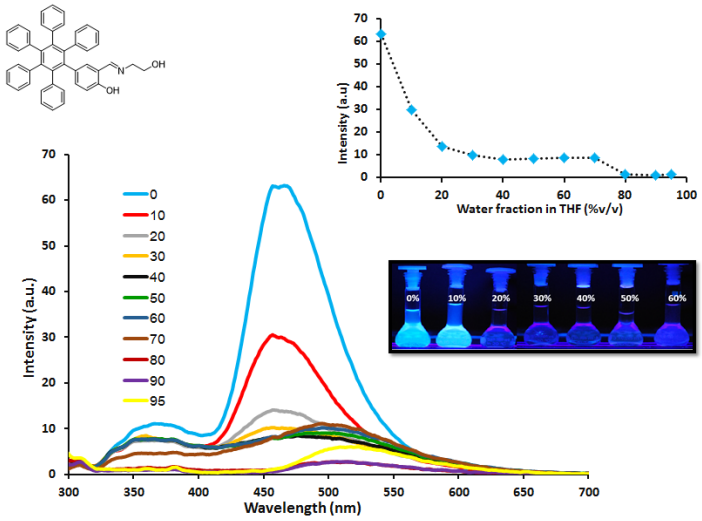

Figure S.37 fluorescence emission spectra of **SW4** (20μM) in variable in variable H_2O: THF λex 280 nm

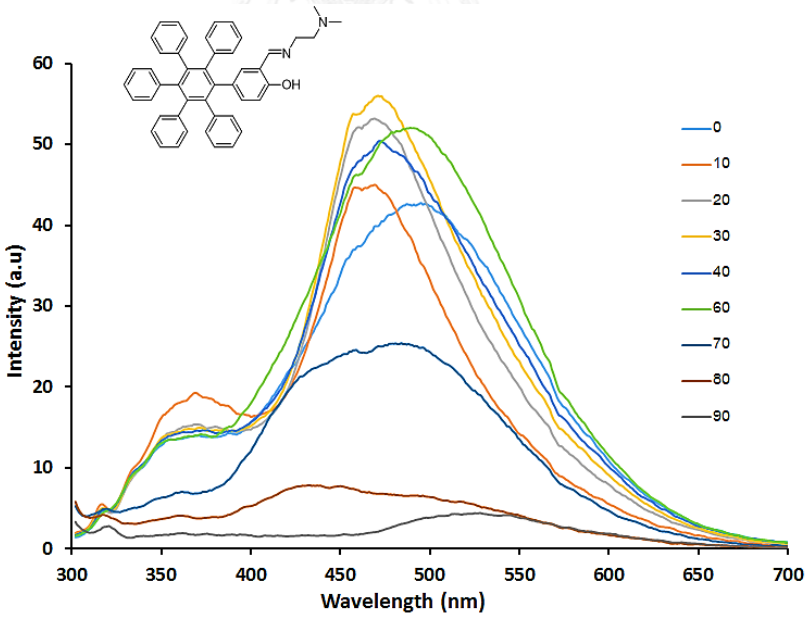

Figure S.38 fluorescence emission spectra of **SW5** (20μM) in variable in variable H_2O: THF λex 290 nm

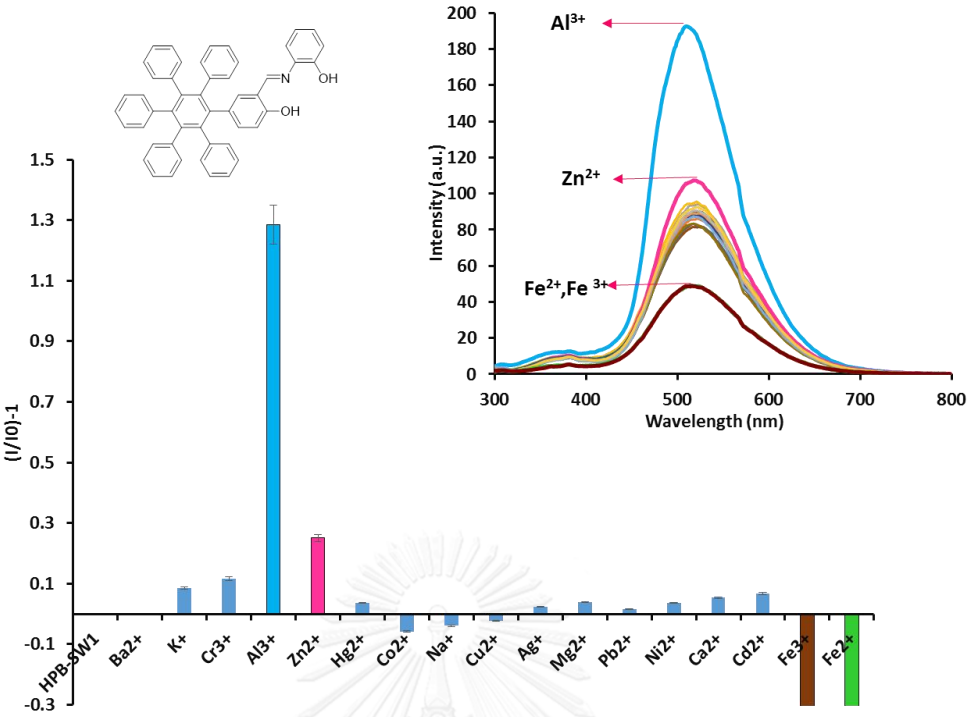

Figure S.39 Change of **SW2** (20 μM) upon mixing with different other metal cations (10eq) in THF: H_2O (4:6, v/v) lex 280 nm.

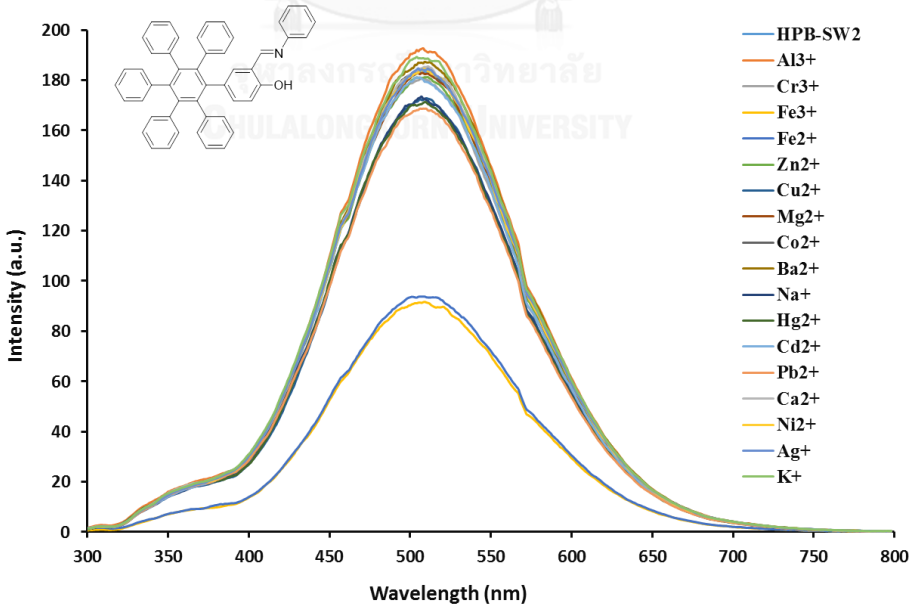

Figure S.40 Change of **SW3** (20 μM) upon mixing with different other metal cations (10eq) in THF: H_2O (4:6, v/v) λex 280 nm.

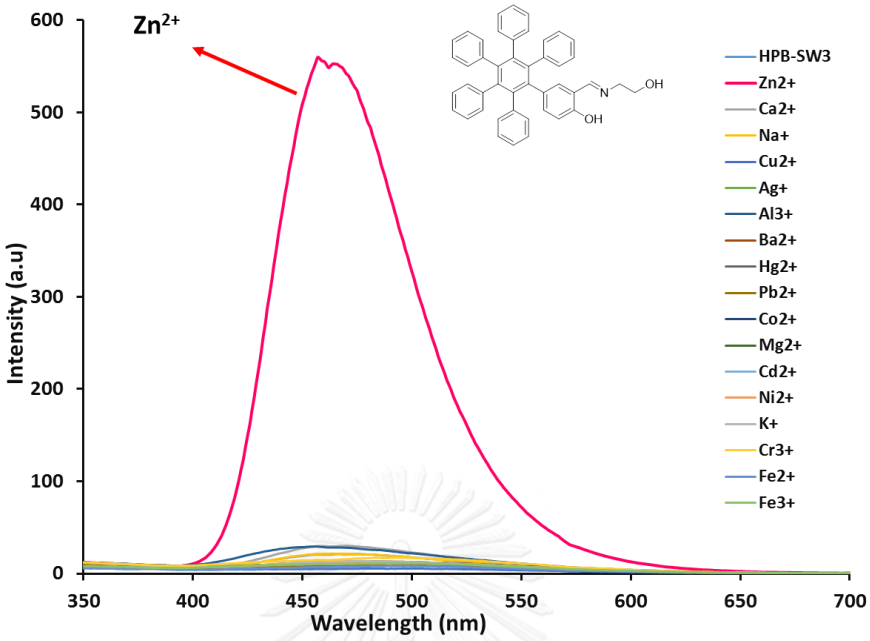

Figure S.41 Change in the fluorescence spectra of **SW4** (20 μM) upon mixing with different other metal cations (10eq) in THF: H_2O (1:1, v/v) λex 280 nm.

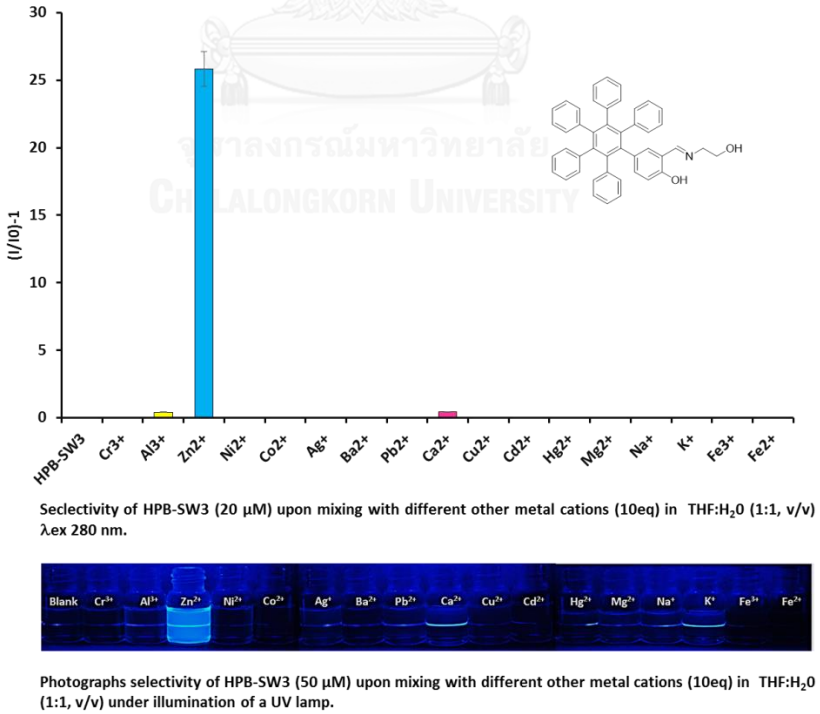

Figure S.42 Bar graphs of **SW4** (20 μM) upon mixing with different other metal cations (10eq) in THF: H_2O (1:1, v/v) λex 280 nm.

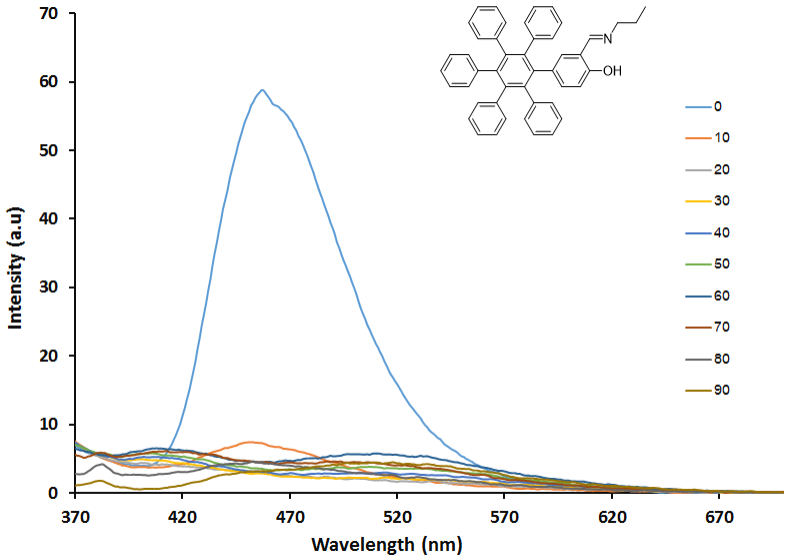

Figure S.43 Fluorescence emission spectra of **SW6** (20μM) in upon mixing with different other metal cations (10eq) in THF: H_2O (1:1, v/v) λex 280 nm.

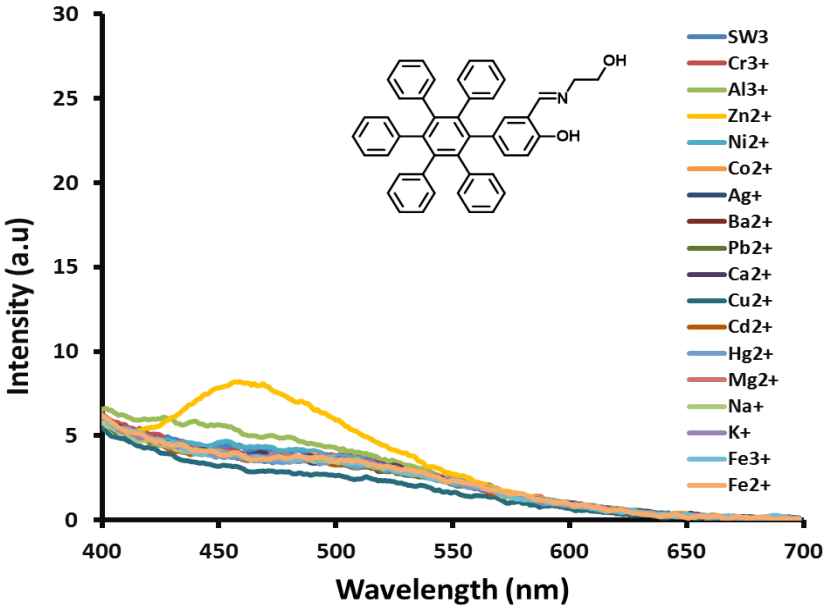

Figure S.44 Fluorescence emission spectra of **SW4** (10μM) in upon mixing with different other metal cations (1eq) in THF: H_2O (1:1, v/v) λex 280 nm.

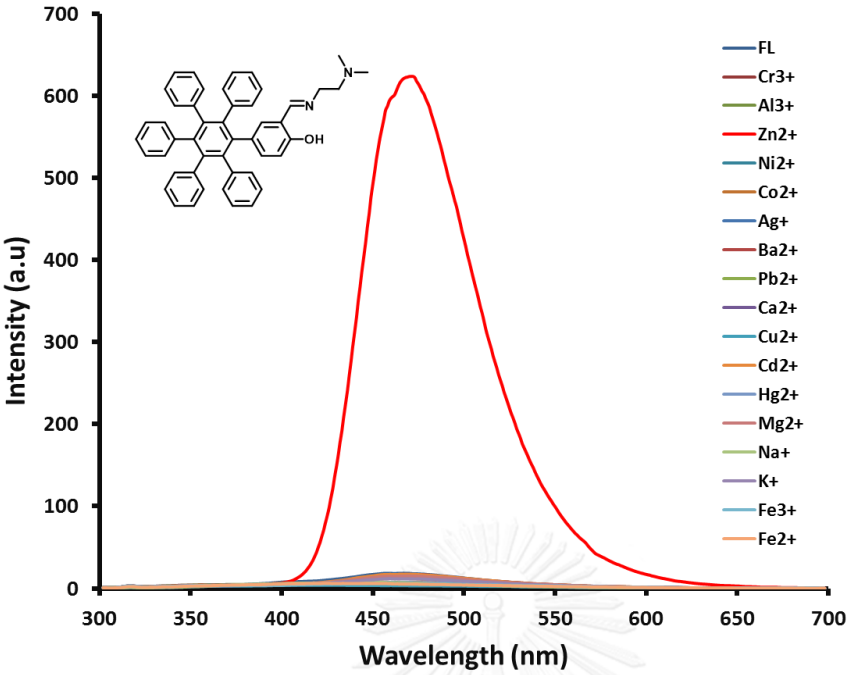

Figure S.45 Fluorescence emission spectra of **SW**5 (10μM) in upon mixing with different other metal cations (1eq) in THF: H_2O (7:3, v/v) λex 290 nm.

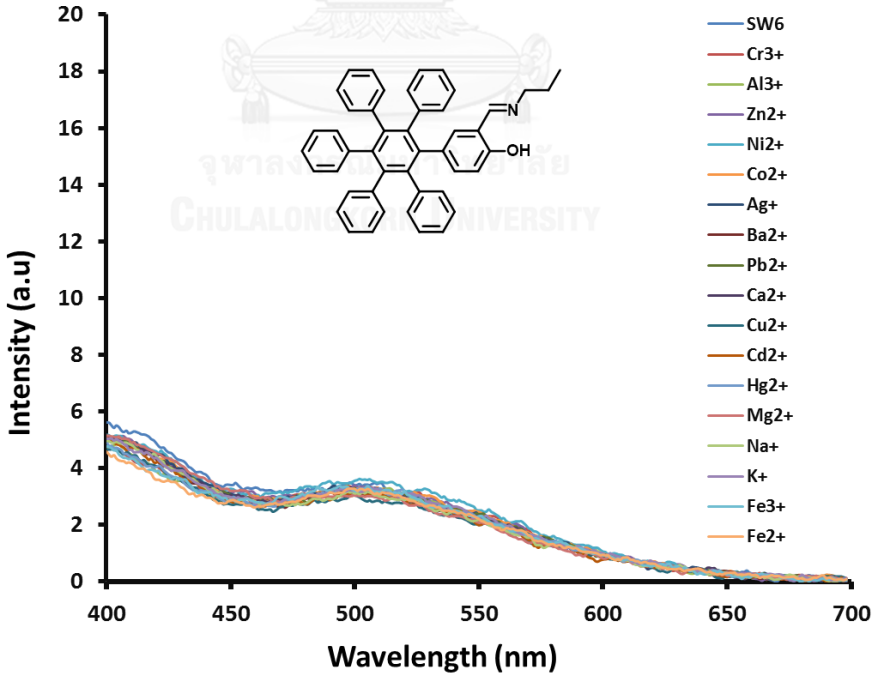

Figure S.46 Fluorescence emission spectra of **SW**6 (10μM) in upon mixing with different other metal cations (1eq) in THF: H_2O (1:1, v/v) λex 280 nm.

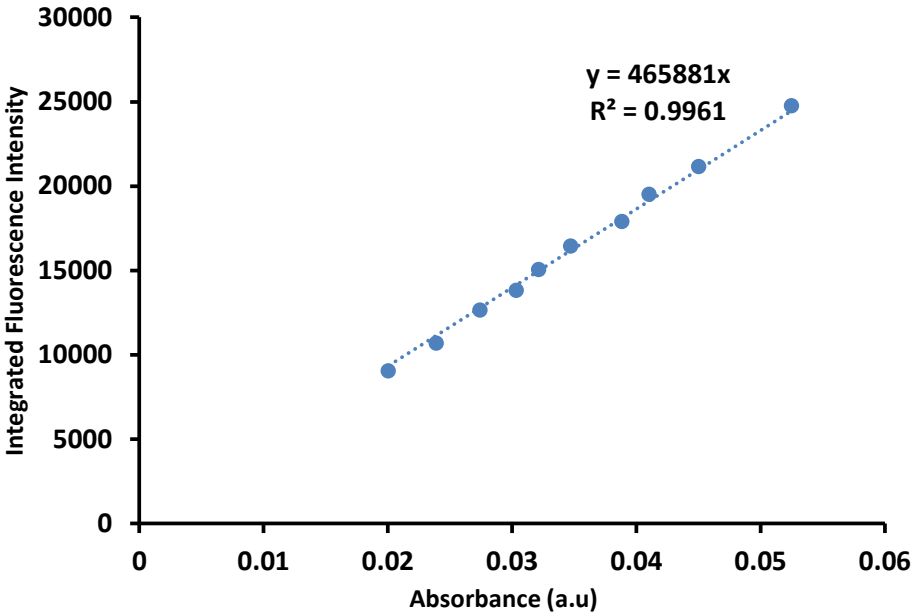

Figure S.47 Quantum yield of quinine Sulfate

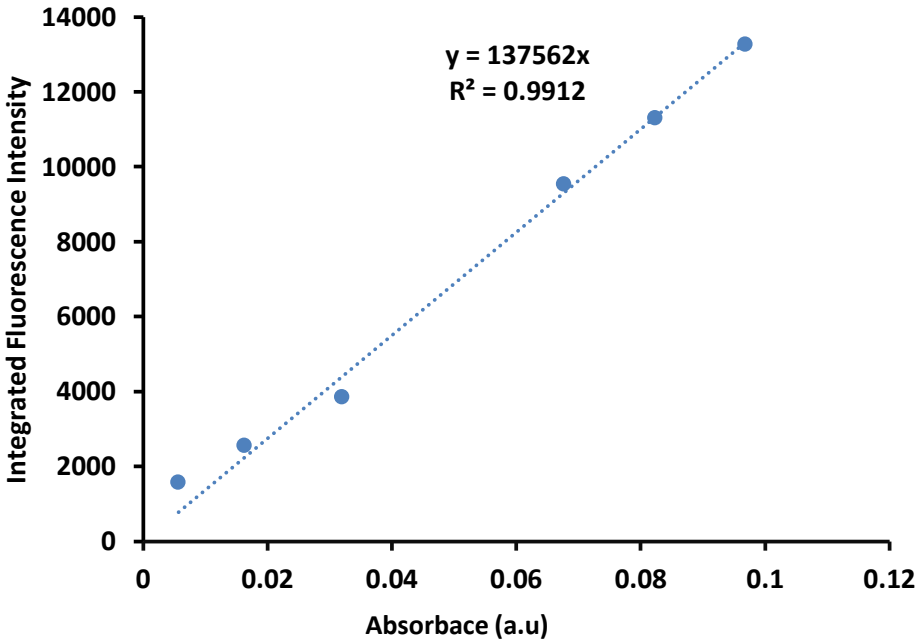

Figure S.48 Quantum yield of **SW5** toward Zn^{2+}

VITA

Mr. Weerawat Sripet was born on August 29, 1989 in Trang, Thailand. He graduated with high school degree from Saparachinee 2 School, Trang. He graduated with bachelor degree of Science, major of chemistry from Prince of Songkla University. In 2012, he had finished a project of organic synthesis and applied a master degree at Chulalongkorn University in the same year. And so, he has joined a group of MAPS research unit under the supervision of Assistant Professor Sumrit Wacharasindhu during him master degree, he was a teaching assistance for Department of chemistry, Faculty of Science, Chulalongkorn University. His present address is 264 Moo 4, Phrong Chorakhe, Yan Ta Khao, Trang, Thailand 92140.